Titre: Title:	Sulfur passivation of InP(100) surfaces
Auteur: Author:	Ye Tao
Date:	1993
Type:	Mémoire ou thèse / Dissertation or Thesis
Référence: Citation:	Tao, Y. (1993). Sulfur passivation of InP(100) surfaces [Thèse de doctorat, Polytechnique Montréal]. PolyPublie. https://publications.polymtl.ca/57985/

UNIVERSITE DE MONTREAL

SULFUR PASSIVATION OF InP(100) SURFACES

par

Ye TAO

DEPARTEMENT DE GENIE PHYSIQUE

ECOLE POLYTECHNIQUE

THESE PRESENTEE EN VUE DE L'OBTENTION

DU GRADE DE PHILOSOPHIAE DOCTOR

(GENIE PHYSIQUE)

Avril 1993

ISBN 0-315-86550-4

UNIVERSITE DE MONTREAL

ECOLE POLYTECHNIQUE

Cette thèse intitulée:

SULFUR PASSIVATION OF InP(100) SURFACES

présentée par: Ye TAO

en vue de l'obtention du grade de: Ph.D.

a été dûment acceptée par le jury d'examen constitué de:

M. M. Meunier, Ph.D., président

M. A. Yelon, Ph.D., membre et directeur de recherche

M. R. Masut, Ph.D., membre

M. T. Jackman, Ph.D., membre

SOMMAIRE

Les mobilités électroniques élevées, les grandes valeurs de plafonnement de la vitesse des électrons, ainsi que les gaps énergétiques directs dans la majorité des matériaux III-V, permettent plusieurs applications en ce qui concerne les dispositifs semi-conducteurs, tels que les oscillateurs micro-ondes, les transistors hautes fréquences à effet de champ, les piles solaires, les diodes laser et les détecteurs opto-électroniques. L'opération de ces dispositifs requiert que la qualité des surfaces et des interfaces (avec d'autres solides) du semi-conducteur soit élevée. Il est cependant bien connu que les surfaces de composés semi-conducteurs III-V s'oxydent facilement une fois exposées à l'air. Les densités d'états élevées à la surface (ou interface), qui causent le piégeage du niveau de Fermi sur ces surfaces (ou interfaces), sont un vrai fléau pour les interfaces avec des métaux ou des matériaux diélectriques. De plus, la nature des composés III-V crée d'autres problèmes telles que l'oxydation préférentielle ou la perte physique d'une des composantes dans la région près de la surface pendant le traitement de la surface ou de la fabrication de l'interface. Ceci introduira des états localisés additionnels dans la région près de la surface. Tous ces facteurs continuent d'empêcher le développement de dispositifs semi-conducteur III-V à surfaces sensibles et limitent les dimensions des dispositifs.

Par conséquent, la physique et la chimie des surfaces des matériaux III-V intéressent considérablement les gens du milieu, autant du côté théorique qu'expérimental. Un des efforts des recherches actuelles dans ce domaine a pour but la synthèse par procédés chimiques de surfaces semiconductrices chimiquement stables et idéales électroniquement, ainsi qu'une meilleure compréhension des inter-relations entre la structure crystallographique, la composition chimique, et les propriétés électroniques des

surfaces ou interfaces.

En 1987, Sandroff, Yablonovitch et al. ont rapporté la passivation de la surface de GaAs avec soufre. Ils ont trouvé qu'à l'application, par 'spin-coating', d'une solution $Na_2S{\cdot}9H_2O$, que les centres de recombinaison non-radiative à la périphérie de transistors GaAs/AlGaAs bipolaires et hétéostructuraux étaient passivés, résultant d'un gain de courant 60 fois plus élevé pour le dispositif. Le temps de vie du porteur à l'interface $Na_2S{\cdot}9H_2O$ et GaAs approche celui d'une interface quasi idéal AlGaAs/GaAs. Par la suite, le traitement par solution sulfide a plus attiré l'attention à cause de la possibilité qu'elle offre de passiver des surfaces semi-conductrices III-V, et d'améliorer les propriétés électroniques de ces dernières. Mais les procédures lors de la passivation utilisées jusqu'à maintenant ne sont pas entièrement satisfaisantes. La composition chimique et la structure des surfaces ne sont pas claires. Ceci empêche la compréhension du mécanisme de passivation.

Nous avons developpé une meilleure procédure de passivation pour l'InP avec une solution $(NH_4)_2S$. Cette procédure surmonte les carences des procédures couramment utilisées, tels que: faible recouvrement de la surface par le soufre, piètre reproductibilité de la composition chimique de surface et les matériaux résiduels sur les surfaces traitées. Cette nouvelle procédure crée des surfaces InP chimiquement stables, et ordonnées (niveau atomique), dont les propriétés électroniques sont supérieures aux surfaces non-passivées.

La spectroscopie des photo-électrons par rayon-X (XPS) fut utilisée pour caractériser la composition chimique de surfaces InP passivées au S. Il fut trouvé à partir de l'analyse des spectres P 2p que le phosphore est absent à la couche supérieure d'une surface InP(100) S-passivée. L'analyse des spectres In $3d_{5/2}$ et S 2p révéla que cette même surface est complètement terminée par une monocouche de composé 1:1 In-S. L'atome de soufre se lie seulement aux atomes d'indium de la surface. Aucun pic d'oxyde de soufre ou

d'InP furent détectés. Les mesures XPS angulaires montrent que l'oxygène et le carbone sont situés au-dessus de la couche de soufre. Par conséquent, ils ne sont pas en contact direct avec le substrat InP.

La diffraction des électrons lents (DEL) fut utilisée pour étudier la structure surfacique d'une surface passivée avec soufre. Due à la profondeur d'échappement très limitée des électrons, les patrons en DEL donnent l'information sur la structure très près de la couche supérieure. En mesurant les patrons en DEL de ces surfaces, il fut trouvé que la surface InP(100) passivée avec du soufre a une structure (1x1), et peut être dénotée: InP(100)-(1x1)-S. Des patrons DEL clairs et distincts peuvent être obtenus d'échantillons qui ont été exposés à l'air pendant 3-4 jours. Ceux-ci démontrent que la surface passivée avec soufre est très stable dans l'air, et résistante à la contamination et à l'oxydation. Un modèle structural correspondant fut proposé pour cette surface. Dans ce modèle, on suppose que l'atome de soufre se lie à ses deux atomes d'indium voisins dans le direction [011], et que ses deux autres orbitales atomiques sont comblées par des paires d'électrons.

La diffraction des photo-électrons-rayons X (XPD) fut aussi utilisée pour l'analyse structurale. Les mesures XPD furent effectuées pour différents angles azimutaux et polaires. Les résultats indiquent que les atomes de soufre sont seulement présents à la couche supérieure. Par conséquent, la possibilité d'échange d'anions (S, P) en grande quantité près de la surface est exclue. L'angle de 38 ± 2^{0} entre la liaison S-In et le plan (100) a été estimé à partir des mesures XPD.

Le modèle structural proposé fut par la suite confirmé par les mesures des 'X-ray absoption near edge structure' (XANES). Ces derniers résultats montrent que la liaison S-In est en effet dans le plan (011), et à 40^{0} du plan (100). Les données en XANES indiquent aussi que l'atome de soufre à la surface n'a pas de liaison pendante.

La position du niveau de Fermi à la surface pour les échantillons S-passivés fut estimée en comparant les énergies de liaison des spectres P 2p avec celui d'un échantillon standard qui est en condition de bandes plates. Il fut montré que le InP S-passivé de type n est presque en condition de bandes plates, et le InP de type p a 0.4 eV de courbure de bande. Ces résultats montrent que le procédé de passivation enlève la majorité des états de surface de type accepteur, réduisant le 'band bending' du InP de type n, mais n'affecte pas les états de type donneur et le 'downward band bending' des échantillons de type p.

Les mesures d'intensités de photoluminescence (PL) de bordure de bande furent utilisées pour étudier le processus de recombinaison aux surfaces passivées avec soufre. L'intensité PL fut augmentée de 2 à 4 fois après passivation, dans le cas des deux types d'échantillons (n et p). Ces résultats indiquent que les centres de recombinaisons non-radiatives à la surface de InP étaient grandement diminués par le traitement. A partir des intensités PL sur les échantillons recuits, il fut montré que les échantillons S-passivés sont résistants aux traitements de chaleur, et à la formation de centres de recombinaisons non-radiatives.

Les mesures caractéristiques courant-voltage (I-V) furent employées afin d'étudier les propriétés électroniques de diodes Schottky préparées sur des échantillons S-passivés. La hauteur de la barrière et le facteur d'idéalité d'une diode Au/n-InP furent améliorés par le traitement. La hauteur de la barrière sur le n-InP passivé montre quelque dépendence sur la fonction de travail du métal. Cela indique que les propriétés électroniques à l'interface sont améliorées par le passivation.

La grande stabilité chimique et l'amélioration des propriétés électroniques à la surface sont attribuées à la formation d'une structure InP(100)-(1x1)-S. Les atomes de soufre saturent les liaisons pendantes des atomes d'indium à la surface en formant des

liaisons 'pont' avec leurs deux atomes voisins d'indium, et conservent deux orbitales atomiques comblées par deux paires d'électrons.

Abstract

In recent years, sulfide solution treatment has attracted much attention due to its possible application in passivating III-V compound semiconductor surfaces and improving their electronic properties. But the passivation procedures used up to now are not entirely satisfactory. The surface chemical composition and the surface structure on these surfaces are not clear. This impedes the understanding of the passivation mechanism. We have developed an improved $(NH_4)_2S$ solution passivation procedure for InP. This procedure overcomes the deficiency of commonly used sulfur passivation procedure, such as: low sulfur coverage on the surface, poor reproducibility of surface chemical composition, and residual material on the treated surfaces. The procedure provides chemically stable, and atomically ordered InP surfaces with superior electronic properties.

X-ray photoelectron spectroscopy (XPS) was used for surface chemical analysis. It has been found that phosphorous is absent at the topmost surface of the S-passivated InP(100) surface, and that the surface is completely terminated by one monolayer of 1:1 In-S surface compound. The sulfur atom bonds only to the surface indium atoms.

Low energy electron diffraction (LEED) was employed in surface structural study. It has been found that the S-passivated InP(100) surface has a (1x1) structure, and can be denoted as InP(100)-(1x1)-S. A corresponding structural model has been proposed for this surface. In this model the sulfur atom was assumed to form bridge bonds with its two neighboring surface indium atoms along the [011] direction, and its two other atomic orbitals are filled with paired electrons.

From X-ray photoelectron diffraction (XPD) measurements, the sulfur atoms were found to exist only at the topmost layer. The angle between the S-In bond and the (100)

plane was estimated as 38 ± 2^0 from the XPD measurement.

The proposed structural model has been further confirmed by the X-ray absorption near edge structure (XANES) measurements. It has been shown that the S-In bond is in the $(0\bar{1}1)$ plane, and is 40 ± 2^0 from the (100) plane. The XANES data also indicates that the surface sulfur atom is free of dangling bonds.

The surface Fermi level measurements by XPS have shown that the S-passivated n-InP is nearly at flat band condition, and the p-InP has an about 0.4 eV downward band bending. This shows that the passivation process removes most acceptor-like surface states, reducing the band bending on n-type InP, but do not affect donor-like states and downward band bending on p-type material.

Band edge photoluminescence (PL) intensity on passivated InP surfaces was increased by 2-4 times as compared to chemically etched InP. The results indicate the reduction of the non-radiative recombination centers at the InP surface by the treatment. The PL intensity measurements on the annealed samples show that the S-passivated samples are resistant to heat treatment, and to the formation of non-radiative recombination centers, as compared to the etched samples.

Schottky diode I-V characteristics measurements were also used to study the interface electronic property of treated InP surfaces with metals. The barrier height and ideality factor of Au/n-InP diode were found to be improved by the treatment. The barrier height on the treated n-InP shows some dependence on the metal work functions. It indicates that the interface electronic property was improved by the treatment.

The high surface chemical stability and the improved surface electronic properties

are attributed to the formation of InP(100)-(1x1)-S structure. The sulfur atoms saturate the dangling bonds of surface indium atoms by forming bridge bonds with its two neighboring In atoms, and leaves itself two atomic orbitals filled with lone-pair electrons.

Acknowledgements

First of all, I would like to express my gratitude to my supervisor, professor Arthur Yelon, for his guidance, encouragement, and much personal assistance, during my studies, and also for his thorough revision of the drafts of this thesis. In my four-year-stay in Ecole Polytechnique, I have greatly benefited from his deep understanding in physics and science, through our frequent discussions. His great patience in correcting my English writing is highly appreciated.

I am also especially grateful to Dr. E. Sacher, for many instructive discussions about chemistry and for providing valuable references.

I am very grateful to Drs. M. Graham, and Z. H. Lu at National Research Council of Canada, for providing the opportunity to use their research facility and for our successful collaboration.

I am also very grateful to Dr. R. Leonelli for the photoluminescence measurements and many helpful discussions. I also would like to express my thanks to Dr. R. Masut for kindly providing MOCVD grown InP samples, and for providing helpful references on Schottky diodes.

I would like to express my gratitude to Mr. C. Sundararaman for his experimental help and for providing a pure In_2S_3 sample, many helpful discussions about sulfur passivation is highly appreciated. In addition, I would like to thank Ms. S. Poulin-Dandurand and Dr. B. Lamontagne, for their technical assistance in XPS and XPD experiments, Dr. K. Piyakis for XPS data transfer, Miss E. Poiré and Mr. M. Tabbal for help with the French abstract, and Mr. Y. D. Ma for help printing the thesis.

I can hardly express my gratitude to my parents for their love and dedication.

I shall always remain grateful to my wife, X. Dong, for her love, understanding, supporting and constant encouragement during these years. I also hope that someday my dear daughter, R. Tao, will understand why I cannot go out with her in the weekends during these months.

TABLE OF CONTENTS

LIST OF FIGURES

LIST OF TABLES

LIST OF ACRONYMS

AUDM:	the advanced unified defect model
CBM:	conduction band minimum
CLS:	cathodoluminescence spectroscopy
LEED:	low energy electron diffraction
PL:	photoluminescence
RHEED:	reflected high energy electron diffraction
SRV:	surface recombination velocity
VBM:	valence band maximum
XANES:	X-ray absorption near edge structure
XPD:	X-ray photoelectron diffraction
XPS:	X-ray photoelectron spectroscopy

Chapter 1

Introduction

Compared with silicon (Si) and germanium (Ge), the advantages of the III-V compound semiconductors, including indium phosphide (InP), are primarily in their bulk transport and optical properties. The large electron mobilities, the high values of saturated electron velocity, and the direct energy gaps in most III-V materials lead to many potential applications in semiconductor devices, such as microwave oscillators, high-frequency field-effect transistors, solar cells, laser diodes, and optoelectronic detectors. The operation of these devices demands high quality semiconductor surfaces and interfaces with other solids. However, it is well known that III-V compound semiconductor surfaces, and their interfaces with metals and dielectric materials are plagued by high surface (or interface) state densities which cause the Fermi level pinning at these surfaces (or interfaces) as discussed in ref.[1, 2, 3]. The Fermi level pinning at metal-(III-V) semiconductor interfaces make the Schottky barrier heights insensitive to the metal work functions. The surface (or interface) states also act as recombination-generation centers and carrier traps, which in almost all cases could seriously degrade device performance [4]. In addition, the compound nature of the III-V's creates some other problems, such as preferential oxidation or physical loss of one of the components in the near surface region during surface treatment or interface fabrication. This will introduce additional localized states in the near-surface region [5, 6]. All these factors continue to impede the development of surface sensitive III-V semiconductor devices and limit the dimensions of devices [4, 7-10].

As a result, the surface physics and chemistry of III-V materials have attracted

considerable interest, both experimentally and theoretically. One of the efforts of current research in this area is aimed at the synthesis of chemically stable and electronically ideal semiconductor surfaces by chemical means[11-14], and at obtaining a detailed understanding of the interplay among the crystallographic structure, the chemical composition, and the electronic properties of those surface or interface regions [15,16].

In 1987, Sandroff, Yablonovitch, and co-workers reported sulfur passivation of GaAs surfaces [17-20]. They found that after the application of $Na_2S \cdot 9H_2O$ solution by spin coating, non-radiative recombination centers at the periphery of a GaAs/AlGaAs heterostructure bipolar transistor were passivated, resulting in a 60-fold increase in the current gain of the device [17]. The carrier lifetime at the interface between $Na_2S \cdot 9H_2O$ and GaAs approaches that of the nearly ideal $Al_{0.5}Ga_{0.5}As$/GaAs interface [18]. Band bending of passivated GaAs surfaces was greatly reduced, as shown by Raman scattering measurements [19], and the band edge photoluminescence (PL) intensity was increased by a factor of a thousand after passivation [20]. All these experimental results showed that the surface recombination velocity and the surface state density on GaAs surfaces were greatly reduced by this sulfide-solution treatment. Since then, chemical reagents including sodium sulfide and ammonium sulfide solutions, and hydrogen sulfide vapor have been used to passivate GaAs surfaces [21-23].

Following the success of sulfur passivation of GaAs, Iyer and his collaborators have found that a sulfurization procedure, in which the semiconductor was immersed in a boiling ammonium sulfide solution and dried by N_2 gas, was also effective in reducing surface states on InP [24, 25]. Enhancement mode metal-insulator-semiconductor field-effect transistors (MISFET's) with less than 5% drain current drifts in 12 hours have been obtained using such passivation procedure. The measured surface state density is in the

range of 10^{10} to a few10^{11} cm^{-2} eV^{-1}.

Considerable work has been done since, by many groups, on passivating III-V compound semiconductor surfaces. Sulfide solution treatment seems to be able to improve the surface properties for all III-V compound semiconductors, including their ternary and quaternary compounds [26, 27]. Se and Te have also been used to passivate GaAs surfaces [28-30].

In spite of the early success of sulfur passivation of III-V compound semiconductors as shown by the improvement of surface electronic properties, the surface chemical composition and the surface structure of the treated surfaces, and the passivation mechanism are still controversial. In the case of GaAs, some groups [26, 31, 32] reported dominant S-As bonds, some groups [33] found both S-Ga and S-As bonds, and several other groups [23] reported dominant S-Ga bonds on passivated GaAs(100) surfaces. In the case of InP, Wilmsen and co-workers [34] have shown that, as a result of the sulfurization treatment used in ref.[24], no phosphorous sulfide was present on the InP(100) surface; an indium sulfide layer (> 20 Å) was present on the sulfide treated InP surfaces. Lau et al [35, 36] have more recently found that there was no S-P bonding on InP(100) surfaces which were treated in sulfide solution at room temperature, but both S-In and S-P bonding were found on their sulfide vapor treated InP surfaces. Oigawa et al. have found that both S-In and S-P bonds on InP surface after sulfide solution treatment [26].

These differences may result from the different passivation procedures used by each group. Generally speaking, the sulfur passivation procedures used up to the present, involving the use of $Na_2S{\cdot}9H_2O$ or $(NH_4)_2S$ solution, have not been entirely satisfactory. Sulfur coverage on these surfaces is relatively low and varies widely from sample to sample [34]. For example, Tiedje et al. [37] estimated that the sulfur coverage on GaAs

surface treated with $Na_2S \cdot 9H_2O$ or $(NH_4)_2S$ solution at room temperature is about 0.3 monolayer. The resulting surface was found to be a mixture of oxide and sulfide. From the work of Lau et al [35, 36], the sulfide solution-treated InP surface was found to be covered with about a monolayer equivalent of indium sulfide (In-S) plus one to two monolayers of indium oxide.

Despite the fact that Tiedje et al.[23] have shown that the GaAs surface, completely terminated by a GaS_x species, after treatment with filament-excited hydrogen sulfide in vacuum, is stable in air or when flushed with DI water, the most commonly used final step in sulfide solution treatments is to dry the surface with N_2 gas as soon as the sample is removed from the solution. This is done in order to avoid oxidation caused by rinsing the sample in water. However, this final step leaves a clearly visible residue on the surface. According to some reports [22, 38], this residue can be removed from the GaAs surface by vacuum sublimation, but not from InP [39] and InAs surfaces [40]. Almost all the III-V semiconductor surfaces treated in this way failed to give clear, distinct, low-energy electron diffraction (LEED) pattern. This impedes surface structural analysis and getting a better understanding of the passivation mechanism.

There are three possible reasons for the failure to obtain clear LEED patterns from these surfaces: 1) sulfur coverage may be too low, with too much oxide on the surface; 2) the crystalline surface may be covered by some residual materials resulting from the treatment, and which cannot completely sublime in vacuum; 3) the sulfide treated surfaces themselves may be disordered.

Because of the difficulty of obtaining clear LEED patterns, a few surface structural studies have been done using other techniques such as reflected high energy electron diffraction (RHEED) [26, 41], and coaxial impact collision ion scattering spectroscopy

(CAICISS) [40]. But these experiments were carried out on the surfaces which failed to give a clear LEED pattern. Obviously, the results cannot reflect the structure of the top-most surface, but give average information over a few atomic layers from the top.

Several different mechanisms have been proposed to explain the decrease of surface recombination velocity (SRV) on the sulfide treated GaAs surfaces. From the point of view of Yablonovitch and his collaborators [18, 20, 42], the sulfide treatment will lead to a robust covalently bonded sulfide layer which can greatly reduce the surface state density on GaAs surfaces by satisfying all surface dangling bonds so that the surface Fermi level will be unpinned from a mid-gap position after the treatment. This explanation is supported by the following experimental results: the decrease of band bending after sulfide treatment [19, 23], the substantial decrease of SRV, the dependence of Schottky barrier height on metal work functions [22, 26] .

However, from their surface Fermi level measurement and PL measurement on sulfur passivated GaAs, Besser and Helms [43] found that for n-type GaAs, while the reduction of SRV is attained, the surface Fermi level, instead of being unpinned, is pinned closer to the valence band maximum (VBM). A similar observation was also made by Hasegawa et al. [44].

Based on these results, the passivation mechanism was then explained by Spindt, Spicer et al [45, 46] using the advanced unified defect model (AUDM) [47], which attributes the surface states to antisite defects. They propose that As_{Ga} defects are double donors with energy levels at 0.65 and 0.90 eV from the CBM. These donor states are compensated by Ga_{As} double acceptors near the VBM. The Fermi-level will then be determined by the relative densities of these two kinds of defects. GaAs is usually grown As rich, and there is evidence that excess As will accumulate near the surface, so there will

be more of the As_{Ga}-type defects, and the Ga_{As} will not be able to fully compensate them. Depending on how much the As_{Ga} are compensated by Ga_{As}, the Fermi-level will lie somewhere at or between the two donor levels. The sulfide treatment removes some of As_{Ga} antisite defects from the surface region, and that will allow the Ga_{As} to pull the Fermi level down towards the lower of the two As_{Ga} donor levels.

This AUDM predicts that the reduction in the number of mid-gap states will not flatten the bands, but will in fact cause an increase in band bending on n-type GaAs. The SRV decrease (or PL intensity increase) is then explained by two effects: the reduction in the density of As antisite defect states, and the increased band bending, which will reduce the number of electrons which are able to reach the recombination centers at the surface.

The main difference between these two explanations is that the first considers the dangling bonds as the main cause of high surface state density on GaAs surface, and emphasizes the importance of the chemical bonding between the passivating overlayer and the substrate, whereas the second considers the As antisite defects as the main source of non-radiative recombination centers on GaAs surface. It does not attribute the passivation to the overlayer itself, or to what the overlayer does, but rather to the restoration of a stoichiometric surface region after the sulfide solution treatment. The actual surface structure after passivation is not important in this model.

In contrast, the importance of the surface chemical bonding to the surface state density of the sulfide treated GaAs has been shown by a recent theoretical calculation carried out by Ohno [48]. He has investigated the structural and electronic properties of the GaAs(001)-(1x1) surface adsorbed with a monolayer of chalcogen atoms (S, Se, Te) using *ab initio* pseudopotential method. He has shown that the formation of the chalcogen-Ga bond remarkably reduces the surface state density in the mid-gap region, but the formation

of the chalcogen-As bond does not. The chalcogen-Ga bond was found to be stronger than the chalcogen-As bond. He suggests that chalcogen-Ga bonds are formed at chalcogen-treated GaAs (001) surfaces, and are responsible for the improvement in surface electronic properties. In addition, his results indicate an increased band bending for n-GaAs surfaces after sulfide treatment. This agrees with the experimental results obtained by Besser and Helms [43].

The two mechanisms discussed above were based on different experimental results of surface band bending after sulfide treatments, and can be used to plausibly explain their respective experimental results. In our opinion, it is possible to have different surfaces states at the same time: those due to surface dangling bonds and those related to antisite defects. But the density of antisite defects could not be of the same order of magnitude as that of surface dangling bonds, according to their definition. So, from the surface passivation point of view, surface chemical bonding should be more important. It would not be a proper assumption to ignore the surface states caused by dangling bonds and to attribute the surface states to antisite defects only. The sulfur passivation process may remove both kinds of surface states, to a certain extent, or preferentially remove one of two kinds under different experimental condition. Thus, different results on band bending after sulfide treatments could result from differences in the experimental conditions, wafer qualities, and chemical agents used. In particular, the different surface chemical bonding, and different sulfur coverage on these sulfide treated surfaces could be among the causes of the different band bending measured by various groups [23, 33].

Compared to GaAs, much less work has been done on the sulfur passivation of InP, and the sulfur passivation mechanism of InP is less clear. Wilmsen et al [34] explained the sulfur passivation of InP by proposing that sulfur replaces the surface

phosphorous and fills the phosphorous vacancies in the surface region, removing surface defects and forming an In_2S_3-InP heterojunction. In the work of Lau et al [35, 36], the passivation mechanism was explained in terms of the removal of surface indium oxide, a surface species often associated with donor states near the InP conduction band [49].

Due to limited experimental results available in the literature and the different experimental conditions used by different groups, it is difficult at present to give detailed comments on these explanations or to tell which one is closer to reality. But all the factors considered by different groups could be complementary. This would help us to consider the sulfur passivation in all its aspects.

From the above discussion, we may conclude that a small amount of sulfur coexisting with surface oxide on GaAs surface is effective in improving the surface electronic quality of GaAs. We may expect that a better passivation procedure might produce completely sulfur terminated surfaces, with superior electronic properties. Having this kind of surface would enhance our understanding of the sulfide passivation mechanism of III-V compound semiconductors.

The object of this thesis is to develop a better sulfide-solution passivation procedure for InP, and to obtain a better understanding of the mechanism of sulfur passivation of III-V compound semiconductor surfaces by studying the case of InP. There are two reasons to choose InP(100) surfaces as the research subject:

1) this material is technologically important , but much less research work has been done on it, compared to GaAs;

2) for XPS measurements, there is no interference between the sulfur 2p photoelectron peak, the indium photoelectron peak, and the phosphorous photoelectron peak. This is a great help in quantitative XPS data analysis. In the case of GaAs, there is

peak interference between the S 2p signal and the Ga 3S signal from GaAs substrate.

We have chosen ammonium sulfide solution as the chemical agent for passivation rather than sodium sulfide, in order to avoid unwanted sodium ions. We believe that a detailed surface study of sulfur passivated InP surfaces is of critical importance for our purpose.

In the next several chapters, a new passivation procedure which leads to a chemically and thermally stable InP(100)-(1x1)-S surface, will be described. X-ray photoelectron spectroscopy (XPS) will be used for chemical characterization; low energy electron diffraction (LEED), X-ray photoelectron diffraction (XPD), and sulfur K-edge X-ray absorption near-edge structure (XANES) will be used to investigate the surface structure of sulfur passivated InP(100) surface; band-edge photoluminescence (PL) intensity measurements and Schottky diode current-voltage (I-V) characteristic measurements as well as surface Fermi level measurements by XPS will be used to study the surface electronic properties of sulfur passivated InP. We shall then consider the passivation mechanism in detail.

Chapter 2

Experimental Techniques

Several experimental techniques are used in this thesis to study the surface chemical composition, the surface structure, and the surface electronic properties of S-passivated InP. In order to make the later discussion simple and clear, this chapter presents the basic principles of these experimental techniques.

2.1 X-ray Photoelectron Spectroscopy

2.1.1 The Physical Principles of X-ray Photoelectron Spectroscopy

Photoelectric effect and dispersive electron energy analysis form the cornerstone of photoemission spectroscopy. A basic XPS apparatus is schematically shown in Fig.2.1 The primary excitation is accomplished by irradiating the specimen using a source of X-rays either monochromatic or non-monochromatic, typically Al K_α (1487 eV) or Mg K_α (1254 eV). The X-rays cause photoionisation of atoms in the specimen. The response of the specimen (photoemission) is detected by measuring the energy spectrum of the emitted photoelectrons using an electron energy analyzer.

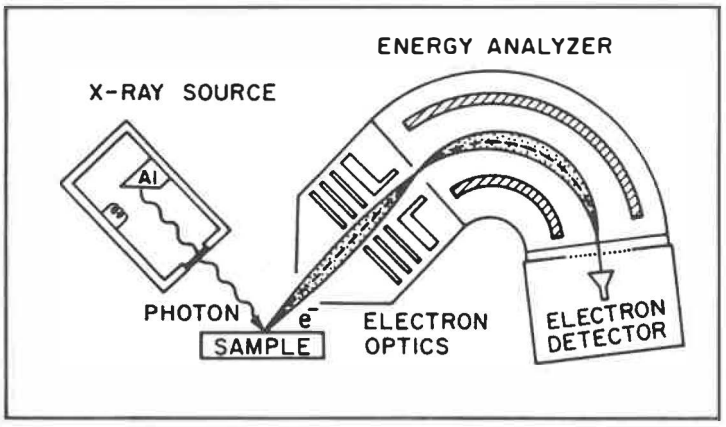

Figure 2.1 Schematic of the basic apparatus used in X-ray photoelectron spectroscopy. X-rays are produced at the Al or Mg anode by bombardment of electrons emitted by the filament. The X-rays impinge on a sample, producing photoelectrons which are detected by the electron energy analyzer.

The kinetic energy of a photoelectron excited from electronic level j in the sample by an incident X-ray photon of energy $\hbar\omega$ is given by the Einstein photoelectric equation [50]:

$$E_{kin} = \hbar\omega - E_B^F(j) - \Phi_s \qquad (2.1)$$

where E_{kin} is the electron kinetic energy at the sample surface, relative to the vacuum level, $E_B^F(j)$ is the binding energy of core level j referenced to the sample Fermi level, Φ_s is the sample work function. The energy level diagram for a conducting sample in an XPS measurement is illustrated in Fig.2.2. The sample is electrically connected with the

spectrometer, so that their Fermi levels are equal. In passing from the sample surface into the spectrometer, the photoelectron will feel a potential equal to the difference between the spectrometer work function Φ_{spec} and the sample work function Φ_s. Thus, the electron kinetic energy E_{kin} at the sample surface is measured as E_k inside the spectrometer, and they are related by :

$$E_k = E_{kin} - (\Phi_{spec} - \Phi_s) \qquad (2.2)$$

so that the binding energy $E_B^F(j)$ is related to the measured kinetic energy E_k through

$$E_B^F(j) = \hbar\omega - E_k - \Phi_{spec} \qquad (2.3)$$

Notice that the sample work function is no longer involved, but that of the spectrometer is.

Photoemission from a solid sample can be thought of as a three-step process [51] consisting of (1) photoexcitation of an electron, (2) its transport through the solid, which includes the possibility for inelastic scattering by the other electrons, and (3) the escape through the sample surface into vacuum. The XPS spectrum $I(E_k, \omega)$ is consequently a sum of a primary distribution of electrons $I_p(E_k, \omega)$ that have not suffered an inelastic collision, which can be described by equation (2.3) and a background of secondary electrons $I_s(E_k, \omega)$ due to electrons that have undergone one or more inelastic collisions [52]:

$$I(E_k, \omega) = I_p(E_k, \omega) + I_s(E_k, \omega) \qquad (2.4)$$

It is $I_p(E_k, \omega)$ that contains the chemical binding state information. Electron inelastic scattering is usually characterized by the electron escape depth, λ_e, (also called electron

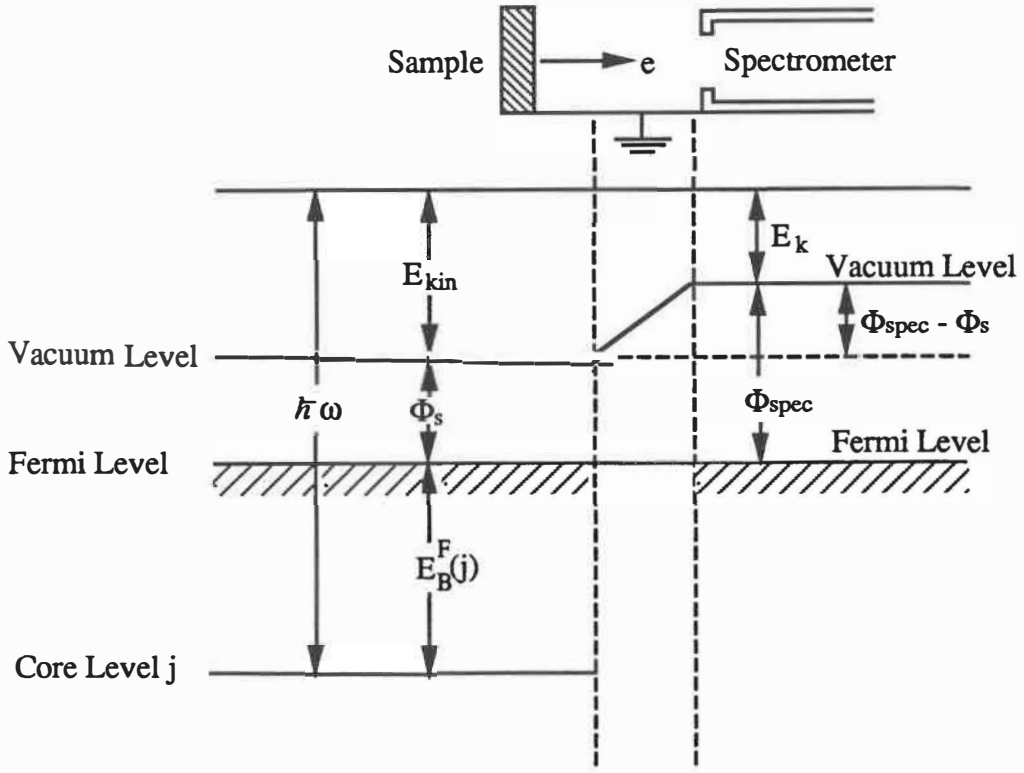

Figure 2.2 Schematic of the relevant energy levels for XPS binding energy measurements.

mean-free-path), which is defined so that an electron has a probability of e^{-1} of travelling adistance of λ_e before being inelastically scattered. The escape depth for electrons with kinetic energies between 5 and 1500 eV, which is the typical energy range interested in XPS, is between 4 and 20 Å [53] (as shown in Fig. 2.3). The short escape depths of photoelectrons effectively limit the sampling depth in XPS, so that XPS can be used to study surface properties. For the same reason, the experiments are very sensitive to surface cleanliness and contamination. Thus, reliable work usually requires ultra-high vacuum and proper surface cleaning procedures.

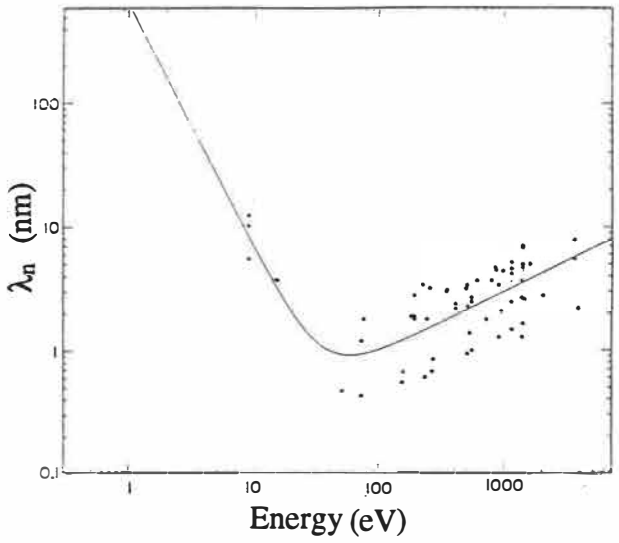

Figure 2.3 Escape depth of electrons in solids as a function of their energy. (From ref.[53]).

2.1.2 Quantitative Elemental Analysis

The numbers of core levels in a certain energy range and their binding energies are characteristic of each element. Adjacent elements throughout the periodic chart can easily be distinguished. For example, the binding energies of adjacent elements are shown in Fig. 2.4 for the 2S (L_1) lines of elements in the third period of the periodic table [54]. Thus, XPS is a straightforward technique for the identification of elemental species at the surface.

For quantitative surface analysis, it is important to note that the ionization cross section of a core level is practically independent of the valence state of the respective element, so that the intensity is proportional to the number of atoms in the detected volume. This is used to determine the relative concentration of the various constituents. The intensity of a core level j from element Z, I(j,Z), is related to the concentration C(Z) of this element by: [52]

$$I(j, Z) = F \cdot \sigma(j, Z, \omega) \cdot C(Z) \cdot T(E) \cdot D(E)\, A(E) \qquad (2.5)$$

where $\sigma(j, Z, \omega)$ is the photoelectron cross section of the core level j of element Z, T(E) is the transmission function related to the electron escape depth, D(E) is called the escape function which accounts for the potential step at the surface caused by the sample work function Φ, A (E) is the energy-dependent transmission function of the electron energy analyzer, and F is an energy-independent scale factor that takes photon intensity and geometrical factors into account.

It is useful and customary to introduce an atomic sensitivity factor, S(j, Z), through

$$S(j, Z) = F \cdot \sigma(j, Z, \omega) \cdot T(E) \cdot D(E) \cdot A(E) \qquad (2.6)$$

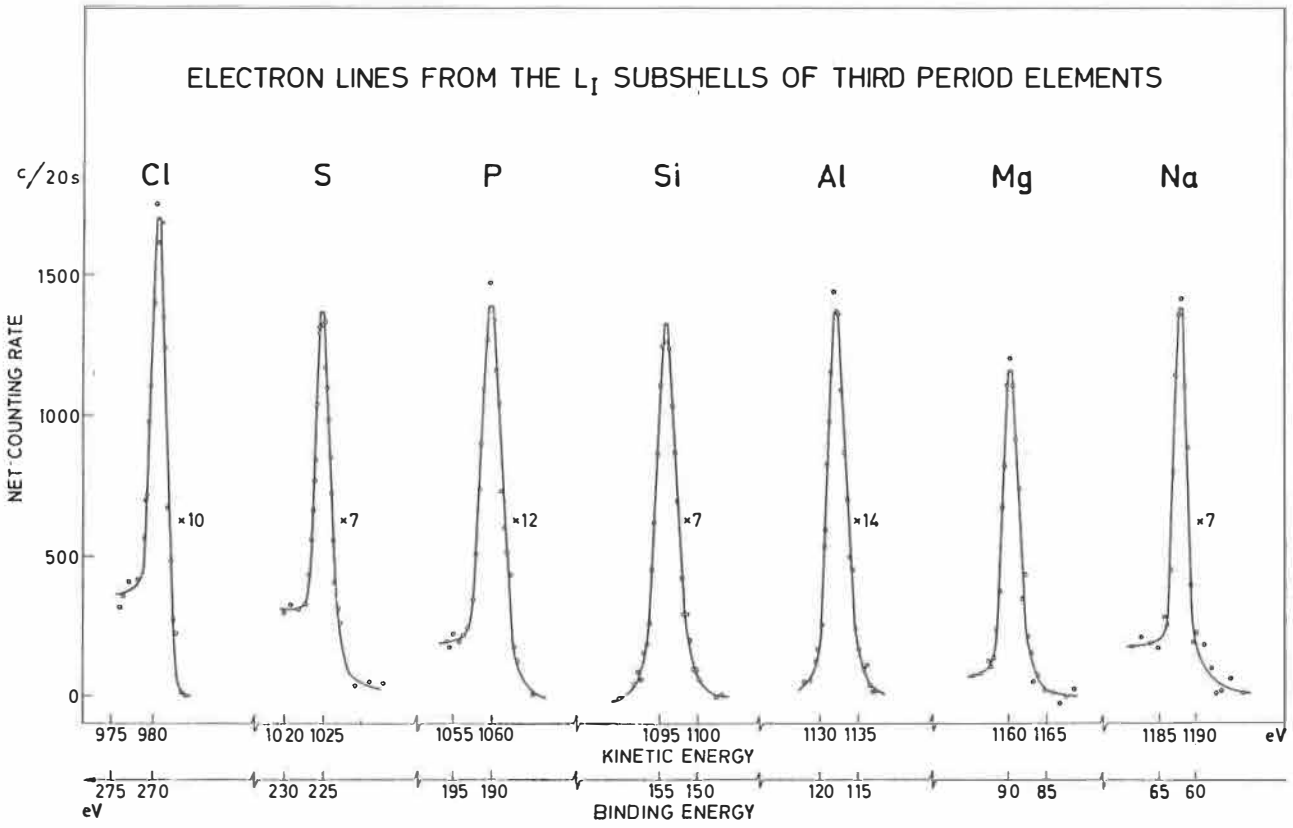

Figure 2.4 Electron lines from the 2S (L_1) subshells of the third period elements (sodium to chlorine) excited with Mg K_α radiation (From ref.[54]).

Obviously, S(j, Z) is the photoelectron intensity from pure element Z matrix. Thus a general expression for the determination of the atom fraction of any constituent in a sample, C (Z_A) can be written as [55, 56]:

$$C(Z_A) = \frac{I(j, Z_A) / S(j, Z_A)}{\sum_i I(j, Z_i) / S(j, Z_i)} \qquad (2.7)$$

S(j, Z) can be determined from standard known compounds, elemental foils, or from calculation [56]. S(j, Z) based on peak height or area can be found in relevant books[55, 57, 58].

2.1.3 Chemical Shift and Spin-orbit Splitting

The exact value of the core-level binding energy measured for a given element depends upon the chemical environment of that element. This effect is called "chemical shift", in analogy to NMR spectroscopy, and is invaluable for the chemistry of molecules, solids and surfaces, and provides a basis for identifying the chemical environment and valence electron state of a given element.

The physical basis for chemical shifts is explained by a so-called charge potential model [54], which describes the binding energy, E_i, of a particular core level, on atom i, in terms of an energy reference E_i^o, valence charge q_i on the atom i and the potential at atom i due to 'point charges' q_j on surrounding atom j:

$$E_i = E_i^0 + kq_i + \sum_{j \neq i} \frac{q_j}{r_{ij}} \qquad (2.8)$$

Where r_{ij} is the separation between atom i and j, and k is a proportionality constant. The physical picture underlying equation (2.8) is the following [57, 59]: the atom i is considered to be essentially a hollow sphere with radius r_v, on the surface of which the charge q_i of the valence electrons is distributed. The potential inside the sphere is q_i / r_v at all points. Neglecting relaxation effects, a change in the valence electron charge of Δq_i will change the potential inside the sphere by $\Delta q_i/r_v$. Thus the binding energy of all core levels will change by this amount, which is indeed often found, to a good approximation. If the last term in equation (2.8) is denoted by V_i, then the chemical shift of an atom between two valence states, (1) and (2), can be written as:

$$E_i(2) - E_i(1) = k\,[q_i(2) - q_i(1)] + [V_i(2) - V_i(1)] \qquad (2.9)$$

Where $E_i(x)$, and $q_i(x)$ (with x=1, 2) denote the binding energy, and the valence electron charge of atom i at valence state (x); and $V_i(x)$ is the electrostatic potential at atom i (due to the valence charges of surrounding atoms). The first term ($k\Delta q_i$) clearly ensures that an increase in binding energy accompanies a decrease in valence electron density on atom i. The last term in equation (2.9) should not be underestimated, since it has the opposite sign to Δq_i and tends to counterbalance the effect caused by the valence charge. More specifically, if q_i is modified by chemical bond formation, the charge is not displaced to infinity, but rather to the adjacent atoms. A more detailed discussion of chemical shifts can be found in ref.[60].

A good illustration of the chemical shifts as a function of the chemical environment or valence states is demonstrated in the spectrum of the carbon 1s levels in ethyl

trifluoroacetate ($C_4F_3O_2H_5$) (Fig. 2.5), recorded by Siegbahn and coworkers [61]. In this molecule, each carbon atom is in a different chemical environment and yields a slightly different XPS line. The binding energies cover a range of about 8 eV.

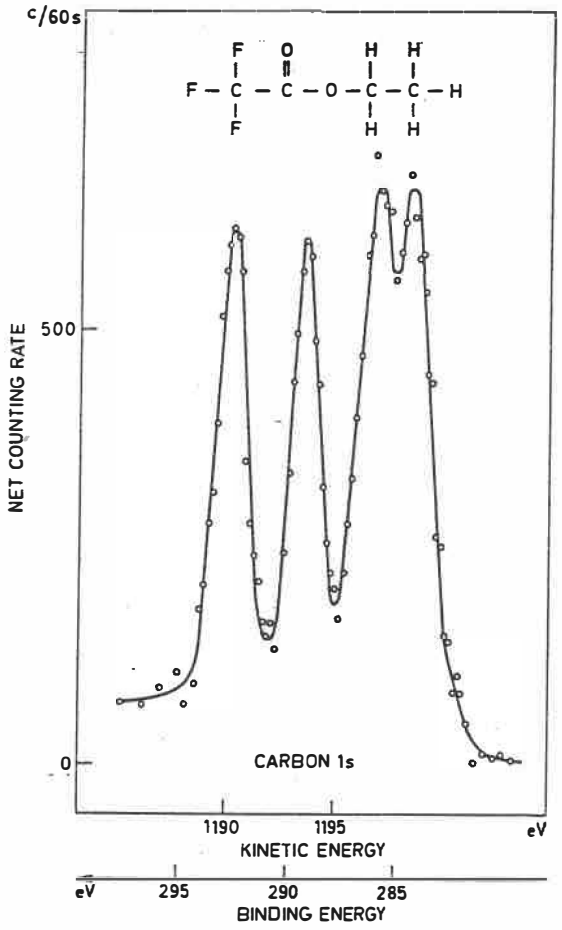

Figure 2.5 Carbon 1s chemical shifts in ethyl trifluoroacetate. The four carbon lines correspond to the four carbon atoms within the molecule (From ref.[61]).

Another important feature in XPS spectra is that non-s levels are doublets. The doublets arise through the fact that an electron is a charged particle, its orbit (with the characteristic quantum number l , l =0, 1, 2, 3, ...) around a nucleus induces a magnetic field, which will interact with the electron's inherent magnetic field produced by the spin (with spin quantum number s, $s=\pm 1/2$) [62, 63]. Under the j-j coupling scheme, the interaction energy E_j can be expressed as

$$E_j = \frac{1}{4m^2c^2}\left(\frac{1}{r}\cdot\frac{dU(r)}{dr}\right)\cdot\left[j\ (j+1) - l\ (l+1) - \frac{3}{4}\right] \qquad (2.10)$$

where m is the electron mass, c is the speed of light, r is the orbit radius, U(r) is the central force potential, and $j=l\pm 1/2$. Two possible states arise when $l > 0$. The spin-orbit splitting ΔE_j, the difference in energy of two states, reflects the "parallel" or "anti-parallel" nature of the spin and orbital angular momentum vectors of the remaining electron.

The spin-orbit splitting, ΔE_j, and relative intensity of the doublet peaks are important parameters in the curve-fitting of XPS spectra. The relative intensities of the doublet peaks are given by the ratios of their respective degeneracies ($2j+1$). The intensity ratios and designations (n, l, j) of spin-orbit doublets are given in Table 2.1.

Table 2.1 Spin-orbit splitting parameters

Subshell	j values	Area ratio
s	1/2	——
p	1/2, 3/2	1 : 2
d	3/2, 5/2	2 : 3
f	5/2, 7/2	3 : 4

2.1.4 Surface Band Bending Estimation with XPS

As discussed in 2.1.1, in XPS measurement, the binding energy reference is taken at the Fermi level, while in semiconductors E_F is free to move within the energy gap. Its position depends upon doping, and upon surface states. With E_F as the fixed reference energy, shifts in E_F are reflected in equal but opposite shifts of the binding energies of the whole photoelectron spectrum. Using the sharp core levels, such movements of E_F can be determined with considerable accuracy. The thickness of the depletion region caused by a band bending of 0.5 eV is estimated to be more than 1000 Å for moderately doped InP, whereas the sampling depth of XPS is less than 100 Å, so that the Fermi level measured by XPS is actually the surface Fermi level. Thus a chosen core level from a sample with upward (or downward) band bending will give a lower (or higher) binding energy than that from a sample at flat band condition as shown in Fig. 2.6. The difference between binding energies gives an estimation on the amount of band bending at surfaces. This binding energy difference should not be confused with "chemical shift" discussed in 2.13, and with the surface charging effect.

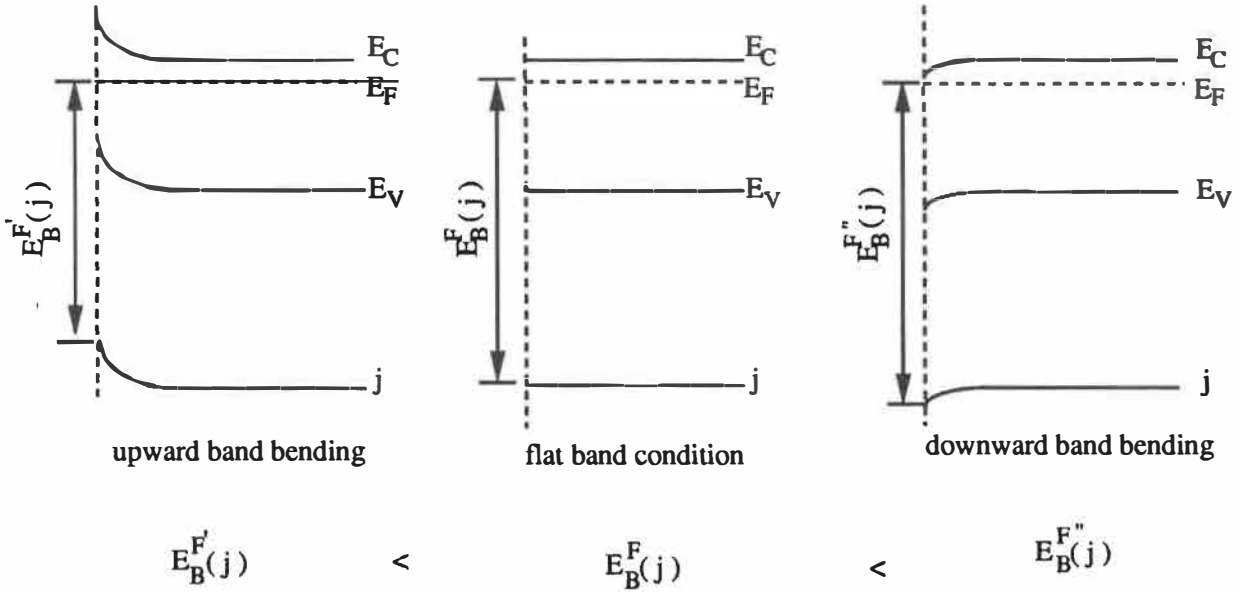

Figure 2.6 A schematic illustration of the relationship between the surface band bending and XPS measured core level binding energies.

2.2 Low Energy Electron Diffraction (LEED)

2.2.1 An Introduction to LEED

Low energy electron diffraction is quite similar in concept to the X-ray diffraction technique used to determine bulk crystal structure. A major difference, however, is the much smaller penetrating capability of electrons relative to X-rays (typical escape depths, λ_e, for the energy range used in LEED, are around 5 Å, as shown in Fig 2.3). As a result of this, all the elastic collisions that lead to diffraction take place in the one or two atomic layers closest to the surface. This makes LEED a highly surface sensitive technique.

A typical LEED configuration is illustrated in Fig.2.7 [57]. The system consists of an electron gun which produces the primary electron beam, three highly transparent hemispherical concentric grids, with the sample at the center of the sphere. The first grid is grounded, as are the sample and drift tube, so that scattered electrons are not deflected electrostatically in the field free region between the sample and the first grid. The second grid is at a negative potential, whose magnitude is slightly smaller that the primary electron energy, and which therefore repels the inelastically scattered electrons. The third grid is generally held at ground, and serves to cut off the inelastically scattered electrons by shielding the retarding (second) grid from the high potential of the phosphor screen. After passing through the second grid, the elastically scattered electrons are accelerated onto a concentric fluorescent screen by a positive potential of a few kilovolts. The screen will then exhibit "diffraction spots" at the position of the interference maxima.

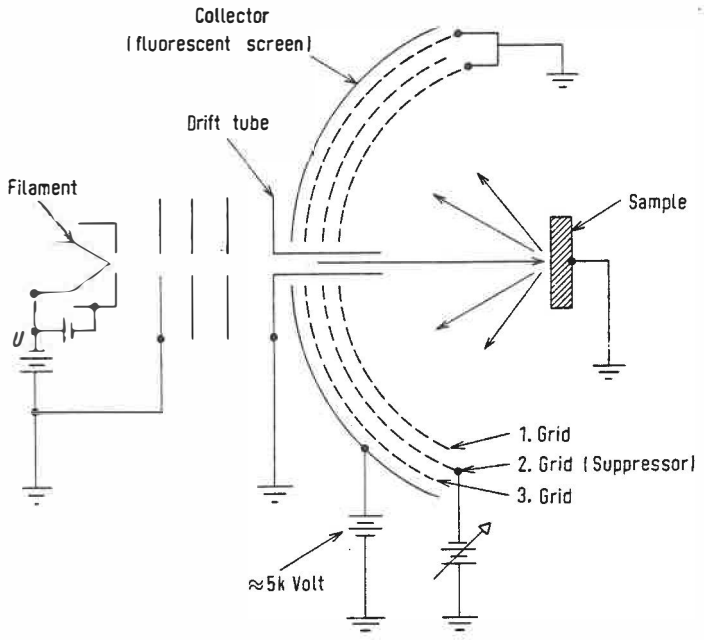

Figure 2.7 Schematic of a three-grid LEED apparatus.

2.2.2 Formation of Diffraction Pattern and Two-Dimensional Reciprocal Lattice

Due to very limited penetrating power of low energy electrons in solids, electron diffraction at a surface can be treated as the scattering of the incident electrons from a two-dimensional array of scattering sites. It will be convenient to characterize the electron diffraction in reciprocal space, as we usually do in three dimensional space. In three dimensions, the primitive translation vectors of the reciprocal lattice **a***, **b***, **c*** are related to those of the real lattice **a**, **b**, **c** by :[64]

$$\mathbf{a}^* = 2\pi \frac{\mathbf{b}\times\mathbf{c}}{V} \qquad \mathbf{b}^* = 2\pi \frac{\mathbf{c}\times\mathbf{a}}{V}$$

$$\mathbf{c}^* = 2\pi \frac{\mathbf{a}\times\mathbf{b}}{V} \qquad V = \mathbf{a}\cdot(\mathbf{b}\times\mathbf{c}) \tag{2.11}$$

The condition for constructive interference in the scattered waves is given by Bragg's law:

$$(\mathbf{k}' - \mathbf{k}) = \mathbf{g}_{hkl} = h\,\mathbf{a}^* + k\,\mathbf{b}^* + l\,\mathbf{c}^* \tag{2.12}$$

where **k** and **k'** are the incident and emerging wave vectors, respectively. The extension of this argument to two dimensions, with a unit cell defined by lattice vectors **a** and **b**, is simply to let $\mathbf{c} \rightarrow \infty$ in equation (2.10) so that :

$$\mathbf{a}^* = 2\pi \frac{\mathbf{b}\times\mathbf{n}}{A} \qquad \mathbf{b}^* = 2\pi \frac{\mathbf{n}\times\mathbf{a}}{A}$$

$$\mathbf{c}^* = 0 \qquad A = \mathbf{a}\cdot\mathbf{b}\times\mathbf{n} \tag{2.13}$$

where **n** is a unit vector normal to the surface. The unit translation along **c*** approaching zero means that the reciprocal lattice "points" along the surface normal are so close that they

form reciprocal lattice rods passing through every point of the two-dimensional reciprocal lattice. In two dimensions, only the component of the electron wave vector parallel to the surface is conserved with the addition of a reciprocal lattice vector, while the vertical component is not conserved in this process[65]. The energy conservation gives

$$\mathbf{k}_{\parallel}^{2} + \mathbf{k}_{\perp}^{2} = \mathbf{k}'^{2}_{\parallel} + \mathbf{k}'^{2}_{\perp} \tag{2.14}$$

where the suffixes, $\parallel$ and $\perp$, denote the parallel and the vertical components of the wave vectors relative to the surface. The conservation of momentum gives

$$\mathbf{k}'_{\parallel} = \mathbf{k}_{\parallel} + \mathbf{g}_{hk} \tag{2.15}$$

with

$$\mathbf{g}_{hk} = h\,\mathbf{a}^{*} + k\,\mathbf{b}^{*} \tag{2.16}$$

The diffraction condition, Eqs. (2.14)-(2.16), can be represented by the Ewald sphere construction shown in Fig 2.8. The construction, superimposed on the reciprocal lattice, involves drawing a vector $\mathbf{k}$ to terminate at a reciprocal lattice rod, taking this intersection point as the origin in the reciprocal space, then constructing a sphere with radius $|\mathbf{k}|$ about the beginning of the vector $\mathbf{k}$. The diffraction condition is satisfied for every beam that emerges in a direction along which the sphere intersects a reciprocal rod. As in three dimensions, the beams are indexed by the reciprocal lattice vector that produces the diffraction. In Fig.2.8, the angle between the incident electron beam and the surface normal is $(180-\theta_0)$, that between the scattered beam and surface normal is θ, so that equation (2.15) can be written as

$$k'\sin\theta = k\sin\theta_0 + |\mathbf{g}_{hk}| \tag{2.17}$$

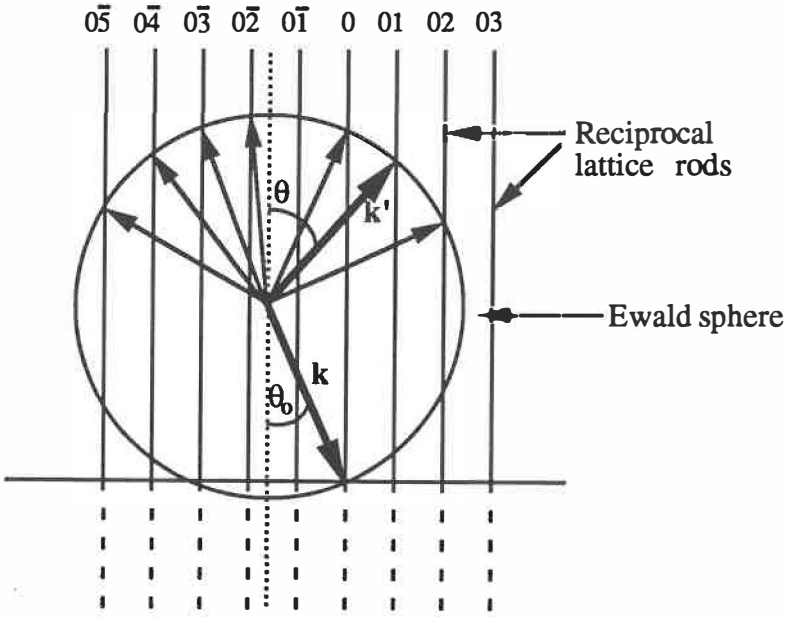

Figure 2.8 The Ewald construction for an electron beam incident to the surface. Seven backscattered beams are shown.

When the direction of the incident electron beam is perpendicular to the surface, equation (2.15) or (2.17) shows that a LEED pattern is an image of two-dimensional reciprocal lattice viewed from the surface normal. Thus, LEED studies can provide information about the periodicity of atoms of the surface and the overall symmetry of the surface. In general, changes in the periodicity or the symmetry of the surface will result in changes in the diffraction pattern which can be observed. It is important to recognize that a LEED pattern photograph can only provide information on the symmetry of the surface structure. In order

to make a unique determination of the atomic positions, it is necessary to resort to dynamical analysis: analysis of the curves of spot intensity *vs* incident electron energy. This analysis is both complicated and tedious because of the high probability of multiple scattering of the very low-energy electrons used. Detailed discussion of LEED and its application in surface studies can be found in refs.[57, 65, 66].

Surface structures are always described in terms of their relationship to the bulk structure beneath the surface. The substrate lattice parallel to the surface is taken as the reference network. A standard notation for surface structures is M(hkl)-(n×m)-C, where M is the chemical symbol for the materials whose surface is being studied, (hkl) indicates the particular crystalline plane to which the surface is parallel, and (n×m) shows that the new surface structure has a periodicity which is n times the original surface periodicity in the **a** direction and m times that in the **b** direction. C is the chemical symbol for the adsorbed material on the surface.

2.3 X-Ray Photoelectron Diffraction

X-ray photoelectron diffraction (XPD) experiment is performed by measuring the angular distribution of core-level photoelectron intensity in specific crystallographic planes from a solid sample. This new application of XPS extends the conventional field of chemical characterization to that of surface structural arrangement.

The phenomenon of photoelectron diffraction by a crystal lattice was first reported in 1970 by Seigbahn et al [67]. XPD has since been developed into a widely used technique in surface crystallography to study the orientation of adsorbed molecules [68], epitaxial growth morphology [69], and reconstruction due to chemisorption [70]. Detailed discussion of XPD can be found in a number of review articles [71-73].

XPD is based on the strong forward-scattering , or forward-focusing, which occurs when X-ray photoelectrons emitted by near-surface atoms are scattered by overlying lattice atoms. This scattering process produces enhanced intensity at polar and azimuthal angles corresponding to the directions connecting the emitting atom with overlying nearest and next-nearest neighbor atoms. Fig.2.9 presents a schematic illustration for describing XPD using a semi-classic model [74]. The photoelectrons originating from the emitter are deflected into the forward direction as they pass through the attractive Coulomb potential of a scatterer (overlying lattice atom). Due to the cylindrical symmetry around the emitter-scatterer axis, this amplitude scattered into the forward direction is all in phase [75] so that, by constructive interference, a strong gain in intensity in the forward direction is possible.

From both theoretical calculations and experiment [73, 76, 77], it has been shown that for photoelectrons with kinetic energies above several hundred electron volts, the forward scattering becomes dominant. Fig.2.10 illustrates schematically how forward scattering comes to dominate. There are many electron paths which can lead to a given

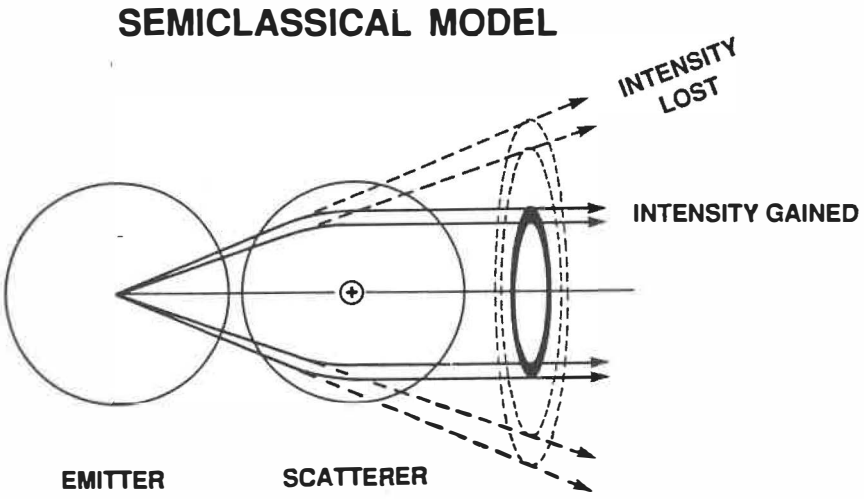

Figure 2.9 A schematic diagram illustrating how an attractive potential produces forward scattering or diffraction of an electron wave. The constructive interference, around the cylindrically symmetric axis, by the part of the wave scattered into the forward direction produces an enhanced intensity.

emission angle, such as those leading to 45^0, as illustrated in Fig.2.10. Viewed in terms of amplitudes added in the complex plane, forward scattering constitutes a vector of large magnitude at given phase angle, ϕ. Scattering by other, more complex path will generally contribute small vectors at random phase angles. The vectors are smaller since the cross section for large angle scattering is small above a few hundred volts. The phase angles tend to be random since the path-length differences are considerably larger than the electron wavelength and since the phase-shifts-on-scattering vary with scattering angle. Thus, the forward-scattering contribution to the sum of amplitude vectors can easily become the dominant contribution.

A single-scattering theoretical model [68, 76, 77] would predict a strongly enhanced emission intensity along the axis of the atomic row even if a number of scatterers are present in front of emitter. However, from both the multiple scattering model and experimental measurements [75, 78], it has been found that the intensity enhancement is strong only if a very limited number of atoms are in front of the emitter. If there are too many, the enhancement is suppressed. Thus, the strong forward-scattering in XPS emission tend to originate from the top few atomic layers (2~4 layers). Atoms deeper than the top few layers tend to make a rather isotropic contribution to the intensity. This makes XPD very surface sensitive.

Since core-level peaks are element specific, observation of the directions in which their intensity is enhanced constitutes a probe of short-range order around a particular element. As a corollary, photoelectrons emitted from the atoms in the top atomic layer do not exhibit such forward scattering enhancements. Consequently, this effect is an excellent indicator of whether or not an atom is at the top-most layer.

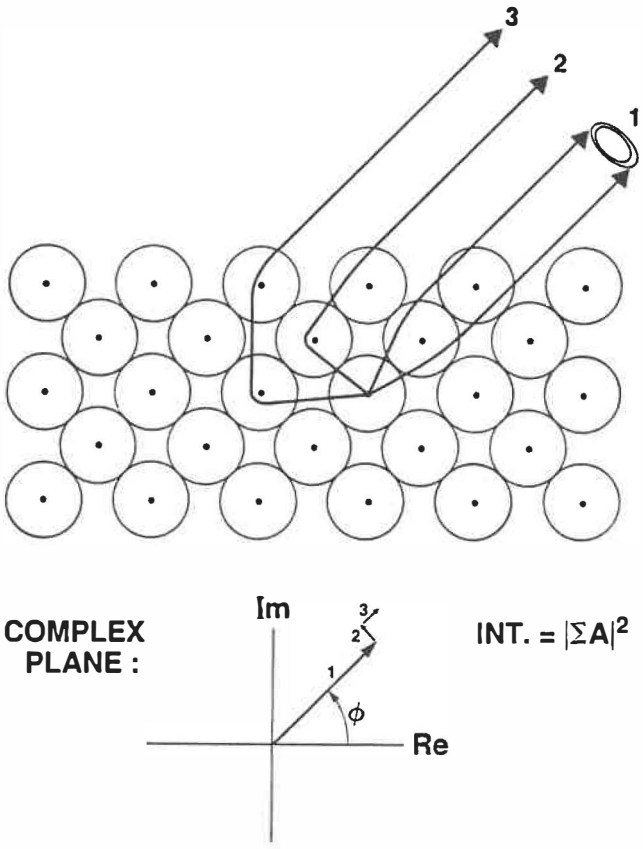

Figure 2.10 A schematic illustration of electron trajectories indicating why rows of atoms are particularly important in determining the angular anisotropy of emission. The cylindrical symmetry of the row yields a large amplitude at one phase angle, whereas other trajectories, usually involving larger scattering angles, contribute a small amplitude at a different phase angle.

2.4 Band Edge Photoluminescence Intensity Measurements

At thermal equilibrium, the distribution of electrons and holes in a semiconductor is determined by thermal excitation in intrinsic material, or by doping in extrinsic material. One of the ways to create an excess minority carrier distribution in a semiconductor is to irradiate the sample surface, using incident radiation with photon energy greater than the minimum energy gap.

After excess minority carriers are produced, in either the conduction or valence bands, they may decay by recombining with majority carriers, either radiatively or non-radiatively. Radiative recombination results in light emission (photoluminescence). Non-radiative recombination means recombination without emission of photons within a specified spectral range: the visible and near infrared [79]. The recombination processes can be further subdivided as follows:

Radiative:

1) band to band recombination (an electron from the conduction band with a hole in the valence band), and free exciton recombination (X).
2) impurity related bound exciton recombination, such as the recombination of neutral acceptor-bound exciton (A^0, X), neutral donor-bound exciton ((D^0, X), ionized donor-bound exciton (D^+, X), and ionized acceptor-bound exciton (A^-, X), etc.
3) band-impurity recombination, such as conduction band-acceptor (e-A^0), and

donor-valence band (D^0–h) recombination; and donor-acceptor pair recombination ($D^0 - A^0$).

3) Recombination via a recombination center.

Non-radiative:

1) Mutiphonon processes which may also involve recombination via defect levels.
2) Auger recombination: a three-carrier process which may be band-to-band or involve recombination centers.

A detailed theoretical description about these recombination processes may be found in ref.[80].

In addition to the bulk recombination mechanisms, excess minority carrier recombination at a semiconductor surface is usually enhanced by surface states. The surface recombination rate, R_s, can be described using Shockley-Read-Hall statistics [81]:

$$R_s = \sum_j N_{sj} \frac{\sigma_n^j \sigma_p^j v_n v_p (p_s n_s - n_i^2)}{\sigma_n^j v_n (n_s + n_s^j) + \sigma_p^j v_p (p_s + p_s^j)} \qquad (2.18)$$

Here N_{sj} is the density per unit area of surface states at an energy level j, σ_n^j (σ_p^j) is the capture cross section for electrons (holes) at surface state j, v_n (v_p) is the electron (hole) thermal velocity, n_s (p_s) is the surface density of electrons (holes), n_s^j and p_s^j are defined as

$$n_s^j = n_i \exp\left(\frac{E_s^j - E_i}{k_B T}\right), \qquad p_s^j = n_i \exp\left(\frac{E_i - E_s^j}{k_B T}\right) \qquad (2.19)$$

where E_i is the intrinsic Fermi level, and E_s^j is the energy level of the surface state j, n_i is the intrinsic carrier density at temperature T. It can be seen from equation (2.19) that the summation of n_s^j and p_s^j reaches a minimum when $E_s^j = E_i$, i.e. R_s becomes maximum. This means that the most effective surface recombination centers are those with energy levels at mid-gap. These processes can be either radiative or non-radiative. The radiative processes via surface states are expected to emit photons with energies far from the band edge energy. Different recombination processes are competitive. Thus, at a fixed excitation level, both radiative or non-radiative surface recombination processes will reduce the photo-luminescence intensity near the band edge. Therefore, a decrease in the density of surface states (especially those at mid-gap) at a semiconductor surface will result in an increase in its band edge photoluminescence intensity. This fact is used in the present work to compare the electronic properties of sulfur passivated InP samples with those of chemically etched ones, and has been used by many other groups [11, 20, 43, 82] to study the quality of semiconductor surfaces.

2.5 Schottky Barrier Diode I-V Characteristic Measurements

A rectifying metal-semiconductor interface is known as a Schottky diode after W. Schottky, who first proposed a model for barrier formation. Schottky diodes have a wide use in device applications. Because many of its important parameters, such as barrier height, reverse current, and ideality factor, strongly depend upon the surface (or interface) state density at the metal-semiconductor interface, it is quite often used to test metal-semiconductor interface properties. In this section, emphasis will be placed upon the basic physics of Schottky barriers and the concepts underlying the parameters used to characterize the electrical properties of such diodes. Detailed reviews of the theory of Schottky diodes may be found in Rhoderick [83], Rhoderick and Williams [84], Sze [85], Sharma and Gupta [86], and Mönch [87] .

2.5.1 Origins of Barrier Height

The earliest model put forward to explain the barrier height is that of Schottky [88] and Mott [89]. The energy diagrams in Fig.2.11 illustrate the process of barrier formation. According to Schottky-Mott theory, the amount of band bending is equal to the difference between the two vacuum levels, which is equal to the difference between the work functions of metal and semiconductor. This difference is given by $V_{do} = \phi_m - \phi_s$, where V_{do} is expressed in volts and is known as the built-in potential of the junction. V_{do} is the

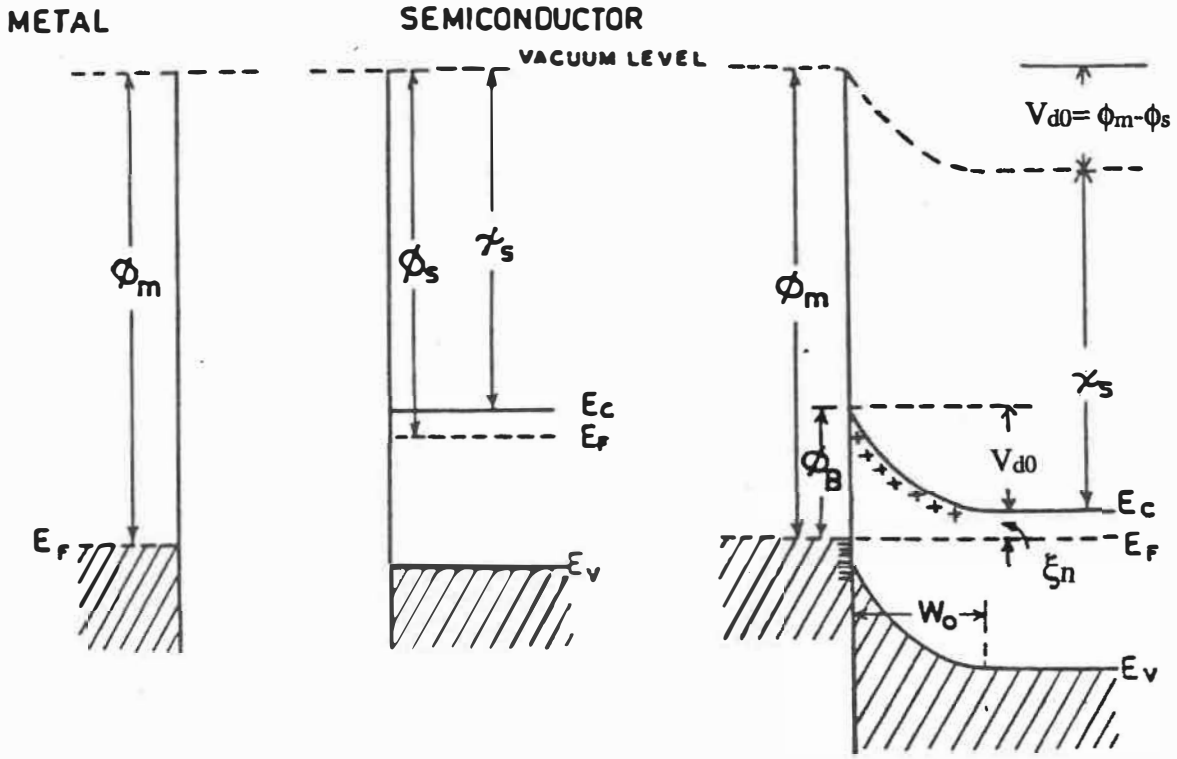

Figure 2.11 Energy level diagram of Schottky barrier formation according to Schottky-Mott theory.

potential barrier which an electron moving from the semiconductor into the metal has to overcome. However, the barrier for an electron from the metal is

$$\phi_B = \phi_m - \phi_s - \xi_n = (\phi_m - \chi_s) \qquad (2.20)$$

where ξ_n is the energy difference between the conduction and the Fermi level, χ_s is the electron affinity in the semiconductor. Equation (2.20) shows that the barrier height ϕ_B should increase linearly with the metal work function, ϕ_m. This ideal case is called the Schottky limit.

Experimentally, it is found that the barrier height is a less sensitive function of ϕ_m than that given in equation (2.20), and in some cases it is almost independent of the choice of metal. An explanation of this weak dependence on ϕ_m was put forward in 1947 by Bardeen [90], who pointed out the importance of localized surface states in determining the barrier height.

The dependence of barrier heights on the presence of surface states was first studied by Cowley and Sze [91] using a generalized Bardeen model. Suppose that the metal and semiconductor remain separated by a thin insulating layer as illustrated for a n-type semiconductor in Fig.2.12 and that there is a continuous distribution of surface states present at the semiconductor surface characterized by a neutral level ϕ_o which is defined as the energy level below which the surface states must be filled for the charge neutrality at a semiconductor surface. In the presence of surface states, the charge neutrality condition becomes $Q_m + Q_d + Q_s = 0$, where Q_m is the negative charge at the metal surface, Q_d is the

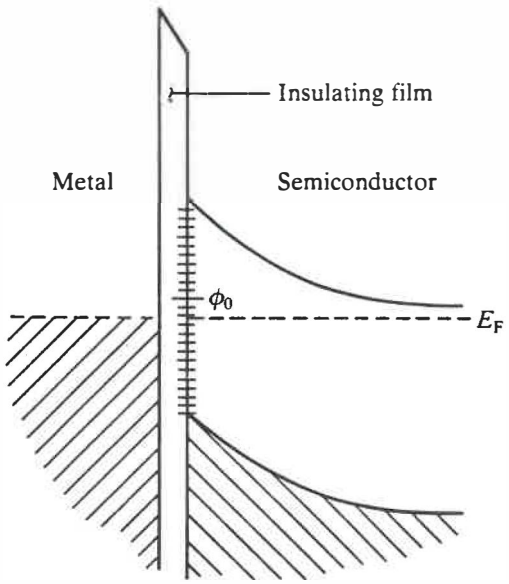

Figure 2.12 Energy level diagram of Schottky barrier formation according to Bardeen theory.

positive charge due to the uncompensated donor, Q_s is the charge in the surface states. According to the definition of the neutral level, the Q_s is given by:

$$Q_s = -qD_s [(E_g - \phi_0) - \phi_{Bn})] \tag{2.21}$$

where D_s is the density of surface states per unit area per eV, and ϕ_{Bn} is the barrier height.

Since Q_m and Q_s reside on opposite sides of the interface, an electric double layer exists at the interface. Its width, δ, is of atomic dimensions. In thermal equilibrium, the energy barrier of that double layer may be written as

$$\Delta = \phi_m - \chi_s - \phi_{Bn} \tag{2.22}$$

By neglecting the contribution from Q_d to the electric field in the interfacial layer (the approximation adopted in ref.[83,84,87,91]), Δ may be expressed as

$$\Delta = \frac{Q_s}{\varepsilon_i \varepsilon_0} \delta \tag{2.23}$$

Here, ε_i is the dielectric constant of the interfacial layer. By combining Eqs.(2.21-2.23) one obtains

$$(\phi_m - \chi_s) - \phi_{Bn} = -\alpha [(E_g - \phi_0) - \phi_{Bn}] \tag{2.24}$$

with

$$\alpha = \frac{q}{\varepsilon_i \varepsilon_0} D_s \delta \tag{2.25}$$

and ϕ_{Bn} can be written as

$$\phi_{Bn} = C(\phi_m - \chi_s) + (1 - C)(E_g - \phi_0) \tag{2.26}$$

with

$$C = \frac{\varepsilon_i \varepsilon_0}{\varepsilon_i \varepsilon_0 + qD_s \delta} \tag{2.27}$$

The Schottky limit, $\phi_{Bn} = (\phi_m - \chi_s)$, is obtained when $D_s=0$. While $D_s \rightarrow \infty$ the barrier height becomes independent of the metal work function and is expressed by

$$\phi_{Bn} = (E_g - \phi_0) \tag{2.28}$$

In this case the Fermi level is said to be "pinned" by surface states, and equation (2.28) is called the Bardeen limit.

The departure of the measured barrier height from that predicted by equation (2.20) and its dependence on metal work functions may be used as an indicator to estimate the surface (or interface) state density on the samples [22, 26, 92, 93].

2.5.2 Current Transport

Once the barrier has formed, the current-voltage characteristics of a metal-semiconductor contact are governed by the transport of the charge carriers (electrons or holes) across the metal-semiconductor interface and its associated space-charge region. There are four different mechanisms by which the carrier transport can occur: (a) thermionic emission over the barrier, (b) quantum-mechanical tunneling through the barrier, (c) carrier recombination in the depletion region, and (d) carrier recombination in the neutral region of the semiconductor, which is equivalent to minority carrier injection. Fig.2.12 schematically shows these processes for a forward biased Schottky barrier on a n-

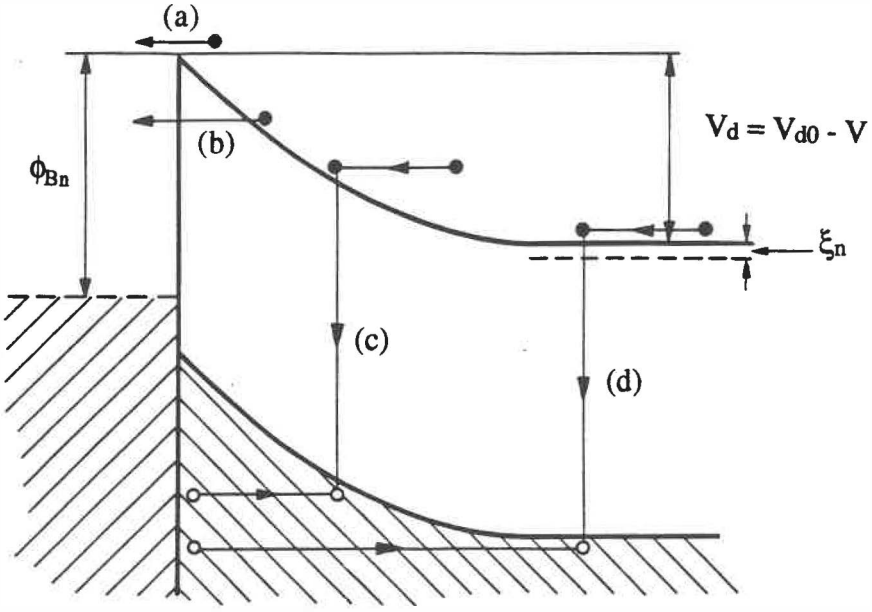

Figure 2.13 Transport processes in a forward-biased Schottky diode.

type semiconductor. The inverse processes occur under reverse bias.

In a diode, if process (a) is the dominant mechanism, such a diode is generally referred to as "nearly ideal" and its current-voltage relationship can be described by Bethe's thermionic-emission theory [94]. A detailed description about this theory is given in Sze [85]. In this theory, the current is assumed to be controlled only by the transfer of carriers across the top of the barrier, and the drift and diffusion that occur as a result of collisions within the space charge region are assumed unimportant. The resulting current density, J, for an applied bias voltage,V (measured positive with respect to the n-type semiconductor), is given by:

$$J = J_0[\, e^{qV/k_BT} - 1\,] \tag{2.29}$$

with

$$J_0 = A^* T^2 e^{-q\phi_B/k_BT} \tag{2.30}$$

where A* is the effective Richardson's constant, k_B is the Boltzman's constant, and T is the measuring temperature.

There are other factors which may affect the current-voltage characteristics, such as [84, 95]:

1) the bias dependence of the barrier height due to the image force and the existence of a interfacial layer will give a current density in the form of:

$$J \propto e^{\frac{qV}{k_BT}(1-\frac{\partial\phi_B}{\partial V})} \tag{2.31}$$

where $\frac{\partial\phi_B}{\partial V}$ represents the bias dependence of barrier height.

2) carrier recombination via localized defect centers will give a recombination current component , J_r, in the form of:

$$J_r \propto e^{qV/2k_BT} \tag{2.32}$$

So, a wide variety of practical metal-semiconductor diodes follow the I-V relationship of the form[84, 95]:

$$J = J_0 e^{qV/nk_BT}[\,1 - e^{-qV/k_BT}] \tag{2.33}$$

where n is often called the "ideality factor". For an ideal Schottky barrier where ϕ_B is independent of the bias and current flows only due to thermionic emission, n=1. The existence of an interfacial layer, image force, carrier recombination, or carrier tunneling through the barrier will make n larger than unity. Therefore, the "ideality factor" is frequently used as the criterion of diode quality. Detailed discussion of the possible factors which may affect the diode I-V behavior may be found in ref.[83, 84, 95].

Chapter 3

Experimental Conditions and Passivation Procedure

3.1 XPS Measurements and Reference Samples

3.1.1 XPS Spectrometers

A VG ESCALAB 3 MKII (illustrated in Fig.3.1), and a PHI-5500 XPS spectrometer were used for surface chemical and structural analysis. The VG XPS spectrometer is equipped with a non-monochromatic twin-anode X-ray source, which is switchable between Al K_α ($\hbar\omega$ =1486.6 eV), and Mg K_α ($\hbar\omega$ =1253.6 eV). Concentric hemispheric analyzers (CHA) are used on both XPS spectrometers to detect the kinetic energy of photoelectrons. When using Mg K_α source and at a pass energy of 20 eV, the energy resolution of the VG XPS spectrometer is about 1.1 eV, as measured by the full-width at half maximum (FWHF) of the Au $4f_{7/2}$ peak. The PHI-5500 XPS spectrometer is equipped with a monochromatic Al K_α source. At a pass energy of 5 eV, the instrument has a resolution about 0.6 eV, as measured by the FWHM of the Au $4f_{7/2}$ peak. The Au $4f_{7/2}$ peak at 83. 8 eV was also taken as the energy reference.

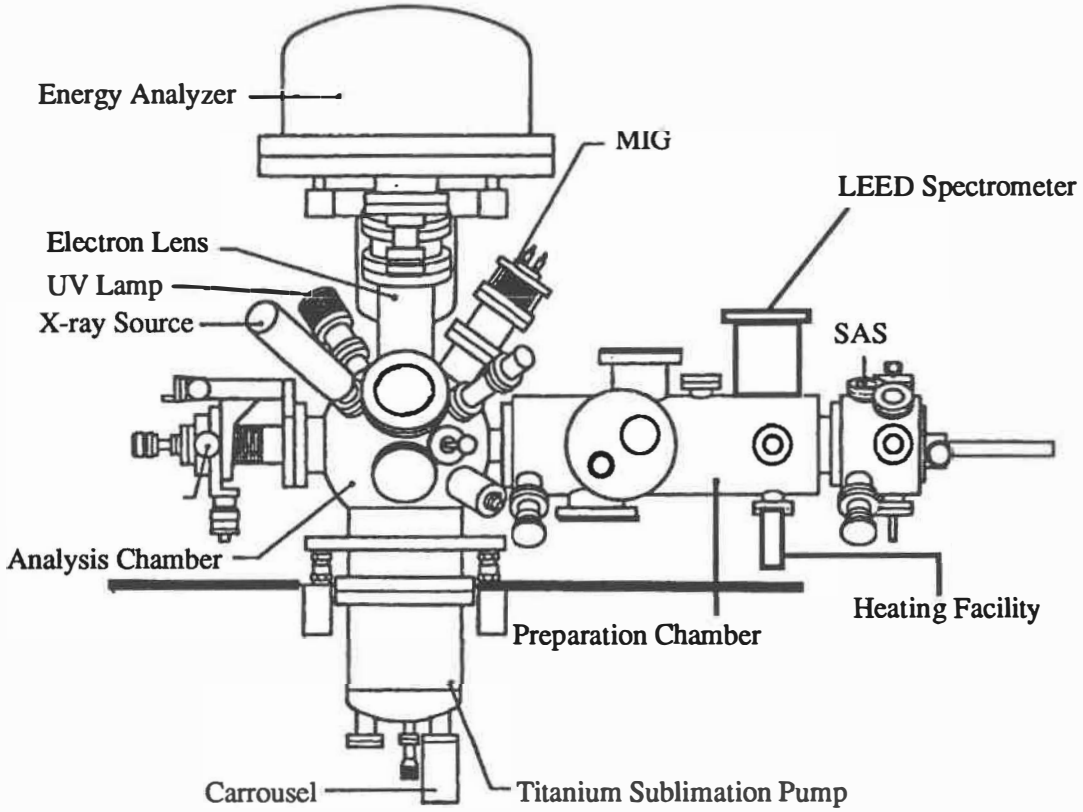

Figure 3.1 A schematic illustration of a VG ESCALAB 3MKII.

3.1.2 Standard Samples for Data Analysis

Although an extensive list of chemical shifts for various binding states of many elements can been found in several books (e.g. ref[55]) or some reference papers, little information is available concerning the full width at half maximum (FWHM) of these photoelectron peaks, since this quantity depends upon both the chemical status and the energy resolution of the spectrometer. But it is an important parameter in data analysis. Therefore when using chemical shifts of core levels as a fingerprint technique to identify the chemical binding state of an element, it is very important to get proper standard samples.

An in-situ UHV cleaved InP(011) surface is free of surface oxide and contamination. Some of the in-situ UHV cleaved InP(011) surfaces in our experiments have mirror-like finish. The low energy electron diffraction pattern from such a surface shows a (1x1) structure confirming a surface unit mesh of the same symmetry as that of the bulk structure in the (011) plane (Fig.3.2). This means that such a cleaved InP(011) surface is nearly undamaged. Due to UHV condition (about 10^{-10} mbar) and short time interval between cleaving sample and measuing XPS spectra (about 4 min.), the cleaved InP(011) surface is free of oxidation and contamination. The photoelectron spectra from this surface will show the feature of indium-phosphorous bonding, so it is an ideal standard sample for InP. High resolution core level spectra of In $3d_{5/2}$ and P 2p from a UHV cleaved n-type InP(011) surface are shown in Fig.3.3.The curve fitting parameters are listed in Table 3.1.

As discussed in §2.1, when taking the Fermi level as the energy reference, the binding energy of a core level depends upon the bulk doping and surface potential. But the

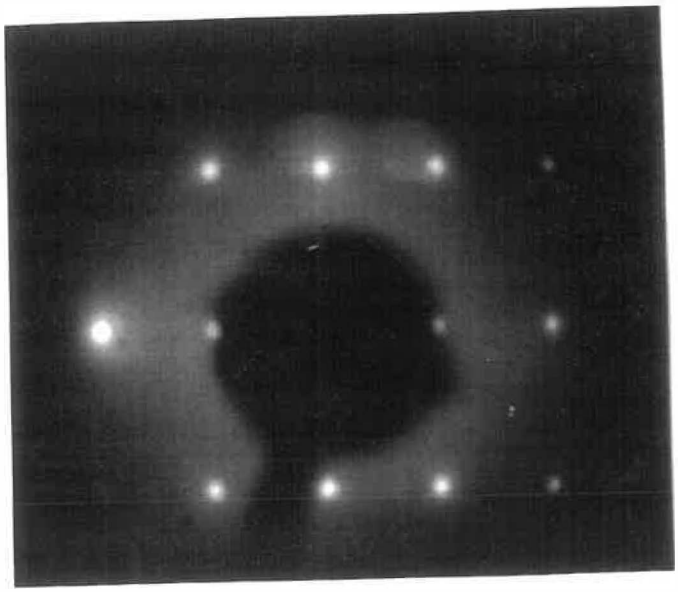

Figure 3.2 A typical (1x1) LEED pattern from in-situ UHV cleaved InP(011) surfaces.

Table 3.1 Curve Fitting Parameters for Vacuum-Cleaved InP(011)

	E_B (eV)	FWHM	ΔE_{spin}	doublet area ratio
In $3d_{5/2}$	444.55±0.01	0.73		
P 2p	128.88±0.01	0.61	0.86	1 : 2
$\Delta E = E_B(\text{In } 3d_{5/2}) - E_B(\text{P } 2p)$		=315.67 eV		

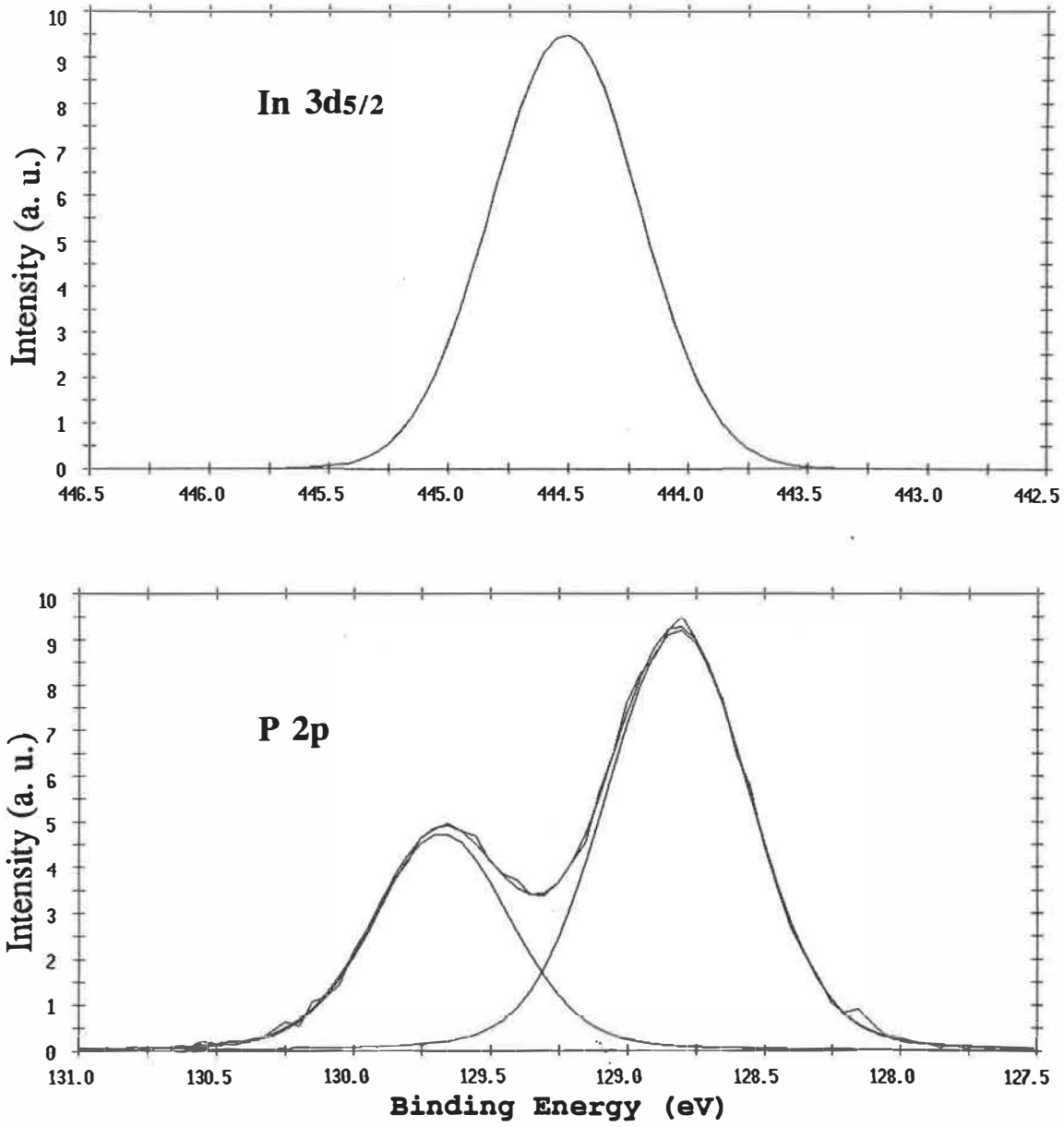

Figure 3.3 High resolution core level spectra of In $3d_{5/2}$ and P 2p from a UHV cleaved InP(011) surface.

energy difference between the core levels measured from a sample, such as the binding energy difference between the In $3d_{5/2}$ and P 2p for InP, is independent of these parameters. Thus, the curve fitting parameters for p-type InP are the exactly the same as those for n-type InP, as listed in Table 3.1, except that there is an energy shift towards lower binding energy for both the In and P peaks. This energy shift is equal to the amount of surface Fermi level movement towards the valence band maximum.

In order to analyze the In-S bonding on the sulfur passivated InP(100) surfaces, a proper standard sample should be chosen. There are two possible In-S compounds: InS or In_2S_3. However, from the experimental results presented in the next chapter, it has been found that the binding energy of the In-S component shifts to a more oxidized chemical state as compared with the InP bulk component. This means that indium bonded to S is more positive than in InP, therefore the indium should not be in the chemical state In^{+2}. Thus, a 99.999% pure In_2S_3 powder sample pressed onto a clean gold foil was measured and taken as a tentative standard sample. The spectra from this sample showed no oxidized sulfur peak, and the In $3d_{5/2}$ peak was very symmetric, and could be curve fitted using a single Gausian. Therefore, the In_2S_3 sample was assumed to be free of oxide. The high resolution spectra of In $3d_{5/2}$ and S 2p from pure In_2S_3 compound are shown in Fig.3.4, and the related curve fitting parameters are listed in Table 3.2.

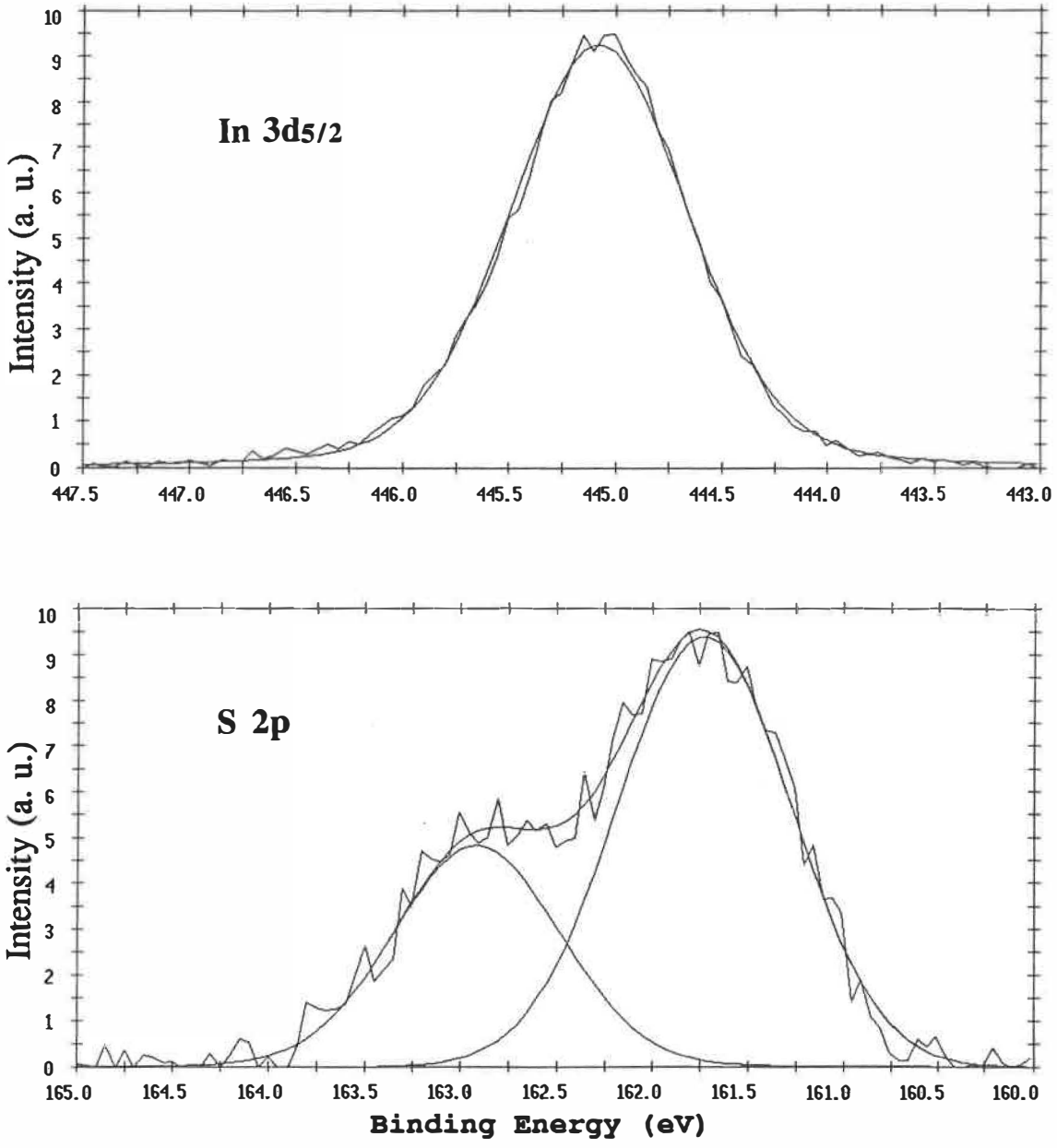

Figure 3.4 High resolution core level spectra of In 3d $_{5/2}$ and S 2p from a 99.999% pure In_2S_3 powder standard sample.

Table 3.2 Curve Fitting Parameters for In_2S_3 Standard Sample

	E_B (eV)	FWHM	ΔE_{spin}	doublet area ratio
In $3d_{5/2}$	445.00±0.01	0.99		
S 2p	161.71±0.01	1.10	1.19	1 : 2
$\Delta E = E_B(In\ 3d_{5/2}) - E_B(S\ 2p)$ = 283.29 eV				

3.1.3 Energy Reference for Surface Fermi Level Measurements

A set of P 2p spectra from in-situ UHV cleaved n-type and p-type InP(011) surfaces were used to establish an energy reference for surface Fermi level measurement. The n-type InP (011) samples (S-doped, carrier density ~10^{16}, and 10^{18} cm^{-3} respectively) gave the highest binding energy for P $2p_{3/2}$, at 128.9 eV. The p-InP sample (Zn-doped, carrier density ~ 10^{18} cm^{-3}) gave the lowest binding energy of P $2p_{3/2}$ at 127.6 eV. Since the difference between the measured binding energy of P $2p_{3/2}$ from the n-InP samples and that from the p-InP samples is about 1.3 eV, which is close to the value of band gap of InP (E_g=1.35 eV), this indicates that these UHV cleaved n-InP(011) and p-InP(011) samples

are nearly at flat band. Therefore, an InP sample with its surface Fermi level at VBM will give a P $2p_{3/2}$ peak close to 127.6 eV, and one with its surface Fermi level at CBM will give a P $2p_{3/2}$ peak close to 128.9 eV. This energy range agrees very well with that obtained by Lau et al [35].

However, some n-InP(011) samples had P $2p_{3/2}$ peaks at 128.7 ± 0.1 eV, and some p-type InP samples (Zn-doped, carrier density ~10^{16}, and 10^{18} cm^{-3} respectively) had P $2p_{3/2}$ peaks at 128.0 ± 0.1 eV. This means that the Fermi levels of these n-InP surfaces were pinned about 0.2 eV below the CBM, and those of the p-InP surfaces were pinned about 0.4 eV above the VBM. This phenomenon was also observed by Spicer et al [3]. It has been shown that high-quality clean cleaved InP(011) samples have no surface states in the band gap, and show no surface band bending [96, 97]. The surface band bending observed on these samples may be caused by extrinsic surface states, due to the poor cleavage of the surfaces.

3.2 LEED and XPD Measurements

3.2.1 Experimental Set-up

Low energy electron diffraction experiments were used to study the surface structure of sulphur passivated InP surface and carried out in the preparation chamber of the VG system, with a VG-640 LEED spectrometer. The incident electron energies can be adjusted in the range of 0 to 1000 eV.

X-ray photoelectron diffraction measurements were used to determine whether or not the sulfur on InP is limited to the topmost layer. The XPD data on polar angle dependence were measured in the VG system. Since there is no azimuthal tilting system on the VG, the XPD data on azimuthal angle dependence were obtained on the PHI-5500 system. The tilting accuracy for the VG system is ±5 degrees for the polar angle, and that for the PHI-5500 system is ±2 degrees for both polar and azimuthal angles.

3.2.2 Reference Sample for LEED Experiments

In the LEED experiment, the incident electron beam was perpendicular to the sample surface. The diffraction patterns were recorded on film with a Minolta X-700 camera. For a LEED pattern taken with incident electron wave length of λ, the distance measured on the film between the diffraction spot and the central spot, x, is related to the diffraction angle θ by (as shown in Fig.3.5):

$$\frac{x}{\beta} = R \sin\theta \qquad (3.1)$$

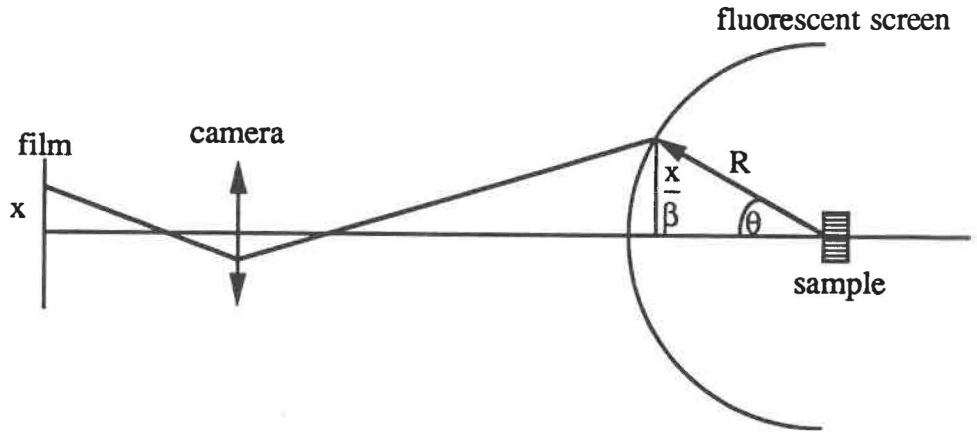

Figure 3.5 A schematic illustration of the geometric parameters involved in LEED experiment.

where R is the radius of the fluorescent screen, β is the magnification coefficient of the camera. θ and λ are related to the two-dimension lattice spacing, d_{hk} (or $1/g_{hk}$) by equation (2.17). There are two ways to calculate diffraction angles. One is to get the angle from a purely geometric calculation. Another way is to use a reference sample. The latter is both simple and accurate. An as-cleaved muscovite mica was used in our experiment. The muscovite mica has a pseudo-hexagonal structure, with a = 5.2 Å [98]. The cleaved (0001) surface is stable and unreconstructed. The interplane distance along the $[10\bar{1}0]$ direction is do = 4.6 Å. One can take a LEED pattern of the mica (0001) surface with incident electron

wave length λ_0 at the same distance from the screen as that for the InP measurement. The distance between the central spot and the first order diffraction spot is measured as x_0. Therefore by using Eqs.(2.17) and (3.1), the quantity $R\beta$ in equation (3.1) can be expressed as $x_0 d_0/\lambda_0$. Thus, it becomes straightforward to calculate the diffraction angles and to index the LEED patterns from the InP surface. The diffraction angle and the corresponding distance between the two dimensional lattice line are related to x and λ by:

$$\sin\theta = x\frac{\lambda_0}{x_0 d_0}, \qquad d = \frac{\lambda}{x}\frac{x_0 d_0}{\lambda_0} \tag{3.2}$$

Equation (3.2) was used in this work to index the LEED patterns.

3.3 Surface Electronic Property Measurements

Band edge photoluminescence intensity and Schottky barrier diode current-voltage characteristic measurements were used to compare the surface electronic properties of sulfur passivated InP(100) samples with those of chemically etched ones.

The photoluminescence was excited using the 5145 Å line of an Ar^+ laser. The signal was dispersed by a 1m double spectrometer and detected by a cooled InGaAs photomultiplier tube. The samples were mounted in a continuous flow liquid helium cryostat for low temperature measurements. The excitation level was kept at 200 mW/cm^2 for n-type InP, and 150 mW/cm^2 for p-type InP.

For Schottky barrier diode current-voltage(I-V) characteristic measurements, ohmic back contacts on n-type InP were prepared by evaporating 100 Å Au / 500 Å AuGe/ 1500 Å Au in an electron beam evaporator at a pressure better than $2x10^{-6}$ mbar, and ohmic contacts on p-type InP were realized by evaporating 50 Å Au/ 500 Å Zn/ 1500 Å Au in an evaporator at a pressure better than 10^{-5} mbar. All the samples were alloyed using rapid thermal annealing at 350^0C in H_2/N_2 forming gas for 3 min. After surface treatment, the samples were annealed at 300^0C for 30 min in the preparation chamber of the VG system at a pressure about 10^{-9} mbar to eliminate the water vapor resulting from solution treatment. Since the $(NH_4)_2S$ passivating solution attacks the photoresist, a lift-off technique cannot be used. The Schottky contacts (1000 Å gold or 1000 Å aluminum) were deposited in the

preparation chamber of the VG system by an electron beam evaporator at pressure better than $1x10^{-8}$ mbar. Then the diode pattern was defined using conventional photolithography techniques as shown in Fig.3.6. The gold film was etched off using KI/ I_2 solution (4g KI + 1g I_2 in 40 ml H_2O) [85], and the aluminum film was etched off using H_3PO_4 : HNO_3 : H_2O (80 : 5 : 15). The dimensions of diodes are either 200 μm x 200 μm, or 100 μm x 100 μm.

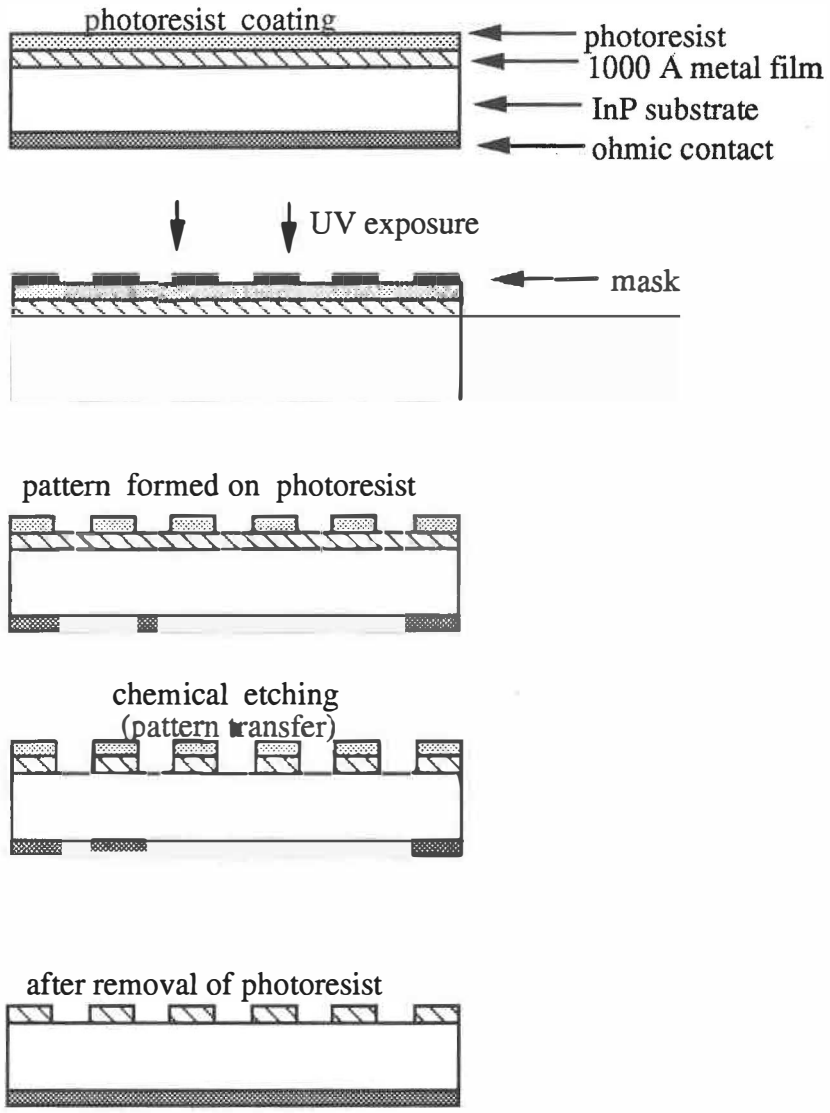

Figure 3.6 A schematic illustration of the pattern transfer in Schottky diode fabrication.

3.4 Passivation Procedure for InP(100) Surfaces

As discussed in the first chapter, a detailed surface study including chemical and structural analysis, is of critical importance for a better understanding of sulfur passivation on InP. Obviously, these investigations should be carried out on well passivated, reproducible, and representative surfaces. Therefore, a good surface passivation procedure becomes a key point in the problem. In the following, we shall discuss and compare two different passivation procedures.

3.4.1 Chemical Etching of InP(100) Surfaces

Most of the InP(100) wafers used in this experiment were supplied by Crystacomm. The n-type InP wafer is sulfur doped (carrier density $\approx 4.7 \times 10^{16}\,cm^{-3}$), and the p-type InP wafer is zinc doped (carrier density $\approx 6.8 \times 10^{16}\,cm^{-3}$). The as-received InP(100) wafers (both n- and p-type) were heavily oxidized, due to long air exposure. From XPS measurements, the oxidized indium components were typically displaced from those of InP by 1.0 ± 0.2 eV towards higher binding energy, and those of phosphorous were displaced by 4.5 ± 0.2 eV. These chemical shifts are not consistent with In_2O_3 or P_2O_5, but are more consistent with $InPO_4$ [99, 100].

Before chemical etching, all the samples were degreased in hot ($\approx 45\,C^0$) trichloroethylene, acetone, and propanol, 5 minutes for each step. Then, the samples were rinsed in 18 MΩ DI water for about 2 min. After that, the samples were chemically etched in 10% HCl at room temperature for 5 min, and then rinsed in DI water. The chemical

etching step apparently removes most of the native oxide, but the InP surface is still covered with a thin $InPO_4$ layer, which is probably the results of oxide regrowth upon exposure to air, rather than the survivor of chemical etching [101]. The oxide regrowth is so rapid that no LEED pattern can be obtained on these surfaces, even immediately after the chemical etching.

3.4.2 A Commonly Used Passivation Procedure

The $(NH_4)_2S$ solution used in this work was supplied by Johnson Matthey Ltd, the concentration is 20 ~ 24% wt. Initially, we tried a passivation procedure similar to that developed by Iyer et al [24]. The InP(100) samples were immersed in a stirred and heated $(NH_4)_2S$ solution (at ~ 65^0C) for about 15 min. Upon removal from the sulfide solution, the samples were directly blown dry by N_2 gas. This step is commonly used by many groups in their sulfur passivation procedure [22, 24, 26, 34, 38, 42]. The InP(100) surfaces treated by this procedure were covered by a clearly visible crust. After the sample was in a UHV chamber for about 20 min, the crust visually disappeared, but it did not completely sublime. No LEED pattern could be obtained on these surfaces. The surface was covered by oxidized sulfur and polysulfide, as well as by sulfur bonded to indium. The surface chemical composition was not reproducible. Fig.3.7(a) and (b) show the S 2p spectra from two samples treated by the same procedure described above. It is obvious that the relative ratio between the three sulfur species is quite different for the two samples. The existence of the residue and its variation among different samples not only keep us from obtaining reliable surface chemical information, but also cause strong surface band bending on S-passivated InP surfaces, as will be discussed in next chapter. It is difficult to perform

systematic studies on such surfaces.

3.4.3 An Improved Passivation Procedure

A DI water rinse is the best known and widely used cleaning procedure in surface preparation. In order to remove residual materials from sulfide treated surfaces using DI water and to avoid possible surface oxidation in water, we must increase the surface coverage of the sulfur species which forms chemical bonding with surface atoms, in order to obtain a completely sulfur terminated InP surface. We believe that once a surface is truly passivated, the passivation effects should not be eliminated by a DI water rinse.

We have combined different steps which were already used separately by others, in order to obtain a procedure for InP which will completely passivate the surface. In this procedure, as described in [102], chemically etched InP(100) samples were put into an $(NH_4)_2S$ solution at 60~65^{0}C for 15 min under 200W tungsten light illumination as used by Vaya and collaborators for GaAs in Na_2S solution [103]. The heating and the illumination were used to promote the sulfur passivation. The samples were then thoroughly rinsed in DI water for about 10 min to remove the residual materials and other possible contamination, and then blown dry with N_2 gas.

In our experiment, lamp-to-sample distance was kept at about 10 cm, the power density at the sample surface was estimated between 200~300 mW/cm^2. The temperature of the tungsten filament is usually around 2000 K, so the main part of the spectrum should be in the infrared. The effect of light illumination will be discussed in more detail in §4.1.4 and §5.

We believe that the sulfur passivation effects on InP are based entirely on the S

which forms chemical bonds with InP substrate. Oxidized sulfur and polysulfide on these surfaces would not do any good to the passivation effects, so that they should be removed from the passivated surfaces.

Fig.3.7(c) shows the S 2p spectrum from a so treated InP(100) surface. Neither oxidized sulfur nor polysulfide were observed. Only one kind of sulfur, which forms a chemical bond with surface indium atoms, was detected. The margin of detection error was estimated better than 10%. No detectable indium or phosphorous related oxide was found on these surfaces, nor was there any P-S bonding. The surface chemical composition is quite reproducible.

Clear and distinct LEED patterns can be obtained from InP(100) surfaces treated in this way. They are still visible after 3 ~ 4 days exposure to the atmosphere, compared with the immediate oxidation of the chemically etched surface upon exposure to the air. These results indicate that the InP(100) surfaces treated by this procedure have been chemically passivated, with very low surface contamination, and are quite inert to air exposure.

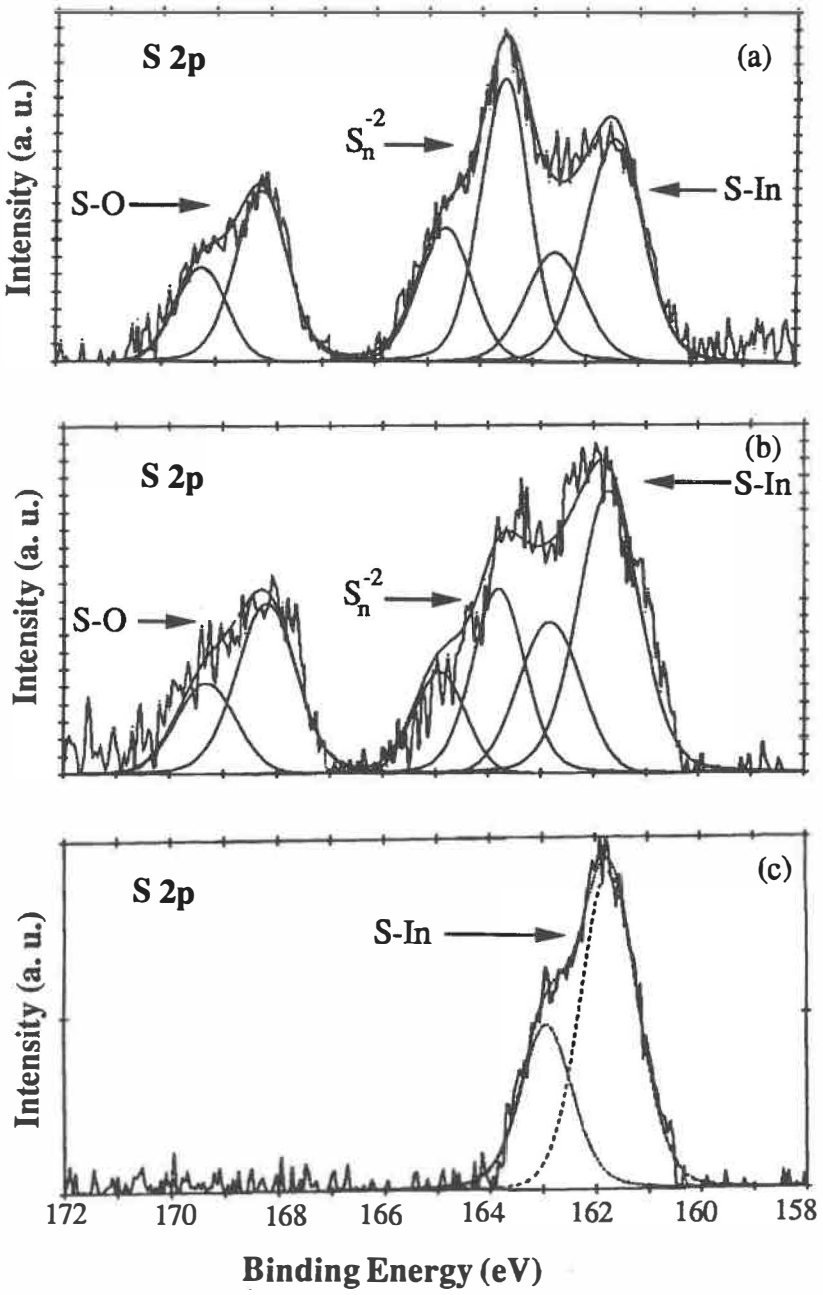

Figure 3.7 (a) & (b) The S 2p spectra from two InP(100) surfaces sulfur passivated using a commonly used procedure. Oxidized sulfur and polysulfide, as well as sulfur bonded to surface indium were found. The amount and the relative ratio of different sulfur species were quite irreproducible; (c) The S 2p spectrum from the improved passivation procedure, only the sulfur bonded to surface indium was found, the surface composition is fairly reproducible.

Chapter 4

Results and Discussion

In this chapter, we present the results of experiments on the sulfur passivation of InP(100) surfaces. The chapter has been divided into three parts: the surface chemical analysis is in §4.1, the surface structural analysis is in §4.2, and the surface electronic properties are in §4.3.

4.1 Chemical Analysis of Sulfur Passivated InP(100) Surfaces

In this section, we consider principally the XPS analysis of InP(100) surfaces treated using the improved sulfur passivation procedure described in §3.4.3. In what follows, we shall use the phrase 'S-passivated InP' to designate such samples. For comparison, samples prepared under other conditions will also be considered. In order to maximize the surface sensitivity, all the XPS spectra shown here were taken at a take-off angle of 30^0 from the surface unless specified otherwise.

4.1.1 Surface Chemical Composition

Experiments were conducted on both n- and p-type InP(100) wafers. As the results of surface chemical analyses, from these two type of InP are identical, within experimental error, only the experimental data from n-type samples will be presented here.

In Fig.4.1, we show high resolution core level P 2p spectra of S-passivated and of UHV cleaved InP. These two spectra coincide to a high degree of accuracy, which means that all the phosphorous atoms in the near surface region of S-passivated InP(100) surface are in the same chemical environment as in the bulk. No indication was found for either P-O or P-S bonding in the vicinity of 133.5 eV, which is the typical binding energy for these two binding states [35]. This indicates that there is only one kind of phosphorus in the sample, which bonds to indium atoms only, and that there are essentially no P atoms at the topmost surface of sulfur passivated InP, whose presence would show the P-O or P-S bonding.

In Fig.4.2, we show the core level spectrum of S 2p of the S-passivated InP. No S-O bonding, which would be at around 168 eV, was observed. The spectra can be curve fitted using nearly the same parameters as those used for the S 2p of the In_2S_3 standard sample, as listed in Table 3.2. The curve fitting results show that there is only one kind of sulfur on the S-passivated InP(100) surface, which bond to the surface indium atoms. A thorough rinse in DI water is necessary for obtaining this result (see Fig. 3.7).

Fig.4.3 shows the comparison between the high resolution core level spectrum of In $3d_{5/2}$ from the S-passivated InP and that from the UHV cleaved InP. The spectra have been normalized in order to compare them. It is found that one or more indium species with higher binding energies than In-P bonding are present on the surface. The most likely are In-O and In-S. As the chemical shifts between the In-S, In-O and In-P bonding are

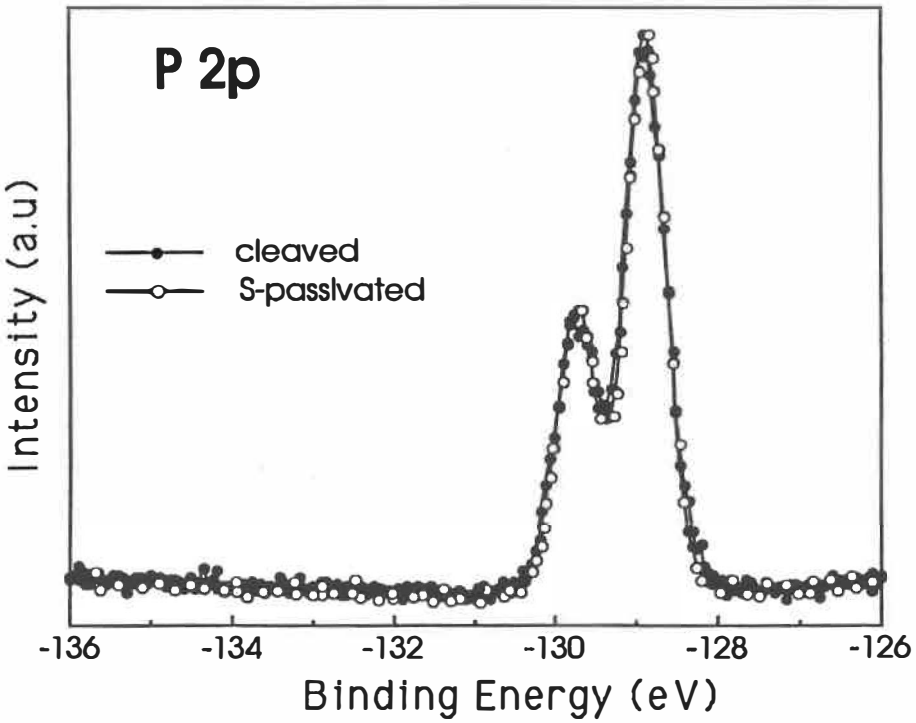

Figure 4.1 High resolution core level spectra of P 2p from S-passivated and UHV cleaved InP.

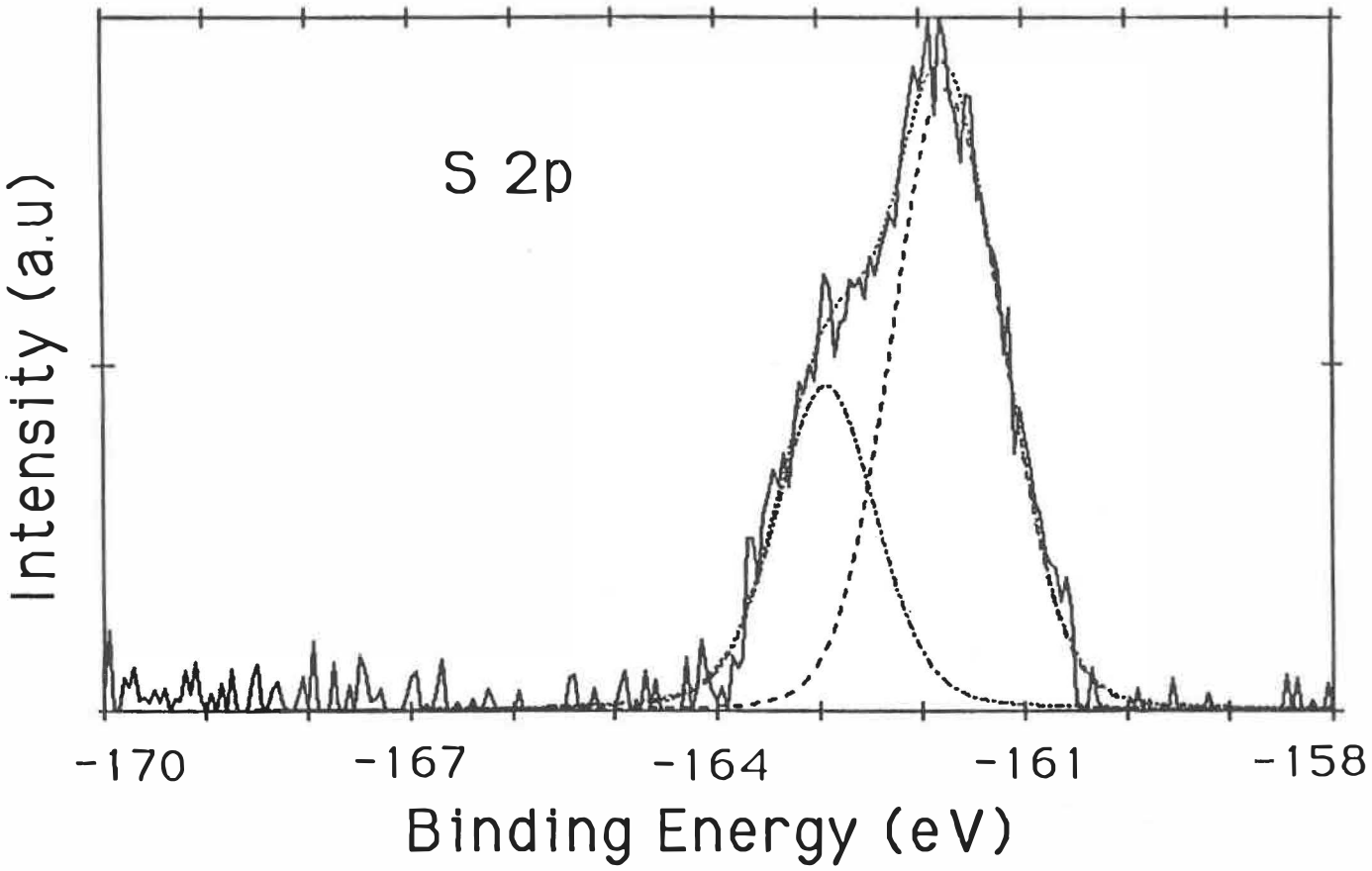

Figure 4.2 High resolution scan of S 2p core level emission from the S-passivated InP(100) surface. The curve fit to a single doublet is shown.

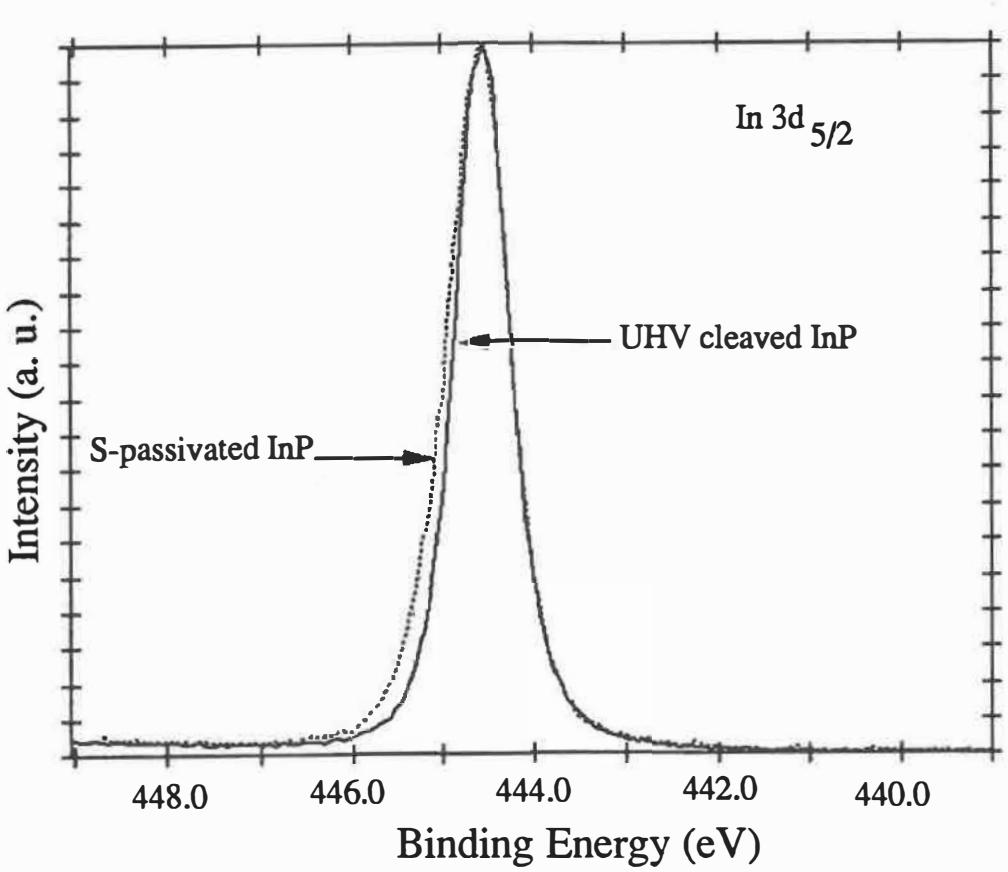

Figure 4.3 Comparison between the In $3d_{5/2}$ spectra of the S-passivated and UHV cleaved InP samples.

quite small, it is not straightforward to identify the different indium species on the surface. We shall take the core level positions and relevant FWHMs from vacuum-cleaved InP, pure In_2S_3 and $InPO_4$ as tentative curve fitting parameters for those possible In species on S-passivated InP surfaces. By so doing, we have in fact made the following assumptions:

i) If there is any In-O bonding on the InP surface, it will be $InPO_4$. This is reasonable since $InPO_4$ is the oxide on as-received InP and on reoxidized InP surfaces after chemical etching.

ii) If there is any In-S bonding on the InP, it will have the same binding energy and FWHM as that of standard In_2S_3 sample. It has been shown that the S 2p spectrum of S-passivated InP can be well curve fitted using the same parameters as those for In_2S_3. Thus it would be reasonable to do the same thing for the In spectrum.

By using the parameters listed in Table 3.1 & 3.2 as tentative parameters to curve-fit the In $3d_{5/2}$ of S-passivated InP, we find that the spectrum can best be fit with a bulk InP peak at 444.52±0.05 eV and an In-S component at 444.92±0.05 eV (Fig.4.4). No appreciable In-O component can be added. This is consistent with the absence of any P-O component on the S-passivated sample. The result again shows that the sulfur atoms at the surface are bonded to indium atoms only. The related curve fitting parameters are listed in Table 4.1.

In Fig.4.5, we show three XPS survey scan spectra: (a) is from an as-etched sample; (b) is from a S-passivated sample; (c) is from a UHV cleaved samples. It is found that although the oxygen and carbon contents have been greatly reduced by the S-passivation, when compared with the as-etched InP, there is still appreciable oxygen and carbon on the surface, as compared to the UHV cleaved InP. From the results we discussed above, it has been found that there are no detectable In-O, S-O, and P-O

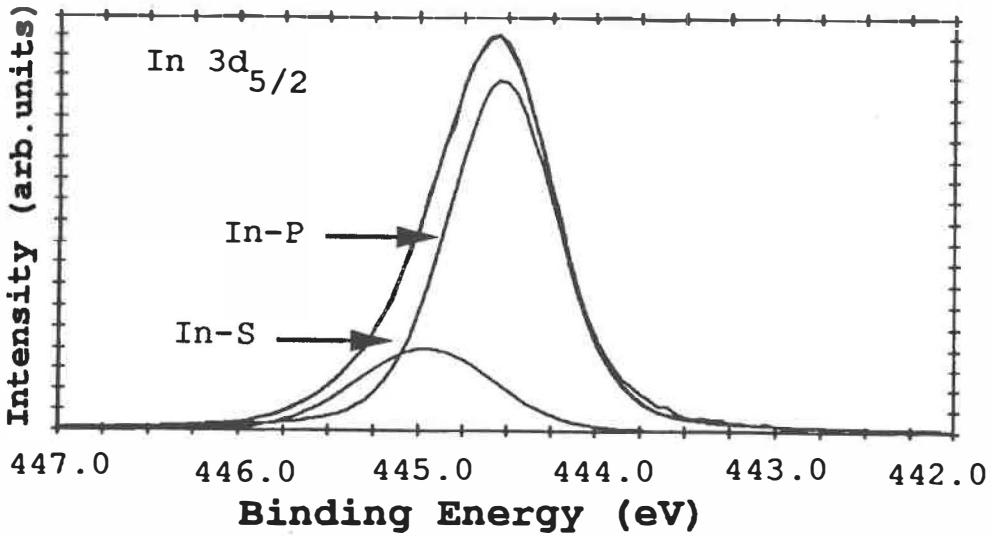

Figure 4.4 High resolution spectrum of In $3d_{5/2}$ of the S-passivated InP surface. The fit to peaks for P- and S-bonded In is shown.

Table 4.1 Curve Fitting Parameters for S-Passivated InP(100)

	E_B (eV)	FWHM	ΔE_{spin}	doublet area ratio
In $3d_{5/2}$ (In-P)	444.52±0.01	0.73		
In $3d_{5/2}$ (In-S)	444.92±0.01	1.00		
P 2p	128.87±0.01	0.61	0.86	1 : 2
S 2p	161.71±0.01	1.20	1.19	1 : 2
$\Delta E = E_B(\text{In } 3d_{5/2}(\text{In-P})) - E_B(\text{P } 2p) = 315.65$ eV				
$\Delta E = E_B(\text{In } 3d_{5/2}(\text{In-S})) - E_B(\text{S } 2p) = 283.21$ eV				

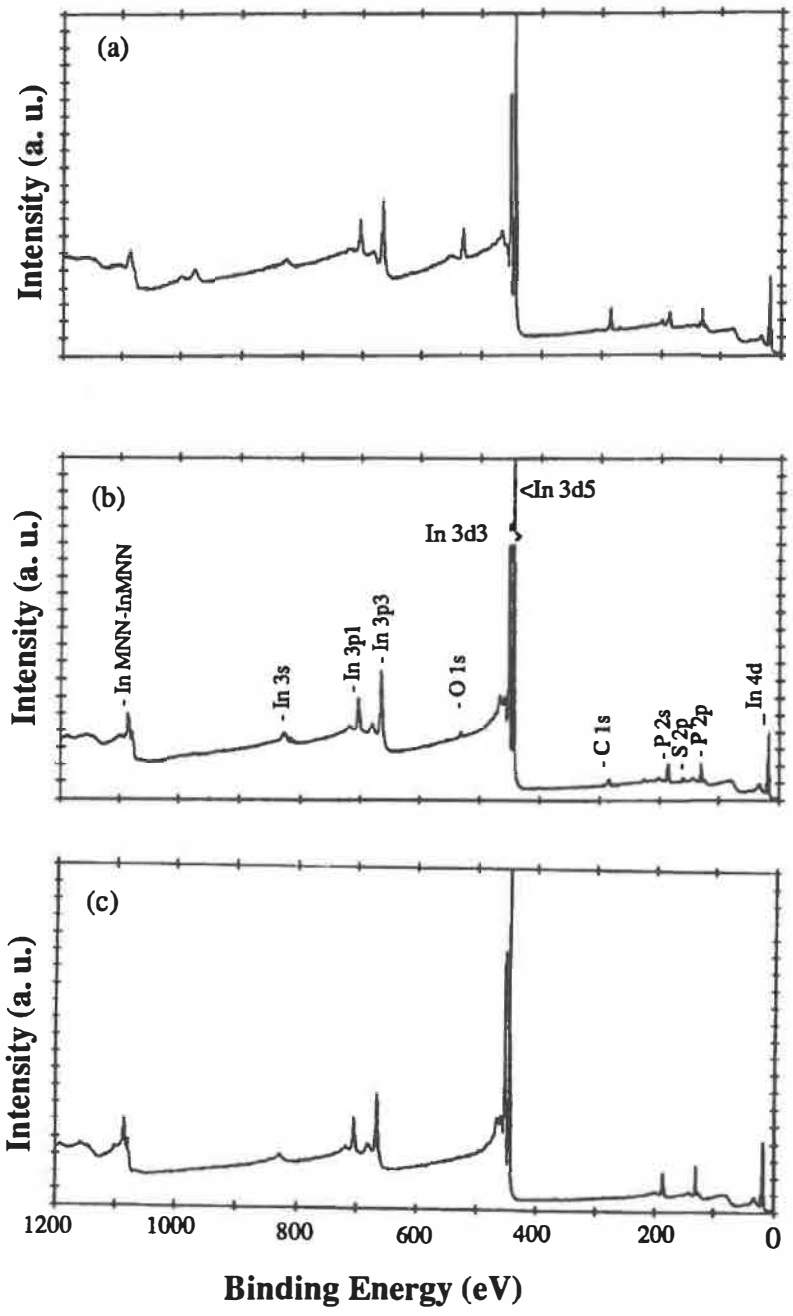

Figure 4.5 Three XPS survey scan spectra from InP(100) surfaces taken at 30 degree take-off angle. (a) is from 10% HCl etched InP; (b) is from a S-passivated InP. (c) is from a UHV cleaved sample.

components on the S-passivated InP(100) surface. Therefore, these oxygen and carbon contents are probably due to physisorbed surface contamination.

From an angle-resolved XPS intensity measurement on the In, P, S, O, and C peaks, it has been found that with the increase of surface sensitivity by reducing the take-off angle (relative to the surface), the relative intensities of In and P peaks drop, those of S, O, and C increase, but those of carbon and oxygen increase much faster than that of sulfur. This means that although S, O, C are surface species, they are all present on the InP surface, but C and O are present above the S layer. Therefore, the oxygen and carbon contents are not bonded to InP surface. These oxygen and carbon contaminants might result from the wet chemical process and air exposure. Fig.4.6 illustrates the relative intensity change with take-off angle. As we may notice, the photoelectron intensity of surface species increases with the decrease of take-off angle. This is explained as follows: the surface area sampled in XPS is of the order of several square millimeters, as defined by the solid acceptance angle of the electron optics. The X-ray flux normally covers a larger area. At take-off angle θ, the sampled area, $\sigma(\theta)$, can be expressed as: $\sigma(\theta)=\sigma(90)/\sin\theta$, where $\sigma(90)$ is the sampled area at take-off angle 90^{o}. The photoelectron intensity of surface species is directly proportional to the sampled area. Therefore the intensity increases with a decrease of take-off angle. The exact values are not significant, as they vary from sample to sample, due to uncontrollable surface contamination during the treatment and sample transfer, but the general tendency is the same for all S-passivated samples.

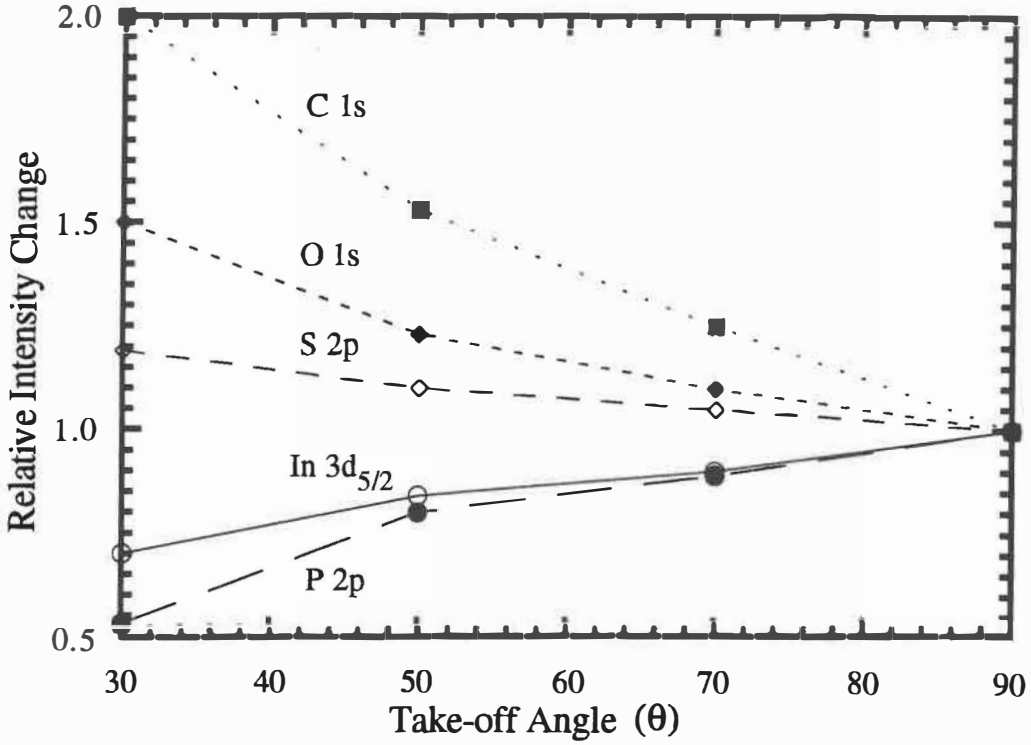

Figure 4.6 The angular dependence of photoelectron intensity of different elements on S-passivated InP(100) surface.

4.1.2 Estimation of Surface In-S Bonding Coverage

By curve-fitting the In $3d_{5/2}$ spectra of the S-passivated InP(100) surfaces taken at different take-off angles, it has been found that the angular dependence of the relative weight of the In-S component in the total intensity of the In $3d_{5/2}$ photoelectron peak (see Fig.4.4) is nearly the same for all S-passivated InP samples. This angular dependence is shown in Fig.4.7 by filled data points. This angular dependence is used to estimate the In-S bonding coverage on the surface [102]. The results from VG and PHI XPS spectrometers are almost the same.

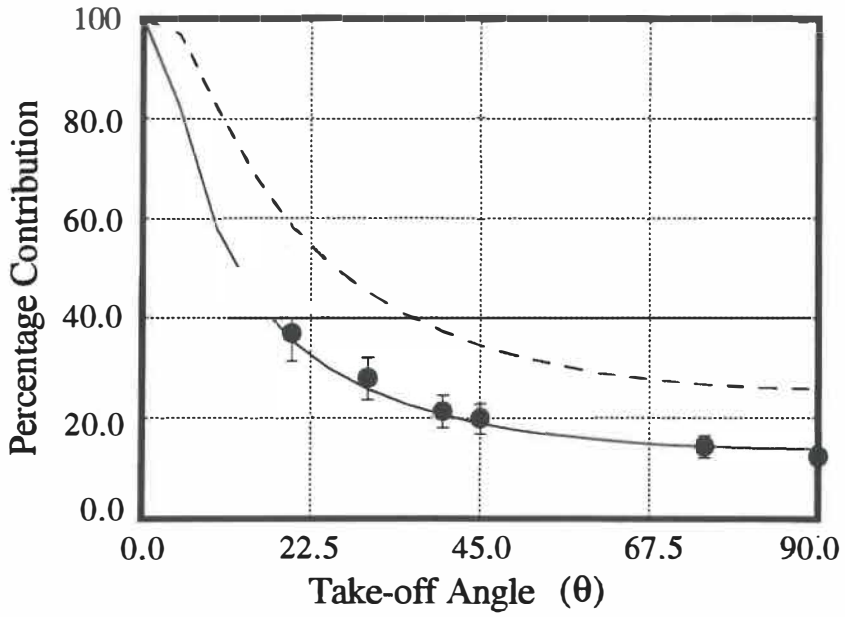

Figure 4.7 Percentage contribution of the In-S bonds to the total detected In $3d_{5/2}$ photoelectron intensity of the S-passivated InP (the filled points); The calculated percentage contribution of one (the solid curve) and two (the dashed curve) monolayers of In atoms at the surface to the total detected In $3d_{5/2}$ photoelectron intensity.

The total In $3d_{5/2}$ photoelectron signal detected by the spectrometer can be thought of as originating from successive indium atomic planes along the [100] direction (Fig.4.8). The penetration depth of the characteristic X-rays is very long (10^3 ~ 10^4 Å) as compared with that of the escaping electrons (10 ~ 20 Å) [56], so that the photoexcitation level within the depth detectable by XPS can be treated as constant. The photoelectrons excited from each indium atomic plane by X-rays can be denoted by I_1, which is the photoelectron

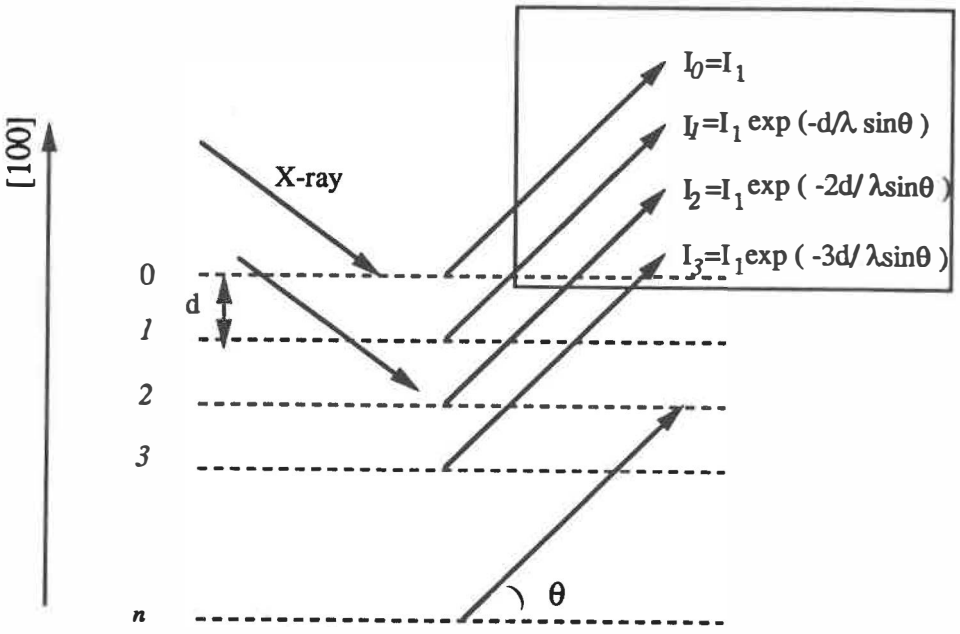

$$I_T = I_1 \sum_{n=0}^{\infty} e^{-(n\lambda/\sin\theta)}$$

Figure 4.8 A schematic illustration about the intensity contribution from successive atomic planes to the total detectable photoelectron intensity.

signal originating from one monolayer of In atoms. As discussed in §2.1, the emitted photoelectrons then have a probability of e^{-1} of travelling a distance characterized by the escape depth λ before being inelastically scattered and no longer appearing in the characteristic XPS spectra. Thus, the flux of photoelectrons decays as $\exp(-l/\lambda)$ as a function of the distance l from the point of origin. Therefore the photoelectrons which originate at the n th indium atomic plane and detected by the spectrometer at a take-off angle θ can be expressed as:

$$I_n = I_1 e^{-n d / \lambda \sin\theta} \tag{4.1}$$

where d is the distance between the successive indium atom planes, about 2.9 Å along the [100] direction. The total detectable photoelectron intensity of In $3d_{5/2}$ is given by adding the contributions from all indium atomic planes from topmost to the bottom of the sample:

$$I_T = I_1 \sum_{n=0}^{\infty} e^{-(n d / \lambda \sin\theta)} = \frac{I_1}{(1 - e^{-(d/\lambda \sin\theta)})} \tag{4.2}$$

The percentage contribution or relative weight of the photoelectrons from the topmost In atomic plane among the total intensity is given by

$$\frac{I_1}{I_T} = (1 - e^{-(d/\lambda \sin\theta)}) \tag{4.3}$$

The kinetic energy of the photoelectrons from the In $3d_{5/2}$ core level is about 1000 eV, if

excited by Al K_α (at PHI), and 800 eV if excited by Mg K_α (at VG). The escape depths at these energies can be calculated using the formula described in ref.[53, 56]:

$$\lambda=0.41\, a^{3/2}\sqrt{E} \qquad (4.4)$$

where a is the average atomic size in the compound expressed in nanometers, 0.29 nm in InP, E is the kinetic energy in electron volts, λ is expressed in nanometers. The escape depth is found to be 20 Å at a kinetic energy of 1000 eV, and 18Å at 800 eV for InP. These values are almost the same as those found from the universal curve in Fig.2.3. We use 19 Å as an average escape depth for fitting the data points from VG and PHI spectrometers.

The percentage contribution from one monolayer of In atoms at the surface to the total In $3d_{5/2}$ intensity in this case is plotted in Fig.4.7 as a solid curve as a function of the take-off angle according to equation (4.3). For comparison, the percentage contribution from two monolayers of surface In atoms (the contribution from In plane #0 plus that from #1, see Fig.4.8) is also plotted in Fig.4.7 as a dashed curve.

The percentage contribution of the In-S component measured from experiment agrees very well with that of one monolayer of surface In atoms as calculated from equation (4.3). This shows that on the S-passivated InP(100) surface the number of the indium atoms which form chemical bonds with sulfur is equal to about one monolayer. The error bars in the plot represents 15% of data scatter among S-passivated InP samples. This scatter gives about 15% fluctuation in the results of surface coverage of In-S compound.

4.1.3 The Atomic Ratio of the Surface In-S Compound

The surface layer formed by one monolayer of indium atoms with the overlying sulfur can be denoted by InS_x. By taking the relative atomic sensitivity factors into account, the atomic ratio, x, can be evaluated by comparing the integrated area under the In-S component of the In $3d_{5/2}$ peak (Fig. 4.4) and that under the S 2p peak (Fig.4.2).

Although there are several sets of atomic sensitivity factors available in the literature [55,57,58, 104], reference data taken on an instrument with one geometry and spectrometer transmission function will show different relative peak intensities from those recorded on an instrument with different geometry and spectrometer transmission function [56], the best way for quantitative analyses of chemical composition is to establish our own atomic sensitivity factors from properly chosen standard samples.

Since we are mainly concerned with the atomic sensitivity factors of In, P, and S in this work, we used a large set of UHV cleaved InP(011) samples and pure In_2S_3 as standards to determine the relative atomic sensitivity factors. We assume that the UHV cleaved InP(011) surface has an In/P ratio close to 1, and that the 99.999% pure In_2S_3 powder sample has an S/In ratio close to 1.5. Based on the XPS data from these standard samples, the atomic sensitivity factors, relative to In $3d_{5/2}$=1.00, were obtained (Table 4.2) by comparing their integrated area.

Table 4.2 Relative Atomic Sensitivity Factors

In $3d_{5/2}$	P 2p	S 2p
1.00	0.080	0.123

By using the relative atomic sensitivity factors, we found that the atomic ratio, the x in surface InS_x compound, is approximately equal to one. The data scattering of atomic ratio among different samples is within 20%. Therefore, we conclude that on S-passivated InP(100) surface, surface In atoms form chemical bonds with overlying S atoms, the atomic ratio is close to one. This means that although the chemical bonding between In and S on the S-passivated InP(100) surface is quite similar to that in In_2S_3, the atomic ratio is not the same. This is because the S can only bond to the surface In atom from one side of the In atom plane.

4.1.4 The Influence of Passivation Conditions

As discussed in the previous chapter, a chemically etched InP surface will reoxidize immediately upon exposure to air. An InP surface prepared for sulfur passivation is in fact an oxidized surface, although the amount of surface oxide is much less than for the as-received samples. Therefore, it is necessary for the passivating solution to be able to dissolve the surface oxide, so that it can enter into direct contact with a fresh InP surface.

We have found that the $(NH_4)_2S$ solution has a limited capability for surface oxide removal and for surface passivation of InP at room temperature. But these capabilities can be enhanced, either by raising the processing temperature or by using light illumination. In Fig.4.9, we show a set of P 2p spectra taken from four differently prepared samples. Spectrum (a) is from an as-etched InP surface. The P-O component is clearly visible. Spectrum (b) is from an InP surface treated in $(NH_4)_2S$ solution at room temperature for 15

min without illumination, and then rinsed in DI water. The P-O component is also present on this surface, although the amount is less than that in spectrum (a). It is not clear whether the oxide is the survivor of sulfide solution treatment, due to limited oxide removal capability of the solution at room temperature, or is oxide regrown after the sulfide solution treatment, due to incomplete surface passivation at room temperature. Spectrum (c) is from an InP sample treated at room temperature under light illumination. Spectrum (d) is from an InP sample treated using the same condition as the improved procedure but no light illumination was applied. No detectable P-O component could be found in spectra (c) & (d). This shows that heating and light illumination, are separately effective for promoting the surface oxide removal and the passivation process. But as shown by the surface In-S coverage discussed below, the combination of the two gives the best results .

For the InP samples sulfur treated under the same conditions as that for the S-passivated samples but without light illumination, the relative weight of the In-S component in the total In $3d_{5/2}$ spectrum is relatively low, as compared to S-passivated samples. The number of In atoms bonded to sulfur is in a range from 0.5 to 0.7 monolayers, as estimated using the same method as in §4.1.2. This difference is illustrated in Fig.4.10 by the curve fitting results of the In $3d_{5/2}$ spectra of these two differently treated samples. This shows that both the heating and the illumination used in our procedure is necessary for obtaining one monolayer In-S coverage.

Although the detailed roles of heating and light illumination played in the S-passivation process is not yet clear, the above results show that the combination of heating and light illumination can enhance the surface oxide removal capability, promote the formation of In-S bonds, and terminate the InP(100) surface by one monolayer of 1:1 In-S surface compound.

The experimental results discussed above indicate that temperature has a strong influence on the surface chemical composition, and the surface coverage of In-S species. But a higher passivation temperature (above 70°C) will lead to a thicker InS_x overlayer, with x range from 2 to 2.5. The details about the InP surfaces treated at higher temperature will be discussed in Appendix I.

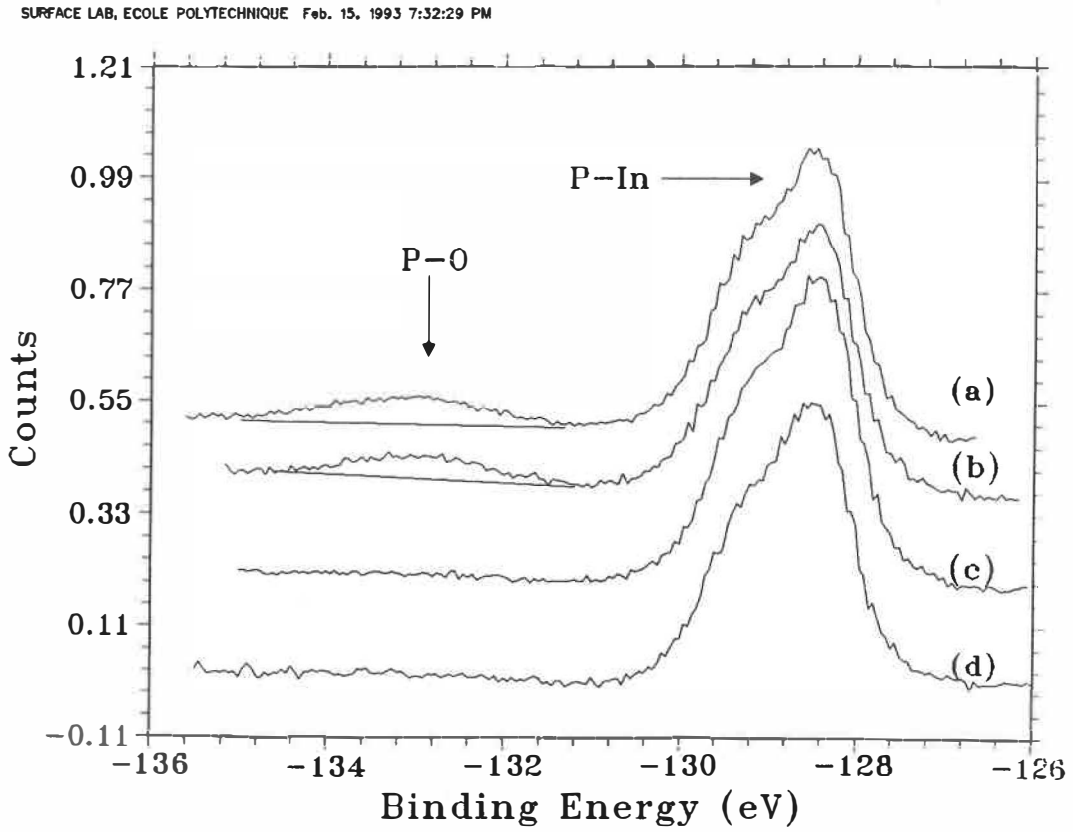

Figure 4.9 P 2p spectra from differently treated InP samples. (a) is from an InP sample etched by 10% HCl. (b) is from an InP sample treated in $(NH_4)_2S$ solution at RT, without light illumination. (c) is from an InP sample treated in $(NH_4)_2S$ solutio at RT with light illumination. (d) is from an InP sample treated in $(NH_4)_2S$ solution at 65^{0}C without light illumination.

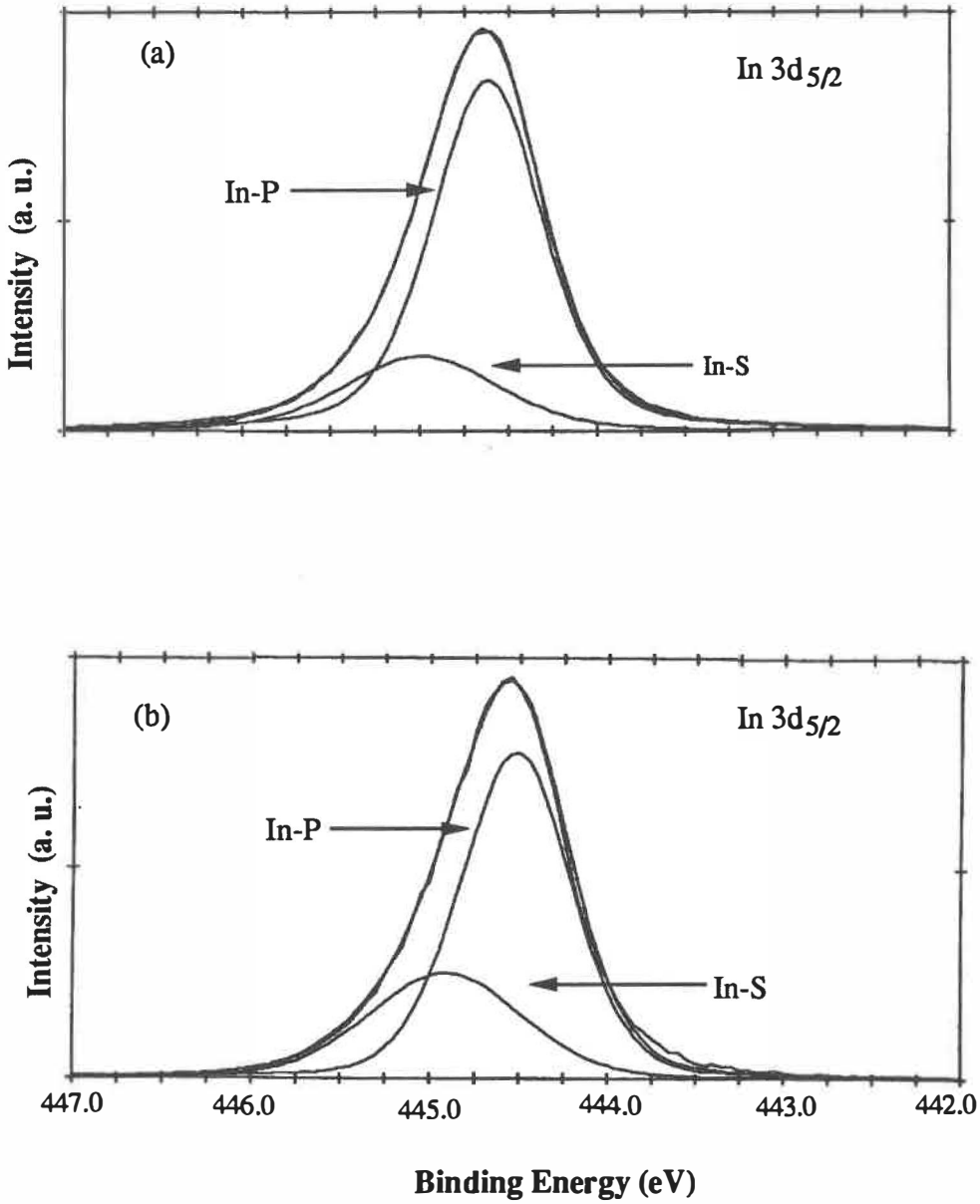

Figure 4.10 High resolution spectrum of In 3d $_{5/2}$ from: (a) InP treated in $(NH_4)_2S$ solution at 65^{0}C without light illumination. (b) S-passivated InP. The fits to peaks for P- and S-bonded In are shown.

4.1.5 The Stability of S-passivated InP

The thermal and chemical stability of the resulting surface is an important parameter for a surface processing procedure. The S-passivated InP(100) surface is quite stable in air, and against DI water rinse. As mentioned before, clear LEED patterns are still visible on the S-passivated surfaces after 3 to 4 days exposure to the atmosphere, or after being annealed up to 400 ± 50^0C in UHV for 60 min. This demonstrates that the surface structure is very stable, and the S-passivated surfaces are highly resistant against air-oxidation and contamination. The surface chemical composition is also quite stable. Fig.4.11 shows the P2p and S2p spectra, which are very sensitive to the oxidation and chemical composition change at the surface, after a sample was either exposed to the atmosphere for 4 days or annealed at 400 ± 50^0C for one hour. No P-O or S-O components were found on these surfaces. The spectra could be well curve-fitted using the same parameters as those used for the as-passivated InP. No intensity decrease in the S 2p spectrum was observed upon annealing. This shows the strong chemical binding between the sulfur and surface indium. The thermal stability of the S-passivated InP surface will be discussed further in relation to photoluminescence experiments in §4.3.

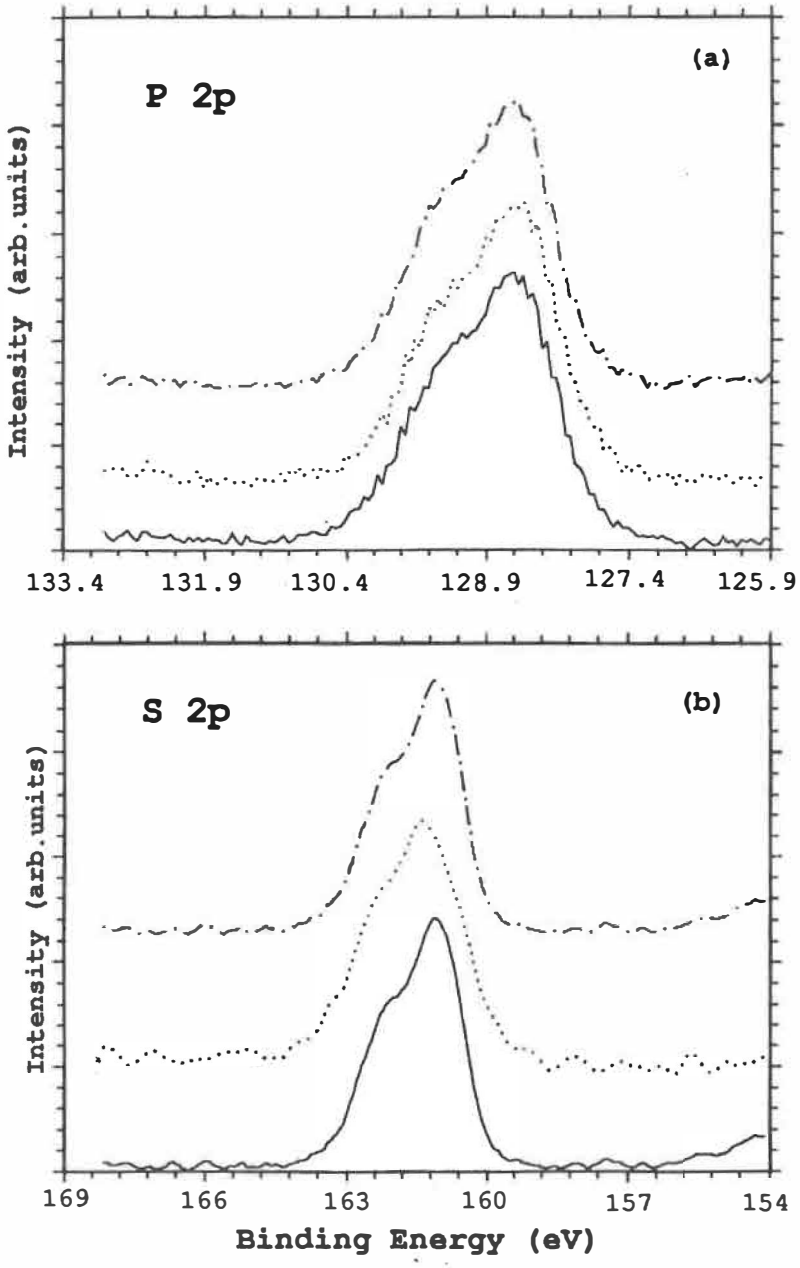

Figure 4.11 (a) P 2p spectra and (b) S 2p spectra from the as-S-passivated sample (the solid curves), the sample which has been air exposed for 4 days after S-passivation (the dotted) curve, and the sample which has been annealed at 400±50°C for 1 h after the S-passivation.

4.2 Structural Analysis of S-Passivated InP(100) Surfaces

It has been shown in the previous section that on S-passivated InP(100) surface, one monolayer of surface In atom forms chemical bonds with the overlying sulfur atoms. The surface is terminated by one monolayer of InS_x with x near one. Here, we shall describe surface structural analysis of these surfaces using LEED , XPD, and XANES. A structural model consistent with this data will be presented.

4.2.1 InP(100)-(1x1)-S Surface

Low energy electron diffraction was used to study the surface structure of S-passivated InP(100) wafers. Clear and distinct LEED patterns can be obtained from these samples.

The atomic arrangement in an InP crystal when viewed from the [100] direction is schematically illustrated in Fig.4.12. The vectors, $\mathbf{a_1}$ and $\mathbf{a_2}$ denote the lattice vectors of bulk InP along the [010] and [001] directions respectively,with $a_1 = a_2 = 5.87$Å. In the analysis of LEED patterns, the elastic interaction between the incident electrons and the surface is treated as the scattering of waves at a two dimensional lattice [57]. It is clear that the atomic arrangement on (100) surface can be represented by a two dimensional lattice defined by lattice vectors $\mathbf{b_1}$ and $\mathbf{b_2}$ along the [011] and [0$\bar{1}$1] directions of the bulk lattice, with $b_1 = b_2 = a_1 / \sqrt{2} = 4.15$ Å. Obviously, the two dimensional unit cell with basis vector $\mathbf{b_1}$, $\mathbf{b_2}$ is a primitive unit cell from which the lattice may be constructed by translation

operations (obviously it is also possible to use $\mathbf{a}_1$ and $\mathbf{a}_2$ as the basis vectors, as in the bulk but this is not a primitive base). A corresponding two dimensional reciprocal lattice for the InP(100) surface, defined using the basis vectors $\mathbf{b}_1^*$, $\mathbf{b}_2^*$ which are related to $\mathbf{b}_1$ and $\mathbf{b}_2$ by equation (2.13), is illustrated in Fig.4.13. A reciprocal vector, g_{hk}, can be calculated using $\mathbf{b}_1^*$, $\mathbf{b}_2^*$ and vector algebra.

LEED patterns from a S-passivated InP(100) sample obtained with incident electron energies of 54 and 84 eV, together with the indexed patterns, are shown in Fig.4.14. From a series of LEED patterns, the related reciprocal lattice vectors were measured, using the method described in §3..2.2. The magnitudes of these vectors are listed Table 4.3, together with the vectors calculated from the two dimensional reciprocal lattice of the InP(100) surface discussed above.

It can be seen the the reciprocal lattice vectors measured from the LEED patters are in good agreement with the calculated ones. This means that the diffraction patterns from the S-passivated InP(100) surface can be completely indexed using the two dimensional reciprocal lattice parameters of an ideal InP(100) surface. No diffraction spots having fractional Miller indices were observed between the main spots in the entire range, 5-200 eV. We conclude that the S-passivated InP(100) surface has a (1x1) structure, which can be denoted as InP(100)-(1x1)-S.

There are four possible adsorption sites for sulfur to bond with surface In atoms. These are the bridge site, top site, anti-bridge site, and hollow site as shown in Fig.4.15. Considering the strong characteristic orientation of the sp^3 hybrid orbitals in InP, the most probable site is the bridge site. At the bridge site, a sulfur atom is two-fold coordinated and forms a single covalent bond with each of its two neighboring In atoms along the [011]

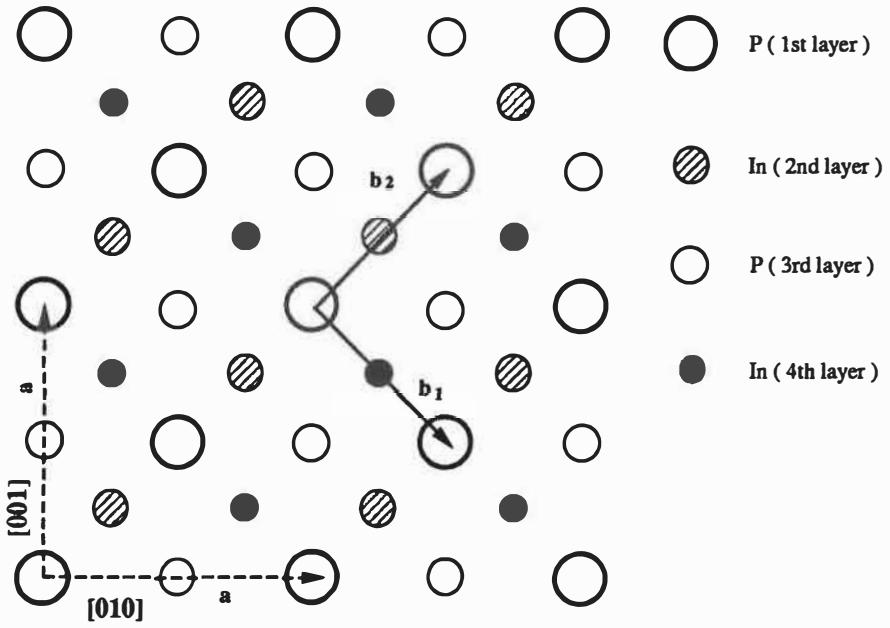

Figure 4.12 A schematic illustration of the atomic arrangement in InP crystal when viewed from [100] direction.

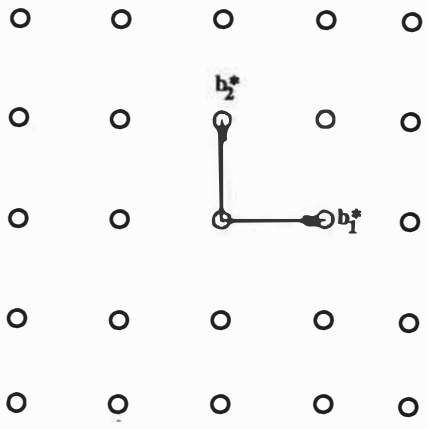

Figure 4.13 The two-dimensional reciprocal lattice for InP(100) surface.

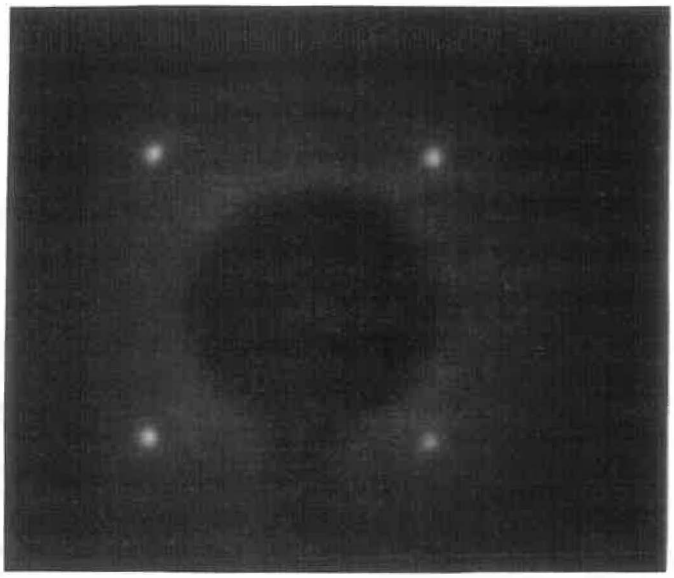

(a)

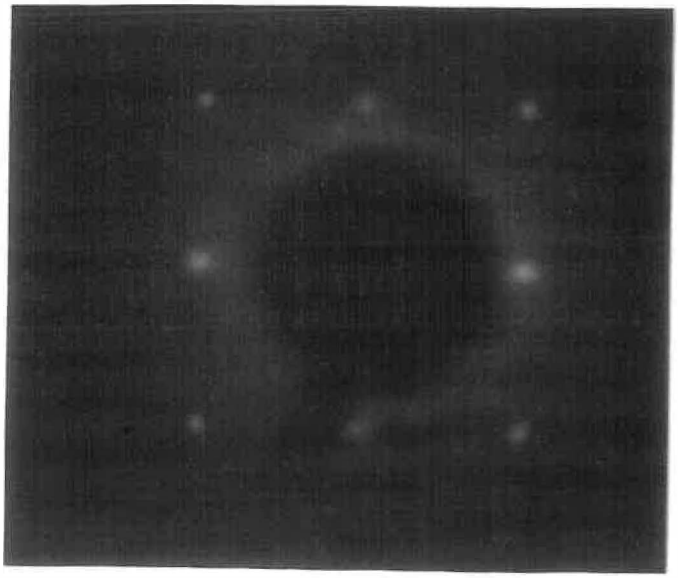

(b)

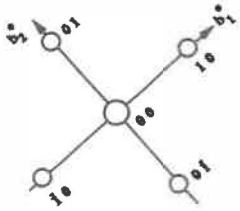

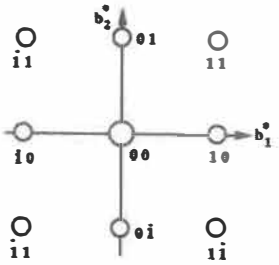

Figure 4.14 LEED patterns of a S-passivated InP(100) surfaces with incident electron energies of (a) 54 eV, (b) 84 eV. The corresponding diffraction indices are shown.

direction. From symmetry considerations, the in-plane coordinates of sulfur atoms in the (100) plane should be the same as those of P atoms, but their out-of-plane distance is not necessarily the same.

Table 4.3 Two-dimensional Lattice Parameters

Index	Calculated from InP(100)	Measured from LEED
< 1 0 >	$\lvert g_{<10>}\rvert = \lvert \mathbf{b}_1^* \rvert = \lvert \mathbf{b}_2^* \rvert = 1.51$ Å^{-1}	1.5 Å^{-1}
< 1 1 >	$\lvert g_{<11>}\rvert = \lvert \mathbf{b}_1^* \pm \mathbf{b}_2^* \rvert = 2.14$ Å^{-1}	2.1 Å^{-1}
< 2 0 >	$\lvert g_{<20>}\rvert = \lvert 2\mathbf{b}_1^* \rvert = \lvert 2\mathbf{b}_2^* \rvert = 3.03$ Å^{-1}	3.0 Å^{-1}

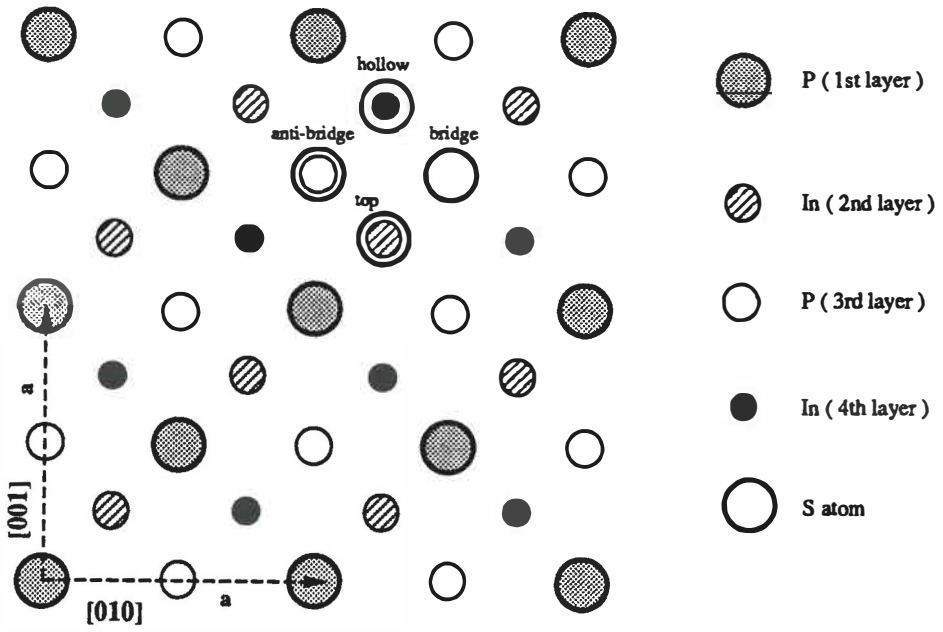

Figure 4.15 Four possible adsorption sites for S to bond to surface In atoms.

Fig.4.16 shows a proposed surface structural model of the S-passivated InP(100) surface, in which S takes the position at the surface that would be occupied by P. This structural configuration is consistent with the experimental results: one monolayer of surface indium atoms form chemical bonds with the overlying sulfur, the atomic ratio between the two is one, and the surface has a (1x1) structure.

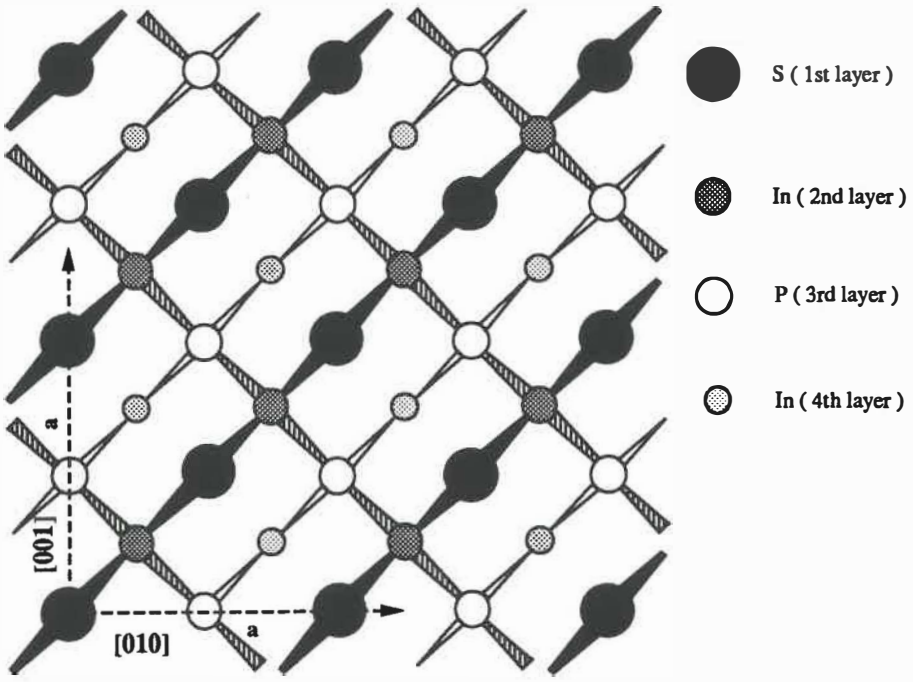

Figure 4.16 A surface structural model for the S-passivated InP(100)-(1x1)-S structure.

4.2.2 XPD Experiments on S-Passivated InP(100)

To confirm the surface structure that we have proposed for S-passivated InP(100) surface, based on the XPS and LEED measurements, we have used XPD to verify two thing. One is if all of the sulfur is in the topmost surface rather than undergoing extensive anion exchange in the near surface region. The latter case was found by Chambers et al [29] on Se and Te passivated GaAs(001) surfaces using H_2Se at 425^0C. The other question is whether the In-S bonds are in the $(0\bar{1}1)$ planes as assumed in the model (Fig.4.16).

As discussed in §2.3, in an X-ray photoelectron diffraction experiment, atoms present in the top atomic layer do not exhibit photoelectron forward-scattering enhancement, due to the lack of a forward scatterer. This effect is an excellent diagnostic of whether or not S atoms extensively exchange with P atoms during the passivation treatment. Based on the same principle, the photoelectron intensity of the In-S component in the In $3d_{5/2}$ signal would be enhanced by the S atom along the In-S bond direction.

In $3d_{5/2}$, P 2p, and S 2p were measured in XPD experiments. S 2p is very well separated from other photoelectron or Auger peaks from InP, with no interference with substrate lines when Mg K_α or Al K_α sources are employed.

The coordinate system for our XPD measurement is shown in Fig.4.17. It is obvious that In and P peaks should exhibit a strong photoelectron diffraction effect along the principle crystal axes, such as <100>, <011>, < 111 >, and along the directions shown in Fig.4.18. If sulfur exchanges with P in the near surface region and takes the place of P in the lattice, the S 2p peak from these samples should exhibit photoelectron diffraction in these specified directions as well. The experimental data are shown in Fig.4.19 and Fig.4.20, for polar and azimuthal angles, respectively.

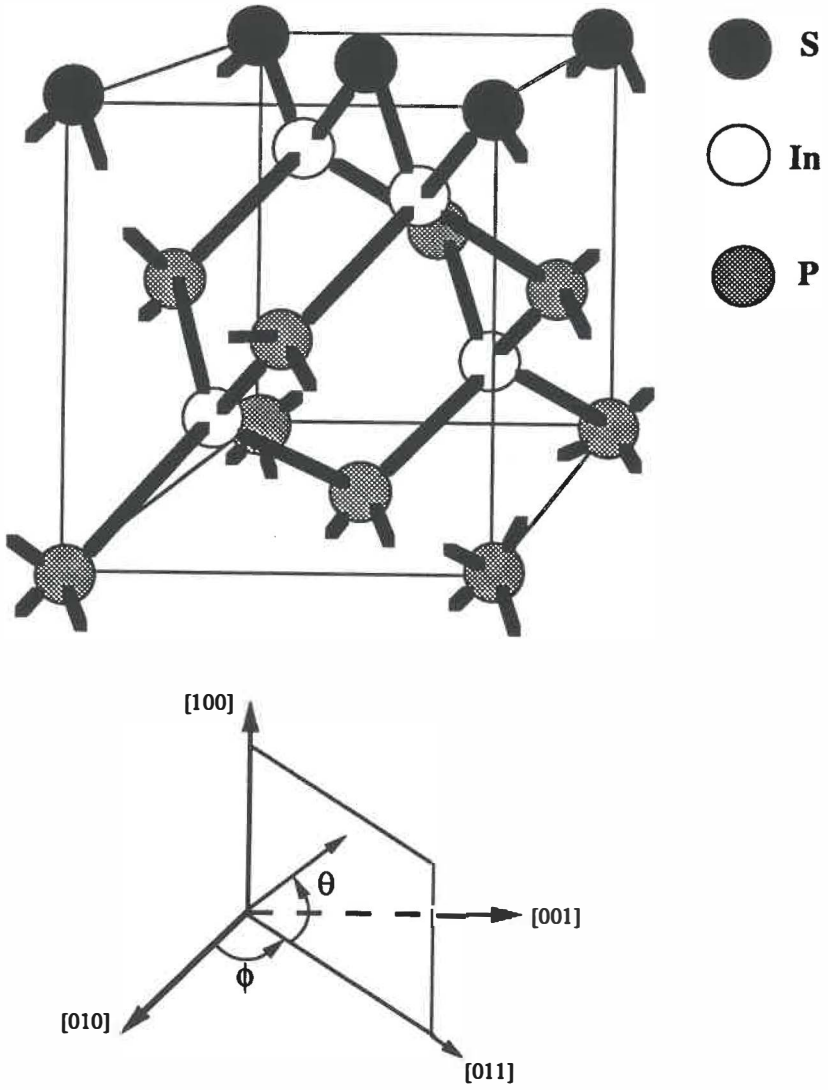

Figure 4.17 The coordinate for X-ray photoelectron diffraction experiment.

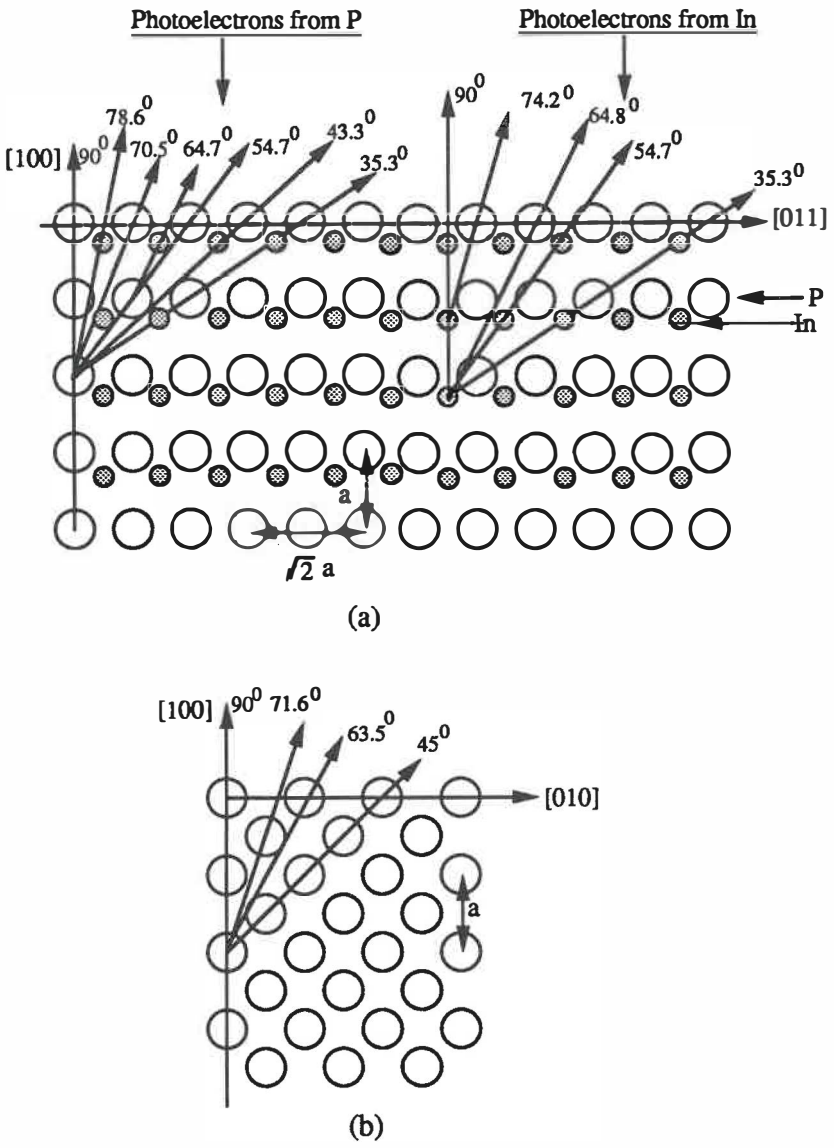

Figure 4.18 The emission plane and various angles of photoelectron forward-scattering, when the polar angle is varied (a) in $(0\bar{1}1)$ plane, and (b) in the (001) plane.

The In and P peaks exhibit strong forward scattering enhancement along the expected directions, as shown in Fig.4.18. The intensity of S 2p shows no such oscillation. This result clearly indicates that the S atoms exist only on the topmost layer.

From the above discussion, we know that the photoelectron intensity of In $3d_{5/2}$ is enhanced by P atoms along [111], the direction of the In-P bond, or more specifically, at a take-off angle of 35.3^0 in the $(0\bar{1}1)$ plane (Fig.4.18). But the intensity of the In-S component of In $3d_{5/2}$ can only be forward scattering enhanced along the In-S bond direction by S atoms at the other ends of the bonds. As shown in Fig.4.4, the high resolution XPS can resolve In(-P) and In(-S) components. Thus it becomes possible to observe the forward-scattering effect of the In-S component. If the In-S bonds are in the $(0\bar{1}1)$ plane, then the intensity enhancement should appear along the bond direction. Fig.4.21 shows the In $3d_{5/2}$ intensity of In-P and In-S components as a function of take-off angle. For In-P, the strong forward scattering peak along the In-P bond direction at 35^0 is clearly seen. The measured intensity enhancement of In-S component is in a rather broad range, from 32^0 to about 45^0 centered at about 38 ± 2^0. This broad distribution may be explained as follows: according to the mutiple scattering model of Tong et al [74] and Egelhoff [73], the first few scattering atoms along a row tend to be forward focusing. The In-P component was scattered by these forward focusing processes, so that it has a well-defined forward-scattering direction. Since the In-S component was only forward scattered once by the overlying S atom, the photoelectron intensity is distributed within a larger off-axis angle. Another possible reason may be due to some fluctuations in the off-plane position of S atoms, caused by surface relaxation.

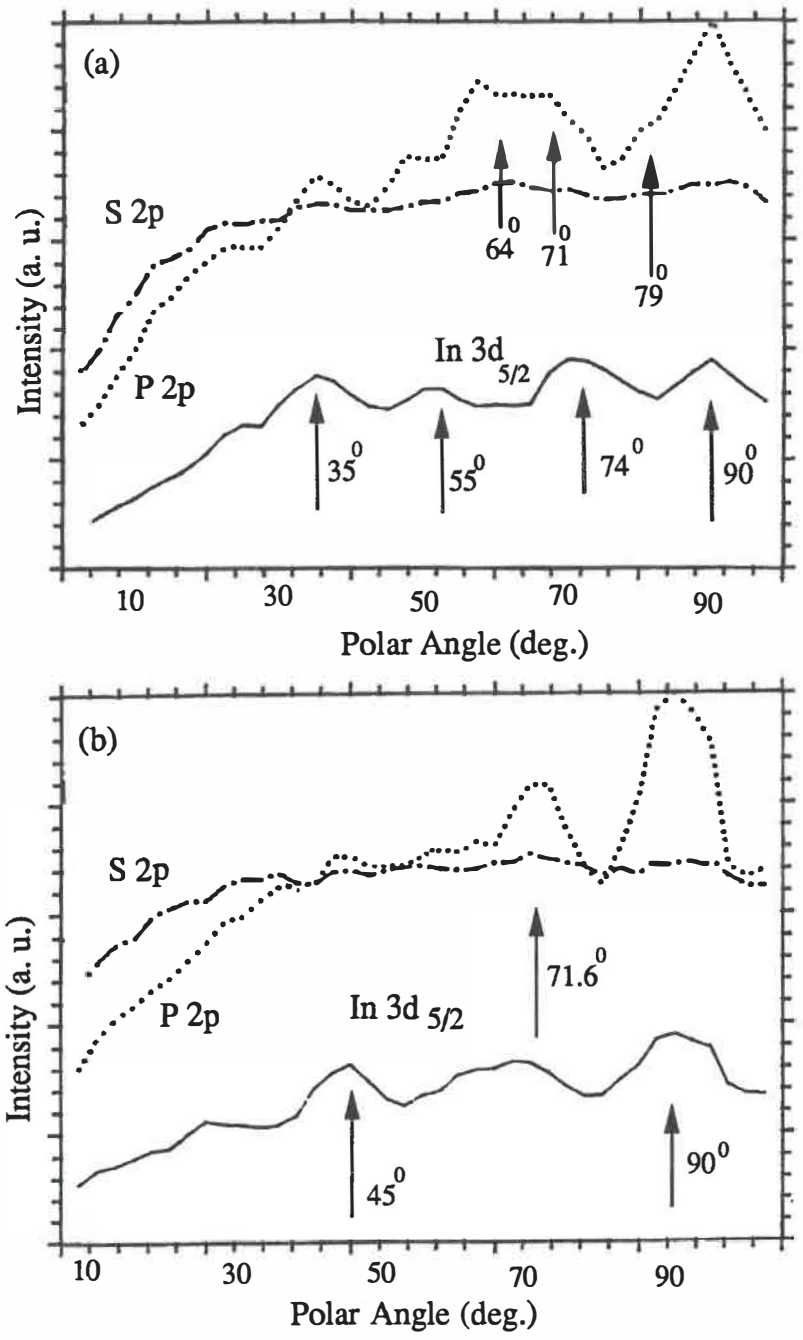

Figure 4.19 The change of photoelectron intensities of In, S, and P core levels with the polar angle, when the polar angle is varied (a) in (0$\bar{1}$1) plane (ϕ=45^0) and (b), in the (001) plane (ϕ=0^0).

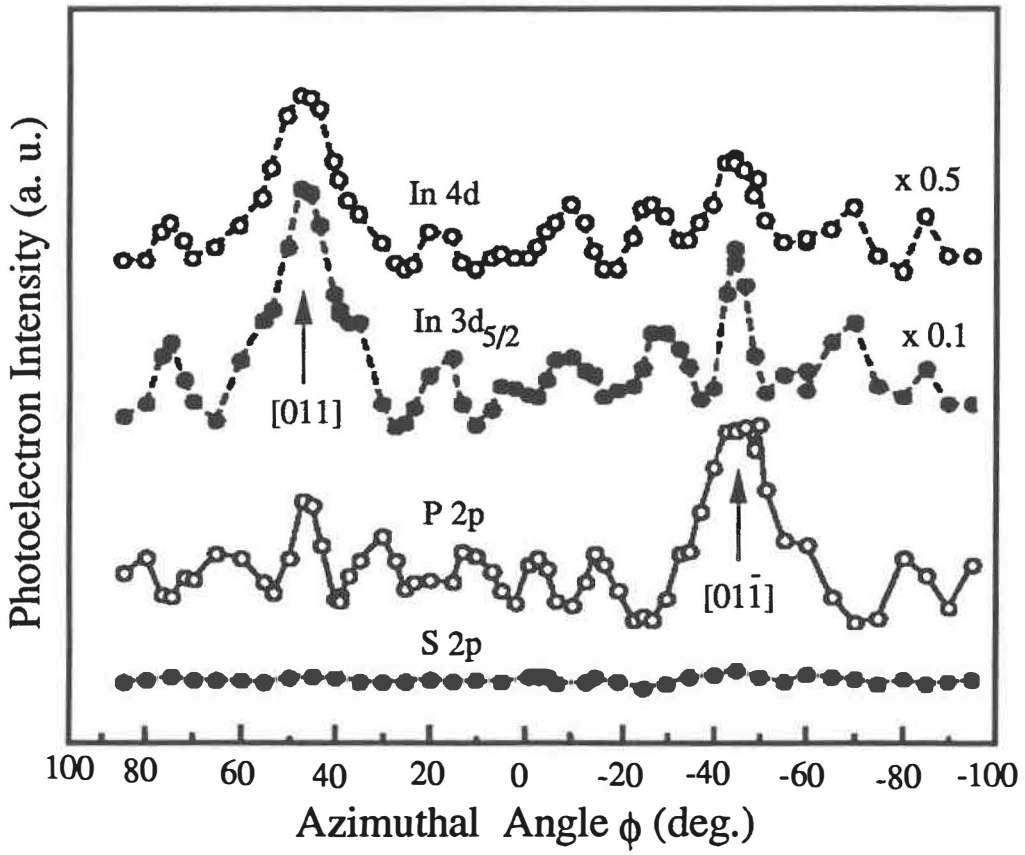

Figure 4.20 Photoelectron intensities of various core levels as a function of azimuthal angles, taken at a constant take-off angle of 35^0 from the (100) plane.

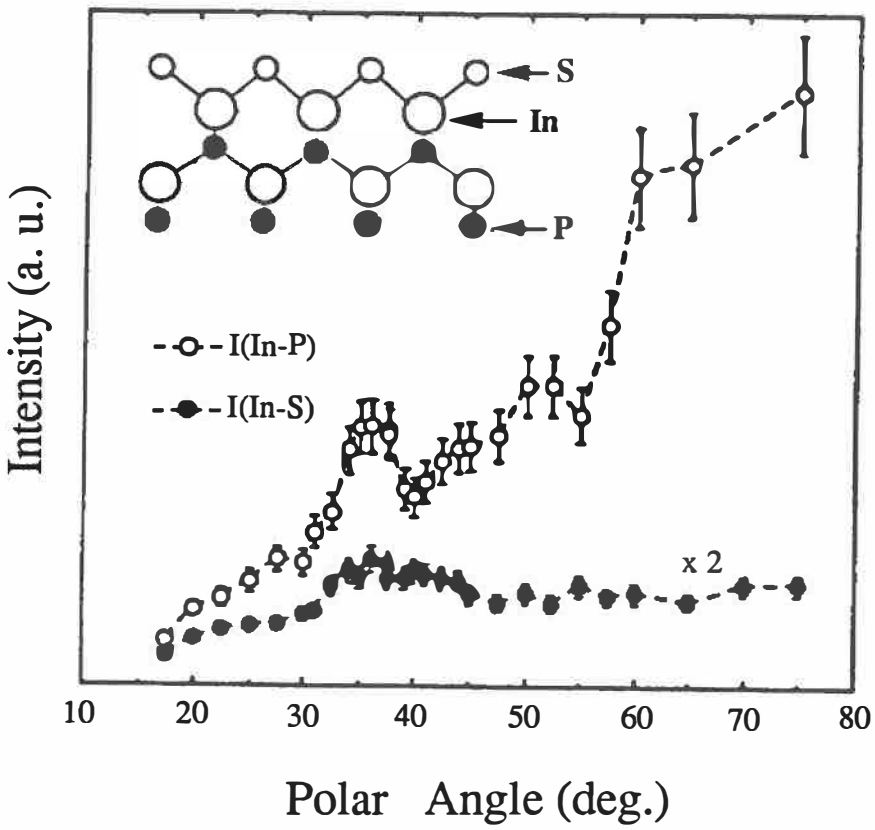

Figure 4.21 In $3d_{5/2}$ photoelectron intensities of In(-P) and In(-S) as a function of take-off angle α, in the [011] azimuth. The error bars represent 10% uncertainty in curve-fitting of In $3d_{5/2}$ into In(-P) and In(-S) components.

4.2.3 X-Ray Absorption Near Edge Structure Measurement

Investigation of the direction of the S-In bridge bond on the S-passivated InP(100) surface, using X-ray absorption near edge structure (XANES), was performed by our collaborators, Dr. Z. H. Lu and co-workers [105], at the double crystal (InSb) monochromator (DCM) beam line of the Canadian Synchrotron Radiation Facility (CSRF) located at the Synchrotron Radiation Center (SRC) of the University of Wisconsin-Madison.

X-ray absorption spectra are due to electronic transitions from atomic core levels to unoccupied final states. The absorption edge occurs when a transitions from a given core level is first energetically allowed. In the experiment, the sulfur K-edge absorption spectra were recorded by measuring total electron yield (TEY). The S K-edge absorption is caused by the photo-induced transition of K-shell electrons to empty valence orbitals, which should be of p-character according to the dipole transition selection rule. The prominent feature in XANES spectra from a covalent bonding system is the transition of s-electrons to antibonding σ-like orbitals, which is often referred to as σ resonance. Since the bonding and antibonding states are along the same axis [106], the σ resonance was used to determined the In-S bond orientation. It is well established [107] that the σ resonance intensity, I_σ, can be expressed as

$$I_\sigma \propto \left|\langle f \left| \vec{E} \cdot \vec{M} \right| i \rangle\right|^2 \qquad (4.5)$$

where $\vec{E}$ is the photon electric vector, $\vec{M}$ is the electric-dipole vector that is associated with the chemical bond orientation. $|f\rangle$ and $|i\rangle$ are the final and initial states involved in the

transition. In Fig.4.22, we define the polar angle, θ, and the azimuthal angle, ϕ, of the photon electric field vector $\vec{E}$ relative to the coordination system of the surface. We assume that the S-In bond is in the $(0\bar{1}1)$ plane, with an angle, α, off the (100) plane. In the case of normal incidence, $\theta = 90^0$, equation (4.5) can be simplified:

$$I_\sigma (\phi, 90^0) = C \cos^2\alpha \cos^2\phi \qquad (4.6)$$

where C is a constant. The σ resonance should reach a maximum when the electric field

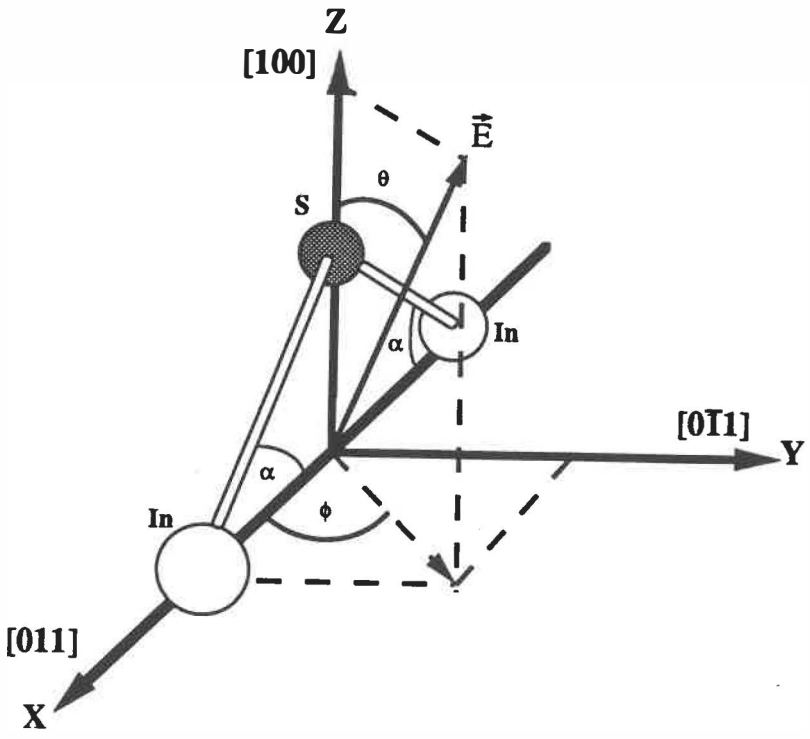

Figure 4.22 The coordinate system for XANES measurements.

vector of the incident photon is parallel to the $(0\bar{1}1)$ plane, that is, at $\phi=0$. Fig.4.23 shows the S K-edge XANES spectra taken at different azimuthal angles. As expected, the σ resonance, the most intense peak at 2470 eV, has its maximum at $\phi=0$. This confirms that the In-S bond is indeed in the $(0\bar{1}1)$ plane. More detailed studies [108] have shown that in the case of normal incidence, I_σ follows rather nicely a $\cos^2\phi$ relationship, although the absorption at $\phi=90^0$ does not drop to zero as one may expect from equation (4.6). This 'background' absorption is most likely due to the presence of residual elemental sulfur on this sample (the sample was prepared by our collaborators, the presence of residual sulfur was probably due to incomplete DI water rinse). This is based on the following observation. In Fig.4.23 the absorption edge energy shifts towards higher energy as the In-S σ resonance intensity decreases, in line with the fact that the K-edge energy of elemental sulfur is about 1eV higher than that of In_2S_3 [108].

When the electric field vector $\vec{E}$ is in the $(0\bar{1}1)$ plane, i.e., $\phi=0$, equation (4.5) can be simplified:

$$I_\sigma(0^0, \theta) = C\cos^2\alpha\,[1-(1-tg^2\alpha)\cos^2\theta] \qquad (4.7)$$

It can be seen that by measuring the intensities with the electric vector at $\theta= 0$, and 90 respectively, one can find the bonding angle by

$$\alpha = tg^{-1}\sqrt{\frac{I(0^0, 0^0)}{I(0^0, 90^0)}} \qquad (4.8)$$

The bond angle relative to the (100) plane is $40^0 \pm 2^0$ as measured using this method[108].

This value is in good agreement with our result got from XPD measurements (38 ± 2^0).

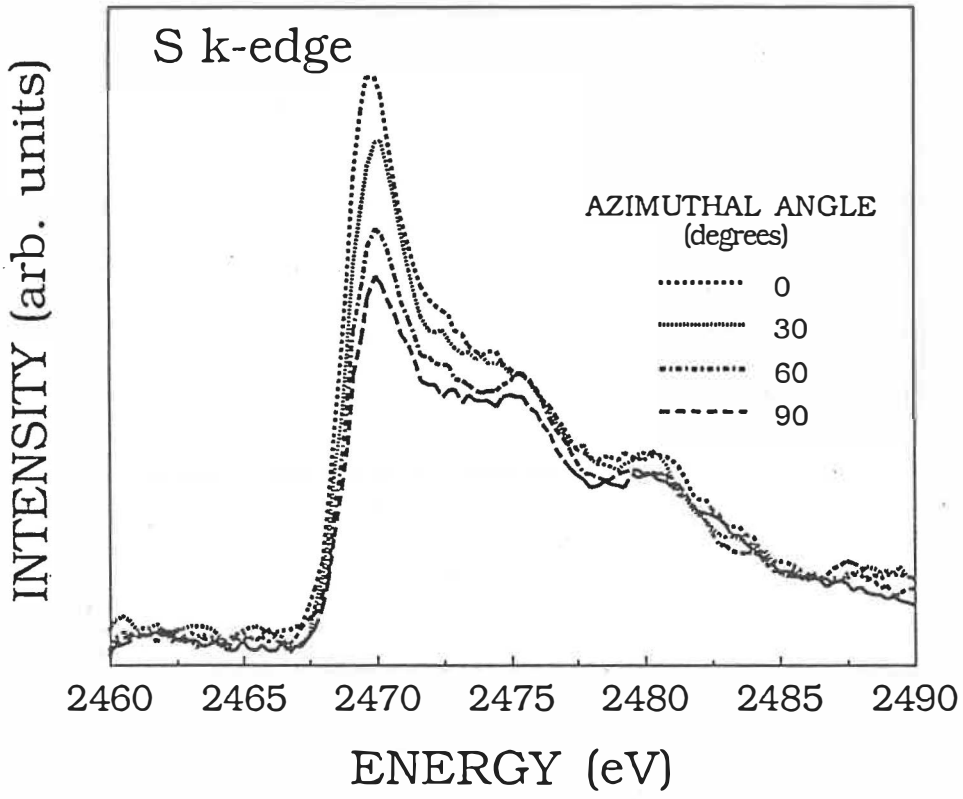

Figure 4.23 S K-edge XANES spectra taken at various azimuthal angles.

4.2.4 Discussion

Our proposed structural model, based on the results from XPS and LEED, has been confirmed by XPD and XANES experiments. In this model, the electronic configuration of the sulfur atom is assumed to be an sp^3 hybrid. Two of its sp^3 orbitals combine with two sp^3 hybrid orbitals from its two neighboring In atoms to form σ bonds as shown in Fig.4.16. The other two sp^3 orbitals are filled with lone-pair electrons and thus are not available for bonding [106]. This can account for the high stability of the surface upon air exposure and annealing.

From the XPD and XANES experiments, it has been shown that the angle between the In-S-In bonds is about 100^0. That means the actual electronic configuration of the sulfur atom is somewhat between pure sp^3 hybrid orbitals (which leads to an angle of 109^0) and a pure 3s3p configuration (which will give an angle of 90^0).

From our experiment, it has been found that annealing the sample at 300^0C in vacuum for 1.5h has little effect on the LEED pattern. We did not observe the surface reconstruction from (1x1) to (2x1) at 250^0C reported by Oigawa et al [26] from their RHEED measurements on the InP(100) surface which had been sulfur treated at room temperature. This is probably due to the difference in the surface chemical composition on the passivated samples, resulting from different passivation procedures.

In Oigawa's experiment, both S-P and S-In bonds were found on as-passivated samples. At 250^0C, the S-P bonds disappeared as indicated by their photoemission results.

After this, the (2x1) RHEED patterns were observed. They explained that at this temperature, the disappearance of S-P bonds cause the formation of stronger S-In bonds, and consequently the RHEED pattern changes from (1x1) to (2x1).

In our opinion, there might be another reason for the structural transition observed for their samples. It is reasonable to assume that the surface is terminated partly by S-P bonds and partly by S-In bonds in their case. The sulfur forms bridge bonds either to its two neighboring In atoms or to its two neighboring P atoms. This will lead to a (1x1) structure. At 250^{0}C, with the breaking down of S-P bonds, the P atoms otherwise bonded to the S atoms will have two dangling bonds available. Two neighboring surface P atoms can form a dimer structure to reduce the number of dangling bonds for each surface P atom from two to one, and thus lead to a (2x1) structure like the dimerization on Si (2x1) surface. The possibility of In dimerization was excluded by the fact that the dimer is along the [0$\bar{1}$1] direction as discussed in ref.[40]. Therefore the cause of this surface structural transition from (1x1) to (2x1) is due to the incomplete coverage of S-In bonding on the surface.

As discussed previously, our S-passivated InP sample surface is completely terminated by one monolayer of S-In bonds, the dangling bonds of surface In atoms are saturated by the sulfur atoms, and the other two sulfur atomic orbitals are filled with lone-pair electrons. There is no driving force to form a (2x1) structure. According to Oigawa et al [26] S-In bonds will remain stable up to 500^{0}C. Therefore, no (1x1) to (2x1) surface structural transition should occur at 250^{0}C on our S-passivated InP(100)-(1x1)-S surface.

4.3 Electronic Properties of S-Passivated InP(100) Surfaces

In this part, we shall compare the surface electronic properties of S-passivated InP samples with those of chemically etched ones, and show that the InP surfaces treated by our procedure is not only chemically passivated, but also with improved surface electronic properties. For quantitative characterization of the surface electronic properties, more detailed and extensive studies are needed.

4.3.1 Estimation of Surface Fermi Level Position by XPS

The surface Fermi level measurement was performed by comparing the binding energy of P $2p_{3/2}$ from the samples with the energy reference which we established in §3.1., i. e., the P $2p_{3/2}$ will be at 128.9 eV if the surface Fermi level is close to CBM; and it will be close to 127.6 if the surface Fermi level is at VBM.

When measuring the surface Fermi level position, it is important to avoid surface charging. Back ohmic contacts were prepared on the samples for good electric contacts by using the method described in §3.3. Each samples was mounted on a holder using a copper ring pressed against the front surface of the sample. The peak position shift caused by surface charging will depend upon the intensity of the X-ray source. Therefore, by changing the X-ray intensity and monitoring the peak position, one is able to tell if there is surface charging or not. This method was frequently used in our measurement to ensure that the peak position is measured for samples without surface charging.

In Fig.4.24, we show the comparison of the measured binding energies of P 2p of

differently prepared n-type InP sample, (a) is from a UHV cleaved InP(011) sample (at flat band condition), (b) is from a S-passivated sample, (c) is from an InP sample prepared under the same conditions as for the S-passivated sample but without a final DI water rinse, i. e., there are oxidized sulfur and polysulfide on the surface (Fig.3.7).

It can be seen that the n-InP sample sulfur passivated without a DI water rinse has a upward band bending, up to 0.35±0.1 eV, while the S-passivated sample is at nearly flat band condition, like the UHV cleaved InP sample. The surface band bending on the unrinsed sample is probably caused by the residual material. Because the oxidized sulfur and polysulfide are very electronegative, they tend to attract electrons from the substrate to form a negative dipole (surface more negative than the layer below). The existence of this negative dipole will cause an upward band bending on the surface.

The surface Fermi level positions for differently treated InP are summarized in Fig.4.25. The error bar in the figure represents ±0.1 eV data scatter among the measured samples (for each surface treatment, more than 10 samples were prepared and measured).

From Fig.4.25, it can be seen that an as-etched n-InP sample has about 0.2 eV upward band bending, and this band bending is eliminated after the S-passivation. From the measurements on p-type InP, it is found that the Fermi level positions on p-type InP surfaces were hardly affected by the treatments. They are all at about 0.4~0.5 eV above the VBM. These experimental results show that the passivation process removes most acceptor-like surface states, reducing the band bending on n-type InP, but do not affect donor-like states and downward band bending on p-type samples.

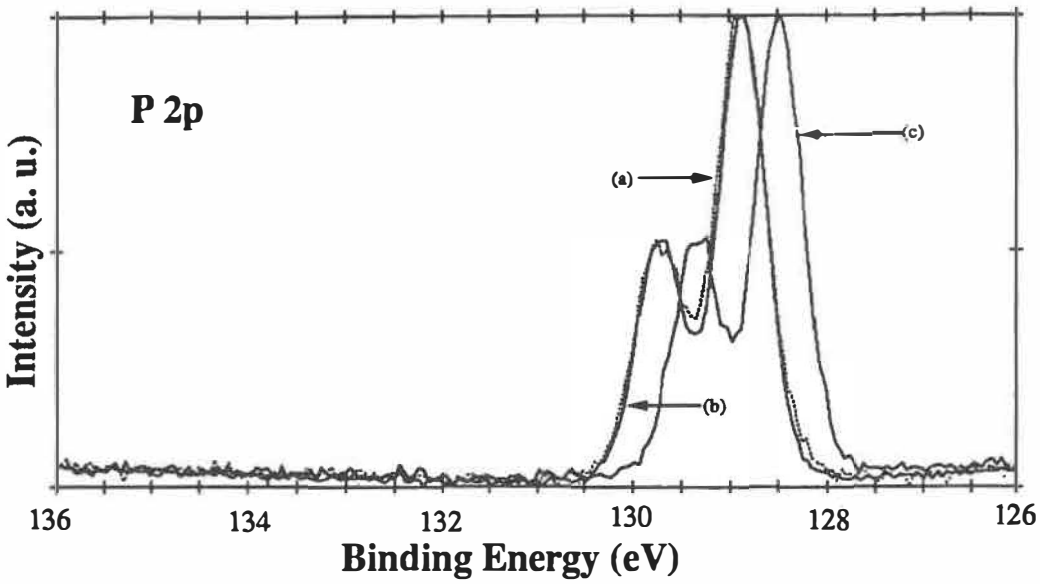

Figure 4.24 Binding energy difference due to the difference of surface Fermi level position. (a) UHV cleaved. (b) S-passivated. (c) sulfur treated but without DI water rinse.

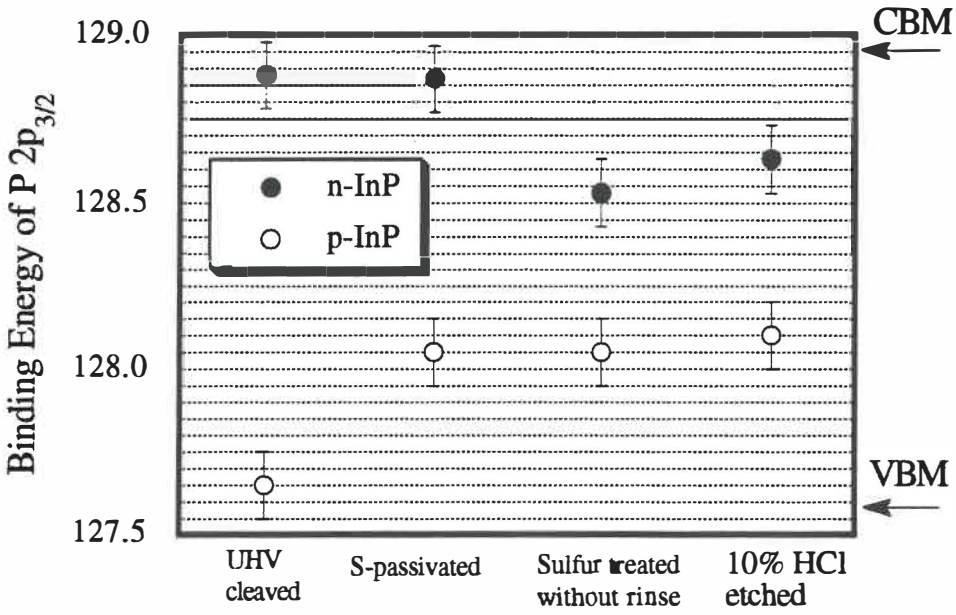

Figure 4.25 Surface Fermi level positions for differently treated InP samples.

4.3.2 Band Edge Photoluminescence Measurements

In this experiment, we investigate the change in the total band edge PL intensity brought about by the S-passivation process. The PL peaks were identified by comparing their peak energies with the data available in the literature. Both n- and p-type InP samples were used in PL intensity measurements. Four groups of samples were prepared for each type. The first group was as-etched, the second was etched and then annealed at 300^0C for 30 min in the preparation chamber of the VG ESCALAB (pressure ~10^{-9}mbar), the third was S-passivated, the fourth was S-passivated and then annealed under the same conditions as the second group.

Fig. 4.26 shows the PL spectra at 9 K for the four groups of n-type InP samples. The strong band-edge luminescence in the 1.3 -1.42 eV range consists of two prominent peaks. That at 1.417 eV is due to the recombination of excitons bound to neutral donors (D^0, X) [109]. That centered at 1.379 eV is most probably due to conduction band-to-neutral acceptor (e-A^0) recombination, but it is also possible that there is some contribution from the recombination of neutral donor-to-neutral acceptor (D^0–A^0), which should have a peak energy several meV lower than 1.379 eV [110]. The neutral acceptors in n-InP might be the residual impurity of Zn incorporated into the sample during crystal growth. The PL intensities for these peaks are listed in Table 4.4. The PL intensity of S-passivated InP (both as-prepared and annealed) is about 2-4 times higher than that of etched InP. Since there is no line-shape change in the spectra, the PL intensity increase is attributed to the reduction of non-radiative recombination centers at the surfaces by the S-passivation.

From Table 4.4, it may be seen that the intensity of the (D^0, X) peak increased

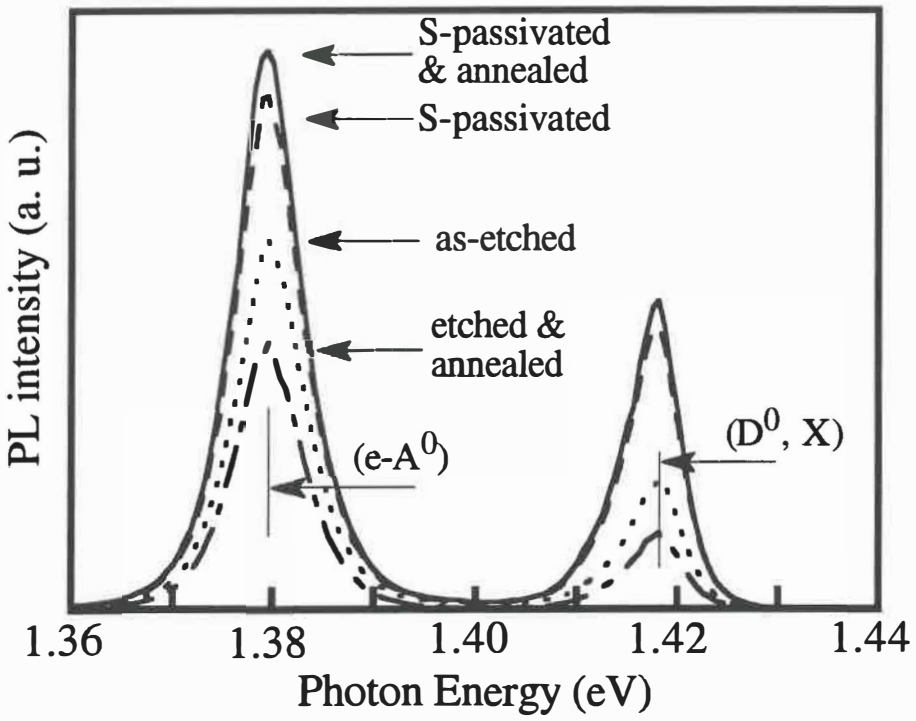

Figure 4.26 Band edge PL spectra at 9 K for differently treated n-InP.

Table 4.4 PL intensity at 9 K (n-InP)

	D^0, X	$e\text{-}A^0$	$D^0, X / e\text{-}A^0$
Etched	0.42	0.67	0.26
Etched & annealed	0.25	0.51	0.20
S-passivated	0.95	0.93	0.42
S-passivated & annealed	1.00	1.00	0.41

more than that of ($e\text{-}A^0$) after S-passivation. There are two possible reasons for this phenomenon. One is that the latter process is minority dopant controlled. That is, its saturated intensity is controlled by the number of neutral minority dopants, A^0, available in the sample, while the saturated intensity of the (D^0, X) peak is controlled by the number of neutral majority dopants, D^0, available in the sample. So the intensity of the ($e\text{-}A^0$) peak will not increase as much as that of the (D^0, X) peak by S-passivation due to the limited number of neutral acceptors in n-InP. Another possible reason is that the S-passivation

process not only reduces the non-radiative recombination centers, which leads to an overall PL intensity increase, but also removes hole traps on the surface, so that the (D^0, X) recombination process will be promoted by the passivation.

Fig.4.27 shows the PL intensities of the four groups of n-type InP at 60 K. Since the thermal excitation energy is about 5.7 meV at this temperature, most shallow donors are thermally ionized. There are fewer D^0 centers available in the sample, so that the peak at 1.379 eV is attributed to the (e-A^0) recombination, and the peak at 1.413 eV is attributed to the recombination of excitons bound to ionized donors (D^+, X). The related PL intensities are listed in Table 4.5. The PL intensity of S-passivated samples (both as-prepared and annealed) are 3~4 times higher than those of chemically etched InP.

Table 4.5 PL intensity at 60 K (n-InP)

	D^+, X	e-A^0	D^+, X /e-Å
Etched	0.23	0.20	1.65
Etched & annealed	0.20	0.19	1.44
S-passivated	0.77	0.76	1.42
S-passivated & annealed	1.00	1.00	1.40

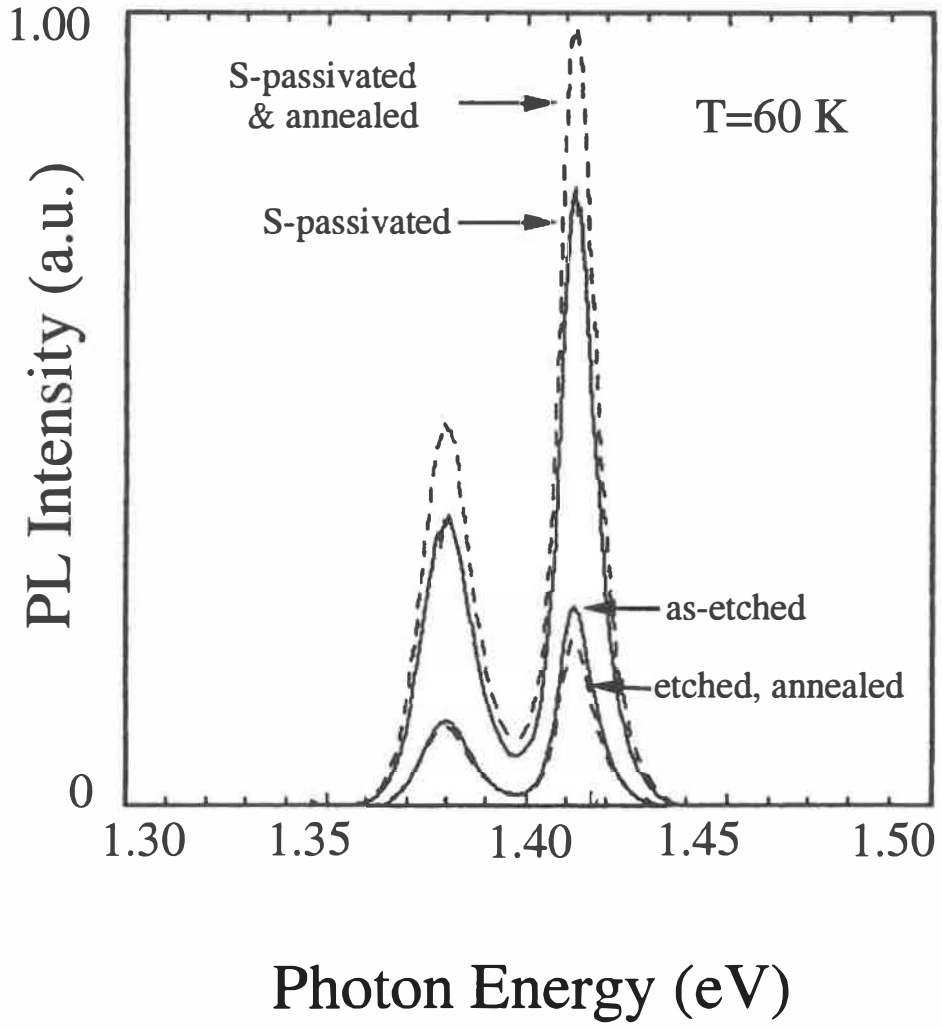

Figure 4.27 Band edge PL spectra at 60 K for differently treated n-InP.

The good resistance of the S-passivated InP surfaces to heat treatment is shown by the fact that in these measurements, there is a decrease in PL intensity for the etched InP samples after annealing, while the PL intensities for the S-passivated sample are nearly the same, improving slightly with annealing. The loss of the band edge PL intensity during annealing has been generally attributed to the incorporation of non-radiative recombination centers, probably due to loss of P, causing lifetime degradation [111]. This result might indicate that the strong chemical bonds between the sulfur and indium atom at passivated surface can reduce the loss of P in the near surface region. The slight increase of PL intensity by the annealing is probably due to the removal of some defects at the surface by the annealing. The PL intensity of the S-passivated and annealed sample is quite uniform over the surface, whereas that of the etched and annealed surface is not (intensities shown in Tables 4.4 and 4.5 are the maximum values). We repeated the measurements on four sets of n-type InP samples, and the tendency of PL intensity change is always the same.

Our result is different from that of Iyer et al [112]. In their experiment, the n-type InP(100) surfaces were treated in a dilute 'polysulfide solution', and the samples were directly dried by N_2 gas. There was a clearly visible crust on these surfaces. The photoluminescence intensity decreased by a factor of more than 20 after the polysulfide solution treatment. The difference between their results and ours might indicate that the InP sample treated with our passivation procedure has a relatively low density of surface non-radiative recombination center. Besides, the residual crust on their prepared surface will surely reduce the PL intensity. A clean surface is essential in order to compare the PL intensity from different samples.

Fig. 4.28 shows the band edge PL intensity measured on four groups of p-type InP samples at 9 K. The peak at 1.4186 eV is due to the recombination of free excitons

(X); that at 1.414 eV is due to the recombination of excitons bound to a neutral acceptor (A^0, X); and that at 1.379 eV is due to conduction band-to-neutral acceptor (e-A^0) recombination [109,110]. The related intensities are listed in Table 4.6. The PL intensity increased after S-passivation by a factor of 2 to 3 as compared to the as-etched sample. This shows that the S-passivation can reduce the non-radiative recombination centers on p-type InP surfaces as well. As in the case of n-type InP, the exciton related peak (A^0, X) increased more than the (e-A^0) peak after passivation. This also indicates the possibility of preferential removal of hole traps by the S-passivation. The absence of donor related peaks in the PL spectra of S-passivated p-type InP excludes the possibility of surface n-type doping caused by sulfur diffusion during the passivation process.

Table 4.6 PL intensity at 9 K (p-InP)

	A^0, X	e-A^0	A^0, X /e-A^0
Etched & annealed	0.15	0.49	0.59
Etched	0.43	0.69	1.19
S-passivated & annealed	0.47	0.69	1.34
S-passivated	1.00	1.00	1.98

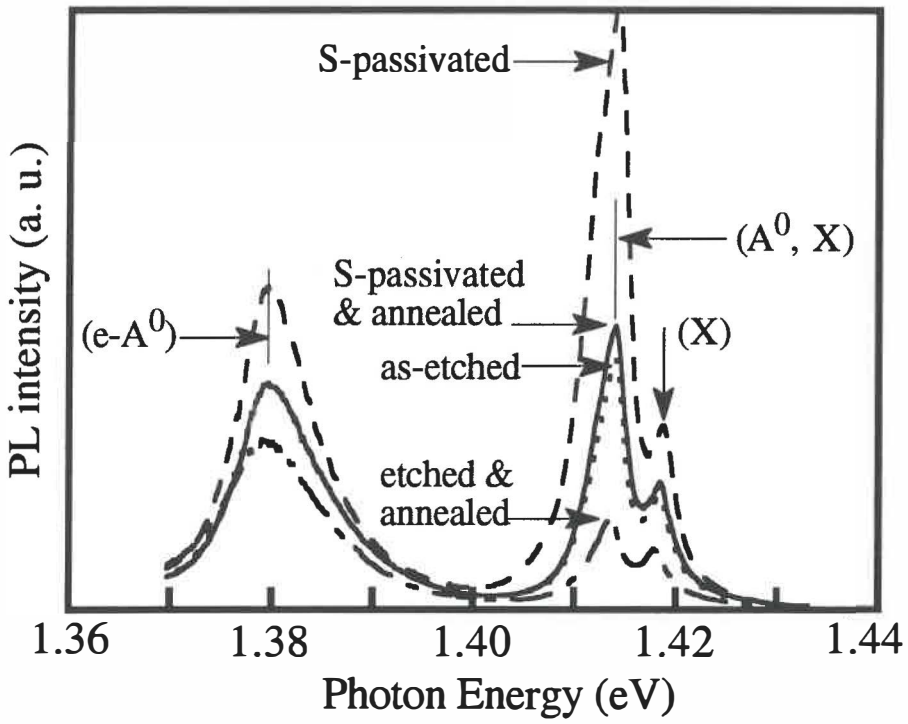

Figure 4.28 Band edge PL spectra at 9 K for differently treated p-InP.

The annealing process seems to have much more influence on the PL intensity of p-type InP than on that of n-type material. For chemically etched samples, the PL intensity decreased dramatically after annealing. The PL intensity of passivated samples also decreased after the annealing, but was still higher than that of as-etched samples. By comparing the relative intensities of the (A^0, X) and (e-A^0) peaks, it is found that the intensity of the (A^0, X) peak decreases much more than that of the (e-A^0) peak. One plausible explanation for this phenomenon is that not only non-radiative recombination centers, but also hole traps were produced on p-type InP during the annealing process. Non-radiative recombination centers reduce the overall band edge PL intensities. Hole traps reduce the population of holes in the valence band and thus reduce the probability of (A^0, X) recombination. Excess electrons, caused by hole trapping will counterbalance the decrease of the (e-A^0) peak, due to the increase of non-radiative recombination centers, produced by the annealing. Therefore the intensity of the (A^0, X) peak decreases more than that of the (e-A^0) peak.

After annealing, the PL intensity of the passivated p-type InP sample is still higher than that of as-etched sample, and the intensity of the (A^0, X) peak decreases much less (relative to e-A^0 peak) than that of the etched sample. This shows that fewer non-radiative recombination centers and hole traps were produced by the annealing of passivated p-type material. This indicates that the S-passivated sample resists the formation of non-radiative recombination centers and of hole traps as well. As in the n-type material, the PL intensity is quite homogeneous on the S-passivated surface both for as-prepared and annealed

sample, while the PL intensity on the etched sample is not homogeneous, especially on etched and annealed samples. The spectrum shown in Fig.4.28 for an etched and annealed sample is a typical one. We repeated the measurements on another set of p-type samples and obtained the same tendency.

The PL experiments have shown that after S-passivation, band edge PL intensity increases were observed for all peaks, for both n- and p- type samples, and at different measuring temperatures. This shows that S-passivation is effective on reducing non-radiative recombination centers on InP surfaces, both for n- and p-type material. In addition, there is indication of preferential removal of hole traps on the InP surface (both for n- and p-type samples) by the S-passivation process. The average enhancement of band edge PL intensity for n- and p-type InP samples after the S-passivation is a factor of 2 to 3. This enhancement is much lower than the three orders of magnitude increase obtained by Skromme et al. [20] on sulfur passivated GaAs samples. This difference is most probably due to the fact that the non-radiative surface recombination velocity on chemically etched InP is 2 to 3 orders of magnitude lower than that of GaAs [114, 115]. Therefore the relative PL intensity increase for InP by the sulfur passivation will not be as high as that for GaAs.

An annealing process can improve the surface properties by restoration of a more ordered structure, and by removal of surface stain resulting from treatment, but it will also produce defect states, as frequently seen for III-V compound materials. The PL intensity after the annealing will then depend upon the competition between these two processes. It is not clear why the PL intensity of the passivated n-type material are nearly the same before and after annealing, while the PL intensity of the passivated p-type material decrease after annealing. One possibility is that the annealing process produces defect states: those at

the mid-gap will act as effective recombination centers, those near the conduction band will act as effective electron traps when they are empty, and those close to the valence band will act as effective hole traps when they are filled by electrons. Since the excitation level used in our experiment is quite low, a relatively low trap density will be effective in reducing the PL intensity, so that we assume that the formation of these defect states will not affect the band bending. (This is a hypothesis, and has to be verified by measuring the surface Fermi level position on annealed samples.)

For the passivated n-type InP, since the surface Fermi level is close to the CBM, the hole traps near the VBM are filled by electrons, and the electron traps near the CBM are also filled, so that only the hole traps are active. The decrease of PL intensity caused by the formation of defect states are balanced by the PL intensity improvement caused by the restoration of a more ordered surface after the annealing, so that the PL intensity is nearly the same before and after the annealing.

But on the passivated p-type material, the surface Fermi level is about 0.4 to 0.5 eV above the VBM, as discussed in §4.3.1. The electron traps near the CBM are empty, and the hole traps near the VBM will also be filled by electrons. Therefore, these two kinds of carrier traps are both active in p-InP. The decrease of PL intensity caused by the formation of defect states can no longer be balanced by the improvement caused by the restoration of a more ordered surface after the annealing, so that a decrease in PL intensity is observed.

Another possibility is that dopant-related defect states formed upon annealing. This is quite similar to the annealing effect on band edge PL intensity of Te-doped GaAs [113], in which the Te-associated defects formed by annealing process act as very effective hole traps and cause a dramatic decrease of exciton peak. A series of PL measurements on differently doped InP samples would help to understand this phenomenon.

4.3.2 Schottky Diode I-V Characteristics Measurements on S-Passivated InP(100)

Schottky diode current-voltage characteristics were measured at room temperature. The Schottky diode parameters on differently treated n- an p-type InP are listed in Table 4.7, more than 20 samples were measured for each kind of diode.

The forward current-voltage behavior of the Schottky diodes that we prepared was assumed to follow equation (2.33). The effective Richardson constant used in the measurements is $A^*=9.4$ A $cm^{-2}K^{-2}$ for n-InP [116], and $A^*=76.8$ A $cm^{-2}K^{-2}$ for p-InP [95]. According the equation (2.33), a logarithmic plot of $[I/(1-\exp(-qV/k_BT))]$ vs V should be linear. Therefore, the barrier height, $q\phi_B$, can be determined by extrapolating the plot to zero bias voltage, and n from the slope of the plot.

The series resistance R_s was deduced at large forward bias voltage from the slop of V-I curve. This method is commonly used in diode I-V measurement [116, 117]. The data shown in the following has been corrected using measured R_s.

Fig.4.29 shows the typical forward bias I-V curves of Au/n-InP diodes prepared from etched, and S-passivated InP samples respectively. The I-V curve measured from S-passivated InP yields $q\phi_b = 0.42\pm0.02$ eV and $n= 1.1\pm0.1$, and that from the etched InP yields $q\phi_b= 0.32\pm0.02$ eV and $n= 1.5\pm0.1$. Both the barrier height and ideality factor were improved by the S-passivation.

The difficulty of using equation (2.25) to quantitatively estimate the interface state density is that the thickness of the interfacial layer on the diodes is unknown, and that the available data on work functions of Au are scattered from 4.70 eV [118, 119], 4.82 eV

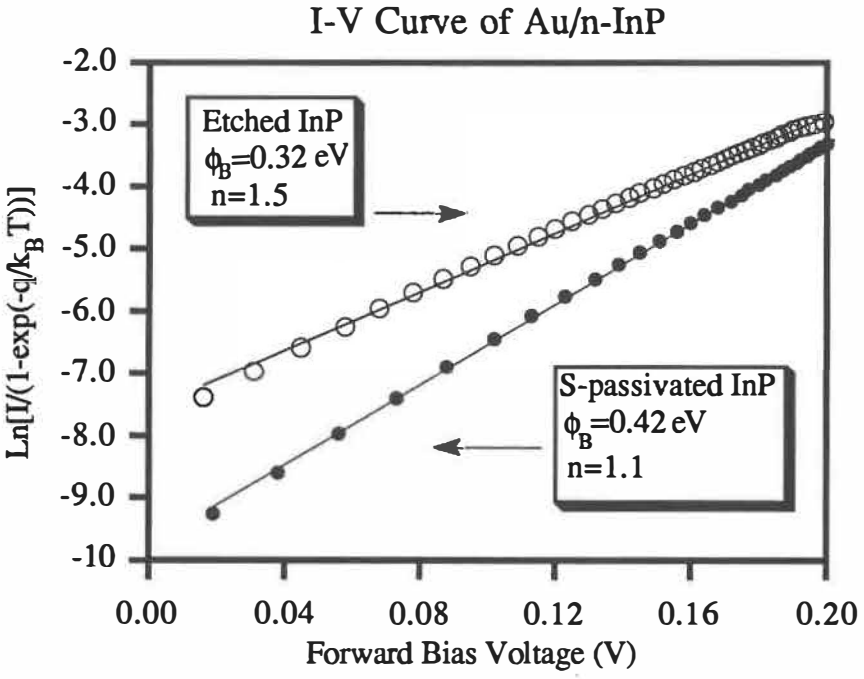

Figure 4.29 The current-voltage (I-V) characteristics of the Au/n-InP Schottky diodes prepared on S-passivated (filled circles), and etched (open circles) samples.

[93, 120] to 5.1 eV [95, 121]. But if we accept 4.87eV as an average value for the work function of Au, and the electron affinity 4.40 eV for InP [86] respectively, according to Schottky model, we would have $q\phi_b$ = 0.47 eV and n= 1 for an ideal Au/n-InP diode. Our experimental results are quite close to these values. The improvement in the ideality factor could be due to two factors (see §2.5.2): one possible cause is the reduction of the recombination current on the S-passivated samples, due to the reduction of surface recombination centers, which has been shown in PL measurements by the intensity increase after the S-passivation. Another possibility is that since the S-passivated sample is very stable in air, and has good resistance to surface oxidation and contamination, the interfacial layer, which is usually caused by surface oxidation and contamination [95], is expected to be much thinner than that on an etched sample. Therefore, the ideality factor will decrease [84].

The Al/n-InP diodes prepared on passivated samples yield $q\phi_b$= 0.30 eV, n=1.45, and $q\phi_b$ = 0.33 eV, n ≥ 2 for chemically etched samples. The quality of Al/n-InP were lower than those Au/n-InP, the linear part of the $\ln[I/(1-\exp(-qV/k_BT))]$ ~ V curve was relatively small. This is probably caused by the reactive metal characteristic of Al on the InP surface [121, 122], which will lead to the failure of the assumption of an abrupt interface. Fig.4.30 shows the barrier height dependance of n-type InP Schottky diodes on the work function of Au and Al. The Schottky barrier height on the etched n-InP is almost independent of the work function of the metal deposited, suggesting Fermi level pinning at the metal-(n-InP) interface. The barrier height of the S-passivated n-InP shows some dependence upon the metal work function. This indicates that the interface state density on the S-passivated samples is lower than that of chemically etched samples, and the Fermi

Table 4.7 The Parameters for Schottky Diodes at 300 K

parameter / Diode	Surface treatment	barrier height (ϕ_B, eV)	ideality factor (n)	reverse saturation current (I_0)	diode area (S)
Au/n-InP	etched	0.32±0.02	1.5±0.1	~ 10^{-3}A	4 x 10^{-4}cm^2
Au/n-InP	S-passivated	0.42±0.02	1.1±0.1	~ 10^{-5}A	4 x 10^{-4}cm^2
Al/n-InP	etched	0.33±0.02	~ 2	10^{-4} ~ 10^{-5} A	1 x 10^{-4}cm^2
Al/n-InP	S-passivated	0.30±0.02	1.4±0.1	~ 10^{-4}A	1 x 10^{-4}cm^2
Au/p-InP	etched	0.83±0.02	1.3±0.1	~10^{-11}A	4 x 10^{-4}cm^2
Au/p-InP	S-passivated	0.84±0.02	1.2±0.1	~10^{-11}A	4 x 10^{-4}cm^2

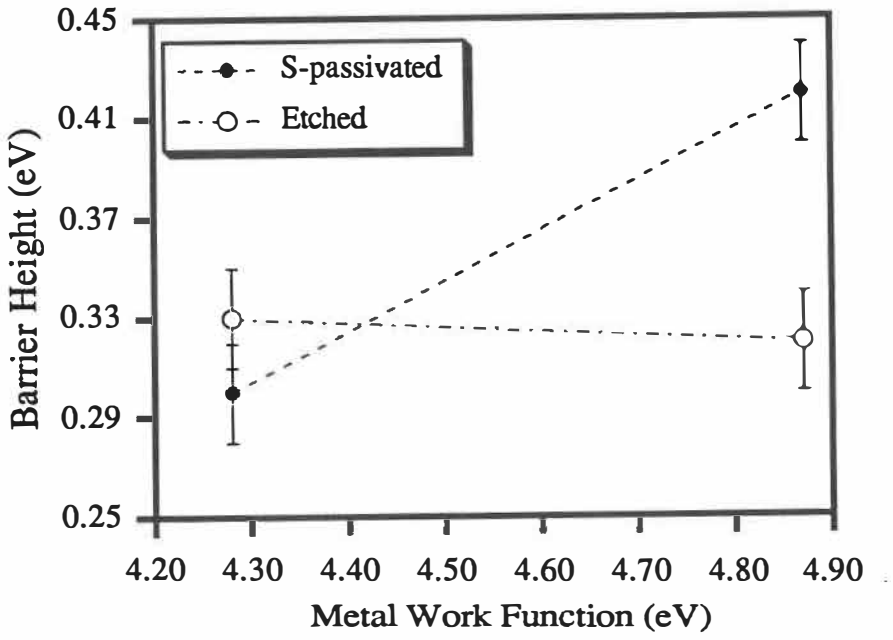

Figure 4.30 Metal work function dependence of Schottky barrier height for S-passivated, and etched n-InP.

level is not pinned, as can be seen from equation (2.26).Au/p-InP diodes prepared on S-passivated samples yield $q\phi_b$= 0.84±0.03 eV, n=1.2±0.1; and those of chemically etched samples give $q\phi_b$=0.83±0.03 eV, n =1.3 ±0.1. The I-V characteristics of Au/p-InP Schottky diodes show no evident difference between the etched and S-passivated samples, except that the ideality factor was slightly improved by the treatment. This may also indicate the decrease of the recombination centers at the interface. But it is not clear why the S-passivation has little effect on the barrier height of p-type InP Schottky diodes.

An anneal (300°C) before the metal deposition was used in order to eliminate the adsorbed water vapor at the surfaces, and to compare the annealing effects with the PL measurements. Especially, we expected to see a difference between the Schottky diodes prepared on annealed and non-annealed p-type material. In contrast to the PL measurements, no evident difference was found from I-V characteristic measurements between the annealed and non-annealed samples. This indicates that although the PL intensity decrease was evident on p-type material, the density of defect states produced by annealing is not so high to be able to change the electronic behavior of Schottky diodes. It also indicates that the electronic properties of a Schottky diode are largely controlled by the interface properties after metal deposition.

4.4 Discussion

From the experimental results discussed in §4.3, it has been shown that the InP(100)-(1x1)-S surface prepared by the S-passivation procedure has surface electronic

properties superior to those of chemically etched samples, and to 90^0C-sulfur-treated samples (as is discussed in Appendix I). The surface chemical composition and surface structural difference among these differently treated samples has been demonstrated. Therefore, it is reasonable to attribute the improved surface electronic properties to the strong and stable S-In bridge bond on the S-passivated InP surface.

Since there are no phosphorous atoms at the topmost layer of S-passivated InP surface, P-related surface states are absent. The surface indium dangling bonds are saturated by surface sulfur atoms, the In atom is fourfold coordinated at the S-passivated surface. The energy position of the S-In bonds are assumed to be below the valence band of InP, due to the strong bonding. The formation of the In-S bond leaves each surface sulfur atom with two atomic orbitals completely filled with two lone-pair electrons. In this way, the S-passivation removes P-related surface states, and replaces the In-related surface states with S-related surface states. These states are filled with paired electrons, and their energy position has to be estimated by theoretical calculation. But we might expect that their energy position should be well below that of In-related dangling bond due to the bound state of these paired electrons, and higher electronegativity of S as compared to In. If their energy position is below the valence band of InP or part of them are below the VBM, the surface state density in the energy gap will be greatly reduced. If some of the S-related states are above the VBM, they will act as donor-like surface states because they are filled when the surface is neutral. This might account for the nearly flat-band condition on n-type and the downward band bending on p-type InP after the S-passivation. Obviously this is only an assumption. A detailed theoretical calculation of the energy position of S-related surface states, and a detailed valence band photoemission study are needed, in order to get a better understanding of the surface electronic structure of the S-passivated surface.

Explanation of the improvement on n-type InP Schottky diode I-V characteristics by the S-passivation is not straightforward. Because a practical Schottky contact is a metal-interfacial layer-semiconductor interface problem, the metal deposition on an S-passivated InP surface is a very complicated process. One of the plausible explanations is that the S-passivated surface itself has a lower surface state density as shown by PL experiments. The nearly flat band condition on S-passivated n-InP surfaces indicates low acceptor-like surface state density in the energy gap. Therefore, the quality of the starting surface for the diode fabrication is better than that of the etched samples. Further, the S-passivated InP(100)-(1x1)-S surface is free of dangling bonds, as discussed above. The probability of chemisorption, which may release energy sufficient to create defects during the metal deposition is reduced. Therefore, the resulting metal-InP interface has a relatively low defect density. But the interface electronic properties can be affected by metal-semiconductor interdiffusion, and by chemical reactions at the metal-semiconductor interface. In particular, chemical reaction between the sulfur overlayer and the deposited metal is quite possible. Depending upon the detailed chemical bonding at the interface, the measured barrier height could be different, due to dipole formation between the metal and the semiconductor constituent. The importance of microscopic chemical effects at the metal-semiconductor interface was considered by Phillips [123], Andrews [124], and Brillson [125-127]. Detailed understanding of the Schottky diode electronic property improvement by the S-passivation requires a combination of electronic property measurements, such as in-situ measurement of surface work function, band banding, and surface chemical characterization using surface sensitive means such as synchrotron excited X-ray photoemission spectroscopy during the metal deposition.

Chapter 5

Conclusion

We have developed an improved $(NH_4)_2S$ solution passivation procedure for InP. While each of the steps employed here have been used by others, their combination (especially the use of a DI water rinse) gives better results than obtained previously. This procedure overcomes the deficiency of commonly used sulfur passivation procedures, such as: low sulfur coverage on the surface, poor reproducibility of surface chemical composition, and residual material on the treated surfaces. We have conducted a series of surface chemical, and surface structural analyses as well as some surface electronic property comparisons on such samples.

From the XPS measurement, we have found that phosphorous is absent at the topmost surface of the S-passivated InP(100) surface, and that the surface is completely terminated by one monolayer of 1:1 In-S surface compound. The sulfur atom bonds only to the surface indium atoms. The atomic ratio and the surface coverage of InS_x surface compound are sensitive to the passivation condition. Both illuminating and heating the solution during the process are necessary for obtaining one monolayer InS coverage. The final 10 min DI water rinse will not oxidize the S-passivated surface. On the contrary, it removes the residual material and leaves a very clean and stable surface.

Based on the high stability and the cleanliness of such treated surfaces, we have obtained clear and distinct LEED patterns for the first time from wet chemical treated InP surfaces. We have found that the LEED patterns can be completely indexed using the two dimensional reciprocal lattice parameters of an ideal InP(100) structure, and we concluded

that the S-passivated InP(100) surface has a (1x1) structure, and can be denoted as InP(100)-(1x1)-S. A corresponding structural model has been proposed for this surface. In this model the sulfur atom is assumed to form bridge bonds with its two neighboring surface indium atoms along the [011] direction.

The possibility of extensive anion (S, P) exchange at the surface region by the S-passivation treatment was excluded by the XPD experiments. We have found that the sulfur atoms are present only at the topmost layer. The angle between the S-In bond and the (100) plane was estimated to be 38 ± 2^0 from the XPD measurement.

Our proposed structural model has been further confirmed by XANES measurements. The XANES results show that the S-In bond is in the $(0\bar{1}1)$ plane, and is 40 ± 2^0 from the (100) plane. The XANES data also indicate that the surface sulfur atom is free of dangling bonds.

By estimating the surface Fermi level position from XPS data, we have found that S-passivated n-InP is nearly at flat band condition, and that p-InP has an about 0.4 eV downward band bending. This indicates the absence of acceptor-like surface states in the energy gap, and the existence of donor-like surface states after the S-passivation. From the band edge PL intensity measurements, we have shown that the S-passivation can effectively reduce the non-radiative recombination centers at the InP surface, both for n- and p-type, increasing the photoluminescence intensity. We have also found that S-passivated samples have good resistance to heat treatment, and to the formation of non-radiative recombination centers.

From the Schottky diode I-V characteristics measurement, we have found that both the barrier height and ideality factor of Au/n-InP diode were improved by the S-

passivation. The barrier height on the S-passivated n-InP shows some dependence on the metal work functions. This indicates improvement of interface electronic properties by the S-passivation.

The high surface chemical stability and the improved surface electronic properties are attributed to the formation of InP(100)-(1x1)-S structure. But our present understanding of the surface electronic structure of this S-InP system is quite limited. More detailed research work has to be done. A valence band photoemission experiment using UPS [16, 127] could be used to study the distribution of occupied surface states in the band gap. Inverse photoemission can be used to study the unoccupied electronic states [128]. These experiments will help to understand the change of the surface state distribution in the energy gap by the S-passivation.

Low temperature band edge PL measurements, including deep level PL spectra (infrared range) can be used to study the recombination process on such surfaces. High purity samples should be used so that the PL spectra will be well separated. By changing the measuring temperature, one will be able to see different peaks, due to the competition among the different recombination processes. The influence of S-passivation on different recombination processes can be deduced by comparing the intensities of these peaks before and after the passivation. This kind of information is very helpful for understanding the surface electronic structure after the passivation and how the passivation improves the surface electronic properties.

It is not clear yet how the light illumination promotes the sulfur passivation. But we believe that this is a photo-electrochemical process. One hypothesis is that we are using the photons with energies greater than the energy gap of InP to create electron-hole pairs on the surface, which participate in the chemical reaction. In $(NH_4)_2S$ solution, HS^- is the

dominant ion species. When the S atom in HS^- ion forms covalent bonds with surface In atoms, a H^+ ion will be ejected into the solution, and two electrons will be transferred to the InP surface. In order to continue the reaction, these electrons must be neutralized by creating holes on the surface. The electrons promoted from the valence band are used to reduce the H^+ ions into H_2. Several experiments can be done to verify this hypothesis. One is to prepare the samples under the illumination with photon energies less than the energy gap; another experiment is to prepare the sample in an electric field with its direction towards the sample surface so that holes will be depleted from the surface region. According to the hypothesis, the chemical reaction will be impeded, and the surface should show lower In-S coverage.

The study of the formation of metal/S-passivated InP interfaces is complicated by the fact that our sample is prepared in air. The sample is usually contaminated by one monolayer equivalent of oxygen and carbon, which will react with the deposited metals. If they can be removed, e.g. by using mild electron bombardment, it will be very interesting to follow and to correlate the electronic and chemical structure of such interfaces as they are built up monolayer-by-monolayer, using XPS or synchrotron-excited photoemission spectroscopy (SXPS).

The ideality factor deduced from I-V measurement reflects the overall effects of interfacial layer thickness, recombination at the interface, and in the whole depletion region. From the ideality factor, it is difficult to obtain detailed information about the recombination process at the interface. Low energy cathodoluminescence spectroscopy (CLS) can be used to probe the recombination properties of metal/semiconductor interface [129]. In this technique, the incident electrons, with kinetic energies from hundreds to thousands electron

volts, penetrate the metal overlayer and produce a cascade of secondaries and electron-hole pairs within the top 100 to 1000 Å. These e-h pairs recombine via band-to-band or deep level transition. By adjusting the energy of incident electrons in CLS measurements, one can preferentially enhance the emission near the top semiconductor surface, so that the electronic structure at the 'buried' interface can be directly probed.

From our preliminary work on GaAs using XPS and LEED, it has been found that the passivation effects of this procedure on GaAs is not as good as on InP. The LEED patterns from these surfaces are quite diffuse, and can only be obtained when the energy of incident electrons exceeds ~150 eV. This indicates the existence of surface oxide or contamination at the surfaces. The XPS results show that the treated surfaces are mainly covered with S-Ga bonds, no S-As and O-As bonds were found. This is quite close to our results on InP material. But O-Ga bonds were found at the treated surfaces, although the amount is much less than that on chemically etched samples. The coverage of S-Ga bonds at the GaAs surfaces is then believed to be less than one monolayer. Since the surface chemical bonding after the passivation are quite similar, the difference between the passivation effects on GaAs and InP seems to be caused by the incomplete removal of Ga-O bonds at the surfaces by the passivating solution under conditions for the InP. The passivation effects of GaAs might be improved by modifying the experimental conditions, such as slightly raising the temperature, using a longer passivation time, or using a stronger light source. When this is done, the procedure is expected to work for GaP as well. Since the passivating solution can remove the surface As, as it does for P, we expect that our present passivation conditions can be directly used for InAs.

references:

[1] WILLIAMS, R. H., in *Physics and Chemistry of III-V Compound Semiconductor Interfaces*, WILMSEN, C. W., ed., (Plenum Press, New York, 1985); MEINERS, L. G., in *Physics and Chemistry of III-V Compound Semiconductor Interfaces*, WILMSEN, C. W., ed., (Plenum Press, New York, 1985)

[2] SPICER, W. E., LINDAU, I., SKEATH, P., and SU, C. Y., "Unified Defect Model and Beyond", J. Vac. Sci. Technol. 17, 1019 (1980).

[3] SPICER, W. E., CHYE, P. W., SKEATH, P. R., SU, C. Y., and LINDAU, I., "New and Unified Model for Schottky Barrier and III-V Insulator Interface States Formation", J. Vac. Sci. Technol. 16, 1422 (1979).

[4] LILE, D. L., in *Physics and Chemistry of III-V Compound Semiconductor Interfaces*, WILMSEN, C. W., ed., (Plenum Press, New York, 1985).

[5] SPICER, W. E., LINDAU, I., PIANETTA, CHYE, P. W., and GARNER, C. M., "Fundalmental Studies of III-V Surfaces and (III-V)-Oxide Interface", Thin Solid Films 56, 1 (1979).

[6] BANERJEE, S., SRIVASTAVA, A. K., and ARORA, B. M., "Thermal Degradation of InP in Open Tube Processing: Deep-Level Photoluminescence", J. Appl. Phys. 68, 2324 (1990).

[7] ZEISSE, C.R., MESSICK, and LILE, D. L., "Electrical Properties of Anodic and Pyrolytic Dielectrics on Gallium Arsendide", J. Vac. Sci. Technol. 14, 957 (1977).

[8] MEINERS, L. G., "Electrical Properties of the Gallium Arsenide-Insulator Interface", J. Vac. Sci. Technol. 15, 1402 (1978).

[9] WIEDER, H. H. "Perspectives on III-V Compound MIS Structures", J. Vac. Sci. Technol. 15, 1498 (1978).

[10] WOODALL, J. M., and FREEOUF, J. L., "GaAs Metallization: Some Problems and Trends", J. Vac. Sci. Technol. 19, 794 (1981).

[11] NELSON, R. J., WILLIAMS, J. S., LEAMY, H. J., MILLER, B., CASEY, H. C., Jr., PARKINSON, B. A., and HELLER, A., "Reduction of GaAs Surface Recombination Velocity by Chemical Treatment", Appl. Phys. Lett. 36, 76 (1980).

[12] MASSIES, J., CHAPLART, J., LAVIRON, M., and LINH, N. T., "Monocrystalline Aluminium Ohmic Contact to n-GaAs by H_2S Adsorption", Appl. Phys. Lett. 38, 693 (1981).

[13] OFFSEY, S. D., WOODALL, J. M., WARREN, A. C., KIRCHNER, P. D., CHAPPELL, T. I., and PETTIT, G. D., " Unpinned (100) GaAs Surfaces in Air Using Photochemistry", Appl. Phys. Lett. 48, 475 (1986).

[14] DUKE, C. B., PATON, A., FORD, W. K., KAHN, A., and Carelli, j., "Dynamical Analysis of Low-Energy Electron Diffraction Intensities from GaAs (100)-p(1x1)-Sb(1ML)", Phys. Rev. B 26, 803 (1982).

[15] MAILHIOT, C., DUKE, C. B., and CHADI, D. J., "Sb Overlayers on (110) Surfaces of III-V Semiconductors: Total-Energy Minimization and Surface Electronic Structure", Phys. Rev. B 31, 2213 (1985).

[16] McGOVERN, I. T., WHITTLE, R., ZAHN, D. R. T., MULLER, C., NOWAK, C., CAFOLLA, A., and BRAUN, W. "Photoelectron Bandstructure of InP(110)-Sb Monolayers", J. Phys.: Condens. Matter 3, S367 (1991).

[17] SANDROFF, C. J., NOTTENBURG, BISCHOFF, J. C., and BHAT. R., "Dramatic Enhancement in the Gain of A GaAs/AlGaAs Heterostructure Bipolar Transistor by Surface Chemical Passivation", Appl. Phys. Lett. 51, 33 (1987).

[18] YABLONOVITCH, E., SANDROFF, C. J., BHAT, R., and GMITTER, T., "Nearly Ideal Electronic Properties of Sulfide Coated GaAs Surfaces", Appl. Phys. Lett. 51, 439 (1987).

[19] FARROW, L. A., SANDROFF, C. J., and TAMARGO, M. C., " Raman Scattering Measurements of Decreased Barrier heights in GaAs Following Surface Chemical Passivation", Appl. Phys. Lett. 51, 1931 (1987).

[20] SKROMME, B. J., SANDROFF, C. J., YABLONOVITCH, E., and GMITTER, T., " Effects of Passivating Ionic Films on The Photoluminescence Properties of GaAs", Appl. Phys. Lett. 51, 2022 (1987).

[21] CARPENTER, M. S., MELLOCH, M. R., LUNDSTROM, M. S., and TOBIN, S. P., " Effects of Na_2S and $(NH_4)_2S$ Edge Passivation Treatments on the Dark Current-Voltage Characteristics of GaAs pn diodes", Appl. Phys. Lett. 52, 2157 (1988).

[22] FAN, J., OIGAWA, H., and NANNICHI, Y., "Metal-Dependent Schottky Barrier Height with the $(NH_4)_2S_x$ -Treated GaAs", Jpn. J. Appl. Phys. 27, L2125 (1988).

[23] TIEDJE, T., COLBOW, K. M., ROGERS, D., FU, Z., and EBERHARDT, W., "Ultraviolet Photoemission Studies of GaAs (100) Surfaces Chemically Stabilized by H_2S Treatments", J. Vac. Sci. Technol. B7, 837 (1989).

[24] IYER, R., CHANG, R. R., and LILE, D. L., " Sulfur as a Surface Passivation for InP", Appl. Phys. Lett. 53, 134 (1988).

[25] IYER, R., CHANG, R. R., DUBEY, A., and LILE, D. L., "The Effect of Phosphorous and Sulfur Treatment on the Surface Properties of InP", J. Vac. Sci.

Technol. B6, 1174 (1988)

[26] OIGAWA, H., FAN, J., NANNICHI, Y., SUGAHARA, H., and OSHIMA, M., "Universal Passivation Effect of $(HN_4)_2S_x$ Treatment on the Surface of III-V Compound Semiconductors", Jpn. J. Appl. Phys. 30, L322 (1991).

[27] OHNO, H., KAWANISHI, H., AKAGI, Y., NAKAJIMA, Y., and HIJIKATA, T., " AES and XPS Studies of Surface of $Al_xGa_{1-x}As$ (110) Treated by ammonium Sulfide", Jpn. J. Appl. Phys. 29, 2473 (1990).

[28] TURCO, F. S., SANDROFF, C. J., HEDGE, M. S., and TAMARGO, M. C., "Thermal and Chemical Stability of Se-Passivated GaAs Surfaces", J. Vac. Sci. Technol. B8, 856 (1990).

[29] CHAMBERS, S. A., and SUNDARAM, V. S., " Passivation of GaAs (001) Surfaces by Incorporation of Group VI Atoms: A Structural Investigation", J. Vac. Sci. Technol. B9, 2256 (1991).

[30] SHIGEKAWA, H., HASHIZUME, T., OIGAWA, H., MOTAI, K., MERA, Y., NANNICHI, Y., SAKURAI, T., "Surface Structure of Selenium-Treated GaAs (001) Studied by Field Ion Scanning Tunneling Microscopy", Appl. Phys. Lett. 59, 2986 (1991).

[31] SANDROFF, C. J., HEDGE, M. S., and CHANG, C. C., " Structure and Stability of Passivating Arsenic Sulfide Phases on GaAs Surfaces", J. Vac. Sci.Technol. B7, 841 (1989).

[32] CARPENTER, M. S., MELLOCH, M. R., COWANS, B. A., DARDAS, Z., and DELGASS, W. N., "Investigation of Ammonium Sulfide Surface TreAtments on GaAs", J. Vac. Sci. Technol. B7, 845 (1989).

[33] SPINDT, C. J., LIU, D., MIYANO, K., MEISSNER, P. L., CHIANG, T. T.,

KENDELEWICZ, T., LINDAU, I., and SPICER, W. E., "Vacuum Ultraviolet Photoemission Spectroscopy of $(NH_4)_2S$-Treated GaAs (100) Surfaces", Appl. Phys. Lett. 55, 861 (1989).

[34] WILMSEN, C. W., GEIB, K. M., SHIN, J., IYER, R., LILE, D. L., "The Sulfurized InP Surface", J. Vac. Sci. Technol. B7, 851 (1989).

[35] LAU, W. M., JIN, S., WU, X. -W., and INGREY, S., " In Situ X-Ray Photoelectron Spectroscopic Study of Remote Plasma Enhanced Chemical Vapor Deposition of Silicon Nitride on Sulfide Passivated InP", J. Vac. Sci. Technol. B8, 848 (1990).

[36] LAU, W. M., JIN, S., WU, X. -W., and INGREY, S., "Studies on Type-Inversion of Sulfide-Treated p-InP", J. Vac. Sci. Technol. A9, 994 (1991).

[37] TIEDJE, T., WONG, P. C., MITCHELL, K. A. R., EBERHARDT, W., FU, Z., and SONDERICKER, D., "UV Photoemission Study of Sulfide Passivated GaAs Surfaces", Solid State Commun. 70, 355 (1989).

[38] NANNICHI, Y., FAN, J., OIGAWA, H., KOMA, A., "A Model to Explain the Effective Passivation of the GaAs Surface by $(NH_4)_2S_x$ Treatment", Jpn. J. Appl. Phys. 27, L2367 (1988).

[39] TAO, Y., YELON, A., SACHER, E., LU, Z. H., GRAHAM, M. J., in *Chemical Surface Preparation, Passivation and Cleaning for Semiconductor Growth and Processing*, NEMANICH, R. J., HELMS, C. R., HIROSE, M., and RUBLOFF, G. W., eds. Mat. Res. Soc. Symp. Proc. 259, 293 (1992).

[40] KATAYAMA, M., AONO, M., OIGAWA, H., NANNICHI, Y., SUGAHARA, H., and OSHIMA, M., "Surface Structure of InAs (001) Treated with $(NH_4)_2S_x$ Solution", Jpn. J. Appl. Phys. 30, L786 (1991).

[41] HIRAYAMA, H., MATSUMOTO, Y., OIGAWA, H., and NANNICHI, Y., "Reflection High-Energy Electron Diffraction and X-Ray Photoelectron Spectroscopic Study on $(NH_4)_2S_x$ -Treated GaAs (100) Surfaces", Appl. Phys. Lett. 54, 2565 (1989).

[42] YABLONOVITCH, E., SKROMME, B. J., BHAT, R., HARBISON, J. P., GMITTER, T. J., "Band Bending, Fermi Level Pinning, and Surface Fixed Charge on Chemically Prepared GaAs Surfaces", Appl. Phys. Lett. 54, 555 (1989).

[43] BESSER, R. S., HELMS, C. R., "Effect of Sodium Sulfide Treatment on Band Bending in GaAs", Appl. Phys. Lett. 52, 1707 (1988).

[44] HASEGAWA, H., ISHII, H., SAWADA, T., SAITOH, T., KONISHI, S., LIU, Y., and OHNO, H., "Control of Fermi Level Pinning and Recombination Processes at GaAs Surfaces by Chemical and Photochemical Treatments", J. Vac. Sci. Technol. B6, 1184 (1988).

[45] SPINDT, C. J., and SPICER, W. E., "Sulfur Passivation of GaAs Surfaces: A Model for Reduced Surface Recombination without Band Flattening", Appl. Phys. Lett. 55, 1653 (1989).

[46] SPICER, W. E., NEWMAN, N., and SPINDT, C. J., ""Pinning" and Fermi Level Movement at GaAs Surfaces and Interfaces", J. Vac. Sci. Technol. A8, 2084 (1990).

[47] SPICER, W. E., LILIENTAL-WEBER, Z., WEBER, E. R., NEWMAN, N., et al. "The Advanced Unified Defect Model for Schottky Barrier Formation", J. Vac. Sci. Technol. B6, 1245 (1988).

[48] OHNO, T., "Passivation of GaAs (001) Surfaces by Chalcogen Atoms (S, Se, and Te)", Surf. Sci. 255, 229 (1991).

[49] BERTNESS, K. A., KENDELEWICZ, T., LIST, R.S., WILLIAMS, M. D., LINDAU, I., and SPICER, W. E., "Fermi Level Pinning During Oxidation of Atomically Clean n-InP(110)", J. Vac. Sci. Technol. A 4, 1424 (1986).

[50] FELDMAN, L. C., and MAYER, J. W., *Fundamental of Surface and Thin film Analysis,* (North-Holland, New York, 1986).

[51] SPICER, W. E., "Photoemissive, Photoconductive, and Optical Absorption Studies of Alkali-Antimony Compounds", Phys. Rev. 112, 114 (1958).

[52] LEY, L. in *The Physics of Hydrogenated Amorphous Silicon II,* JOANNOPOULOS, J. D. and LUCOVSKY, G., eds. (Springer-Verlag, New York, 1984).

[53] SEAH, M. P., and DENCH, W. A., "Quantitative Electron Spectroscopy of Surfaces: A Standard Data Base for Electron Inelastic Mean Free Paths in Solids", Surf. Interf. Anal, 1, 2 (1979).

[54] SIEGBAHN, K., NORDLING, C., JOHANSSON, G., HEDMAN, J., HEDEN, P. F., HAMRIN, K., GELIUS, U., BERGMARK, T., WERME, L. O., MANNE, R., and BAER,Y., *ESCA Applied to Free Molecules*, (North Holland, Amsterdam, 1969)

[55] WAGNER, C. D., RIGGS, W. M., DAVIS, L. E., and MOULDER, J. F., *Handbook of X-Ray Photoelectron Spectroscopy,* MUILENBERG, G. E., ed., (Perkin-Elmer Corporaton , Eden Praire, Minnesota, 1979).

[56] SEAH, M. P. in *practical Surface Analysis by Auger and X-ray Photoelectron Spectroscopy,* BRIGGS, D., and SEAH, M. P., eds, (John Wiley & Sons, New York, 1983)

[57] ERTL, G. and KUPPERS, J., *Low Energy Electrons and Surface Chemistry*,

(VCH Verlagsgesellschaft, Weinheim, 1985).

[58] WAGNER, C. D., in *practical Surface Analysis by Auger and X-ray Photoelectron Spectroscopy,* BRIGGS, D., and SEAH, M. P., eds, (John Wiley & Sons, New York, 1983)

[59] BRIGGS, D., and RIVIERE, J. C., in *practical Surface Analysis by Auger and X-ray Photoelectron Spectroscopy,* BRIGGS, D., and SEAH, M. P., eds, (John Wiley & Sons, New York, 1983)

[60] CARDONA, M. and LEY, L., in *Photoemission in Solids I,* CARDONA, M., and LEY, L. , eds. (Springer-Verlag, Berling, 1978).

[61] SIEGBAHN, K., NORDLING, C., FAHLMAN, A., NORDBERG, K., HARMRIN, K., HEDMAN, J., JOHANSSON, G., BERGMARK, T., KARLSSON, S. E., LINDGREN, I., and LINDBERG, B., *ESCA: Atomic, Molecular and Solid State Structure By Means of Electron Spectroscopy*, (Almqvist and Wiksells, Uppsala, 1967).

[62] EISBERG, R., and RESNICK, R., *Quantum Physics of Atoms, Molecules, Solids, Nuclei, and Particles*", 2nd edition, (John Wiley & Sons, New York, 1985)

[63] COHEN-TANNOUDJI, C., DIU, B., and LALOE, F., *Quantum Mechanics*, 2, (Hermann, Paris; John Wiley & Sons, New York, 1977)

[64] COWLEY, J. M., *Diffraction Physics*, (North-Holland, Amsterdam, 1975).

[65] WOODRUFF, D. P. and DELCHAR, T. A., *Modern Techniques of Surface Science*, (Cambridge University Press, Cambridge, 1986).

[66] CLARKE, L.J., *Surface Crystallography* , (John Wiley & Sons, New York, 1985).

[67] SIEGBAHAN, K., GELIUS, U., SIEGBAHAN, H., and OLSON, E., "Angular

Distribution of Electrons in ESCA Spectra from a Single Crystal", Phys. Lett. 32A, 221 (1970)

[68] KONO, S., GOLDBERG, S. M., HALL, N. F. T., and FADLEY, C. S., "Azimuthal Anisotropy in Core-Level X-Ray Photoemission from c(2x2) Oxygen on Cu (001): Experimental and Single-Scattering Theory", Phys. Rev. Lett. 41, 1831(1978).

[69] EGELHOFF, W. F., Jr., "A New Tool for Studing Epitaxy and Interfaces: The XPS Searchlight Effect", J. Vac. Sci. Technol. A 3, 1511(1985).

[70] PARK, C. Y., ABUKAWA, T., HIGASHIYAMA, K., and KONO, S., "Analysis of The Atomic Structure of the Si (111)$\sqrt{3} \times \sqrt{3}$ – Bi Surface by X-Ray Photoelectron Diffraction", Jpn. J. Appl. Phys. 20, L1335 (1987).

[71] FADLEY, C. S., in *X-rays in Materials Analysis: Novel Applications and Recent Developments*, RUSCH, T. W., Ed. (Springer-Verlag, Berling, 1978).

[72] SHIRLEY, D. A., "Surface and Adsorbate Structural Studies by Photoemission in the $h\upsilon$ = 50- To 500-eV Range", CRC Crit. Rev. Solid State Mat. Sci. 10, 373 (1982).

[73] EGELHOFF, W. F., Jr., "X-ray Photoelectron and Auger Electron Forward Scattering: A New Tool for Surface Crystallography", CRC Crit. Rev. Solid State Mat. Sci. 16, 213 (1990).

[74] TONG, S. Y., PUGA, M. W., POON, H. C., and XU, M. L., in *Chemistry and Physics of Solid Surface* VI, VANSELOW, R. and HOWE, R., Eds. (Springer-Verlag, Berlin, 1986).

[75] EGELHOFF, W. F., Jr., "Role of Multiple Scattering in X-Ray Photoelectron

Spectroscopy and Auger-Electron Diffraction in Crystals", Phys. Rev. Lett. 59, 559 (1987).

[76] POON, H. C., and TONG, S. Y., "Focusing and Diffraction Effects in Angle-Resolved X-Ray Photoelectron Spectroscopy", Phys. Rev. B 30, 6122 (1984).

[77] ARMSTRONG, R. A., and EGELHOFF, W. F., Jr., "An Analysis of Angular Dependent XPS Peak Intensities", Surf. Sci. 154, L225 (1985).

[78] TONG, S. Y., POON, H. C., and SNIDER, D. R., "Importance of Multiple Forward Scattering in Medium- and High-Energy Electron Emission and/or Diffraction Spectroscopies", Phys. Rev. B 32, 2096 (1985).

[79] GERSHENZON, M., in *Semiconductors and Semimetals,* 2, WILLARDSON, R. K., and BEER, A. C., eds., (Academic Press, New York, 1966).

[80] BEBB, H. B. and WILLIAMS, E. W., in *Semiconductors and Semimetals*, 8, WILLARDSON, R. K., and BEER, A. C., eds., (Academic Press, New York, 1972).

[81] PIERRET, R. F., *Advanced Semiconductor Fundamentals*, (Addison-Wesley, Menlo Park, California, 1987)

[82] WILMSEN, C. W., KIRCHNER, P. D., BAKER, J. M., MCINTURFF, D. T., PETTIT, G. D., and WOODALL, J. M., "Characterization of Photochemically Unpinned GaAs", J. Vac. Sci. Technol. B6, 1180 (1988).

[83] RHODERICK, E. H., *Metal-Semiconductor Contacts*, (Clarendon Press, Oxford, 1978).

[84] RHODERICK, E. H., and WILLIAMS, R.H., *Metal-Semiconductor Contacts*, 2nd edition, (Clarendon Press, Oxford, 1988).

[85] SZE, S. M., *Physics of SemiconductorDevices* (Wiley, New York, 1969).

[86] SHARMA, B. L., and GUPTA, S. C., "Metal-Semiconductor Barrier Junctions", Solid-State Technol. 23,90 (1980); 23, 97 (1980).

[87] MONCH, W., "On the Physics of Metal-Semiconductor Interfaces", Rep. Prog. Phys. 53, 221 (1990).

[88] SCHOTTKY, W., "Halbleitertheorie der Sperrschicht", Naturwissenschaften, 26, 843 (1938).

[89] MOTT, N. F., "Note on the Contact between a Metal and an Insulator or Semiconductor", Proc. Camb. Phil. Soc. 34, 568 (1938).

[90] BARDEEN, J. B.,"Surfsce States and Recfitification at A Metal-Semiconductor Contact", Phys. Rev. 71, 717 (1947).

[91] COWLEY, A. M., and SZE, S. M., "Surface States and Barrier Height of Meta-Semiconductor System", J. Appl. Phys. 36, 3212 (1965).

[92] PECKERAR, M., "On the Origin of the Increase in Schottky Barrier Height with Interfacial Oxide Thickness", J. Appl. Phys. 45, 4652 (1974).

[93] HATTORI, K., IZUMI, Y., "The Electrical Characterics of InP Schottky Diodes", J. Appl. Phys. 52, 5699 (1981).

[94] BETHE, H. A., " Theory of the Boundary Layer of Crystal Rectifiers", MIT Radiation Laboratory Reports, 43-12, 1942.

[95] TYAGI, M. S., in *Metal-Semiconductor Schottky Barrier Junctions and Their Applications*, SHARMA, B. L., ed., (Plenum Press, New York, 1984).

[96] WILLIAMS, R. H., VARMA, R. R., and MCKINLEY, A., "Cleaved Surfaces of Indium Phosphide and Their Interfaces with Metals Electrodes", J. Phys. C: Solid State Phys. 10, 4545 (1977).

[97] HUIJSER, A., VAN LAAR, J., and VAN LOOY, T. L., "Electronic Surface

Properties of UHV-Cleaved III-V Compounds", Surf. Sci. 62, 472 (1977).

[98] DONNAY, J. D. H., and ONDIK, H. M., Crystal Data - Determinative Tables, 3rd edition, 2, (National Bureau of Standards, Washington, 1973).

[99] CLARK, D. T., FOK, T., ROBETS, G. G., and SYKES, R. W.,"An Investigation by ESCA of Chemical Treatments of the (100) Surface of n-Type InP Epitaxial Layer for Langmuir Film Deposition", Thin Solid Films, 70, 261 (1980).

[100] HOEKJE, S. J., and HOFLUND, G. B., "Surface Characterization Study of InP(100) Substrate Using Ion-Scattering Spectroscopy, Auger Electron Spectroscopy and Electron Spectroscopy for Chemical Analysis", Thin Solid Films, 197, 367 (1991).

[101] WILMSEN, C. W., in *Physics and Chemistry of III-V Compound Semiconductor Interfaces*, WILMSEN, C. W., ed., (Plenum Press, New York, 1985).

[102] TAO, Y., YELON, A., SACHER, E., LU, Z., H., and GRAHAM, M., J., "S-passivated InP(100)-(1x1) surface prepared by a wet chemical process", Appl. Phys. Lett. 60, 2669 (1992).

[103] WELING, A., S., KAMATH, K., K., and VAYA, P., R., "The effect of external excitation on the sulfur passivation of GaAs surfaces", Thin Solid Films, 215, 179 (1992).

[104] MOULDER, J. F., STICKLE, W. F., SOBOL, P. E., BOMBEN, K. D., *Handbook of X-Ray Photoelectron Spectroscopy,* CHASTAIN, J., ed., (Perkin-Elmer Corporaton , Eden Praire, Minnesota, 1992).

[105] LU, Z. H., TAO, Y., YANG, B. X., FENG, X. H., MITCHELL, D. F., YELON, A., GRAHAM, M. J., and SACHER, E., "Structure of Sulfur-

Passivated In(100)-(1x1) Surface", Mat. Res. Soc. Symp. Proc. 259, 299 (1992).

[106] COMPANION, A. L., Chemical Bonding, (McGraw-Hill Book Company, Toronto, 1964).

[107] HAASE, J., in *Photoemission and Absorption Spectroscopy of Solids and Interfaces with Synchrotron Radiation*, CAMPAGNA, M., and ROSEI, R., eds., (North-Holland, New York, 1990).

[108] LU, Z. H., GRAHAM, M. J. , FENG, X. H., and YANG, B. X., " Structure of Sulfur-Passivated In(100)-(1x1) Surface", Appl. Phys. Lett. 60, 2775 (1992).

[109] RAZEGHI, M., MAUREL, P., DEFOUR, M., OMNES, F., NEU, G., and KOZACKI, A., "Very High Purity InP Epilayer Grown by Metalorganic Chemical Vapor Deposition", Appl. Phys. Lett. 52, 117 (1988).

[110] SKROMME, B. J., STILLMAN, G. E., OBERSTAR, J. D., and CHAN, S. S., "Photoluminescence Identification of the C and Be Acceptor Levels in InP", J. Electron Mat. 13, 463 (1984).

[111] BANERJEE, S., SRIVASTAVA, A. K., and ARORA, B. M., " Thermal degradation of InP in Open Tube Processing: Deep-Level Photoluminescence", J. Appl. Phys. 68, 2324 (1990).

[112] IYER, R., and LILE, D. L., "Role of Polysulfides in the Passivation of the InP Surface", Appl. Phys. Lett. 59, 437 (1991).

[113] WILLIAMS, E. W., and BEBB, H. B. in *Semiconductors and Semimetals*, 8, WILLARDSON, R. K., and BEER, A. C., eds., (Academic Press, New York, 1972).

[114] HOFFMAN, C. A., GERRITSEN, and NURMIKKO, A. V., "Study of Surface Recombination in GaAs and InP by Picosecond Optical Techniques", J. Appl.

Phys. 51, 1603 (1980).

[115] ROSENWAKS, Y., SHAPIRA, Y., and HUPPERT, D. "Picosecond Time-Resolved Luminescence Studies of Surface and Bulk Recombination Processes in InP", Phys. Rev. B 45, 9108 (1992).

[116] SZYDLO, N. and OLIVIER, J., "Behavior of Au/InP Schottky Diodes Under Heat Treatment", J. Appl. Phys. 50, 1445 (1979).

[117] LOUALICH, S., L'HARIDON, H., LE CORRE, A., LECROSNIER, D., SALVI, M., and FAVENNEC, P. N., "Schottky and FET Fabrication on InP and GaInAs", Inst. Phys. Conf. Ser. 91, 517 (1987).

[118] RHODERICK, E. H., "The Physics of Schottky Barriers", J. Phys. D: Appl. Phys. 3, 1153 (1970).

[119] SMITH. B. L., "Au-(n-Type) InP Schottky Barriers and Their Use in Determining Majority Carrier Concentrations in n-Ttype InP", J. Phys. D: Appl. Phys. 6, 1358 (1973).

[120] BOCKRIS, J. O' M., and REDDY A. K. N. *Modern Electrochemistry* (Plenum, New York, 1970).

[121] WILLIAMS, R. H., VARMA, R. R., and MONTGOMERY, V., "Metal Contacts to Silicon and Indium-Phosphide-Cleaved Surfaces and the Influence intermediate Adsorbed Layers", J. Vac. Sci. Technol. 16, 1418 (1979).

[122] WILLIAMS, R. H., MONTGOMERY, V., VARMA, R. R., "Chemical Effects in Schottky Barrier Formation", J. Phys. C: Solid State Phys., 11, L735 (1978).

[123] PHILLIPS, J. C., "Chemical Bonding at Metal-Semiconductor Interfaces" J. Vac. Sci. Technol. 11, 947 (1974).

[124] ANDREWS, J. M., and PHILLIPS, J. C.," Chemical Bonding and Structure of Metal-Semiconductor Interfaces", Phys. Rev. Lett. **35**, 56 (1975).

[125] BRILLSON, L. J., "Transition in Schottky Barrier Formation with Chemical Reactivity", Phys. Rev. Lett. 40, 260 (1978).

[126] BRILLSON, L. J., "Chemical Mechanisms of Schottky Barrier Formation", J. Vac. Sci. Technol. 16, 1137 (1979).

[127] BRILLSON, L. J., and BRUCKER, C. F., "Systematics of Chemical Structure and Schottky Barriers at Compound Semiconductor-Metal Interfaces", Surf. Sci. 132, 212 (1983).

[128] PLUMMER, E. W., and EBERHARDT, W., "Angel resolved Photoemission as a Tool for the Study of Surfaces", Adv. Chem. Phys. 49, 533 (1982).

[129] HIMPSEL, F. J., FAUSTER, Th., and HOLLINGER, G., "Electronic Structure of Si(111) Surfaces", Surf. Sci. 132, 22 (1983).

[130] PENDRY, J. B., "Theory of Inverse Photoemission", J. Phys. C: Solid State Phys. 14, 1381 (1981).

[131] BRILLSON, L. J., VITOMIROV, I. M., RAISANEN, A., CHANG, S., and VITURRO, R. E., "Process-Dependent Electronic Structure at Metallized GaAs Contacts", Proc. of 1992 MRS Spring Meeting, Symposium C, San Francisco, U. S. 1992 (in press).

Appendix I:

The Influence of Passivation Temperature

As discussed in §4.1.4, heating and illumination are effective for promoting surface oxide removal and surface passivation. But for the samples treated under almost the same conditions as those for S-passivated InP but at a temperature between 80~90^{0}C, the coverage and the atomic ratio deviate substantially from that of S-passivated samples. In that temperature range, the ammonium sulfide solution becomes dark red (it is dark yellow at a temperature below 80^{0}C). The treated surface is covered by a visible crust which cannot be completely removed by a DI water rinse. XPS shows that there are more than two monolayers of In atoms bonded to sulfur on such InP surfaces. The atomic ratio of InS_x is higher than that on the S-passivated InP (the sample treated at 65^{0}C), ranging from 2 to 2.5. The overlayer is a rather complicated In-S complex. Fig.A.1 shows a comparison between the normalized S2p spectra from this surface and from the S-passivated surface. The difference between the two is appreciable. The S 2p peak of this sample is wider than that of the S-passivated sample, and can no longer be curve-fit by a single doublet, using the parameters listed in Table 3.2. The reason for this broadening is not clear at present. More detailed work is required to investigate this. These surfaces are not of good crystalline quality. The LEED patterns from these surfaces are very weak and diffuse. Some samples failed to give LEED patterns. This may indicate that the In-S complex overlayer is disordered. But these samples do have some surface electronic properties which are preferable to those of as-etched samples, as will be discussed in the following.

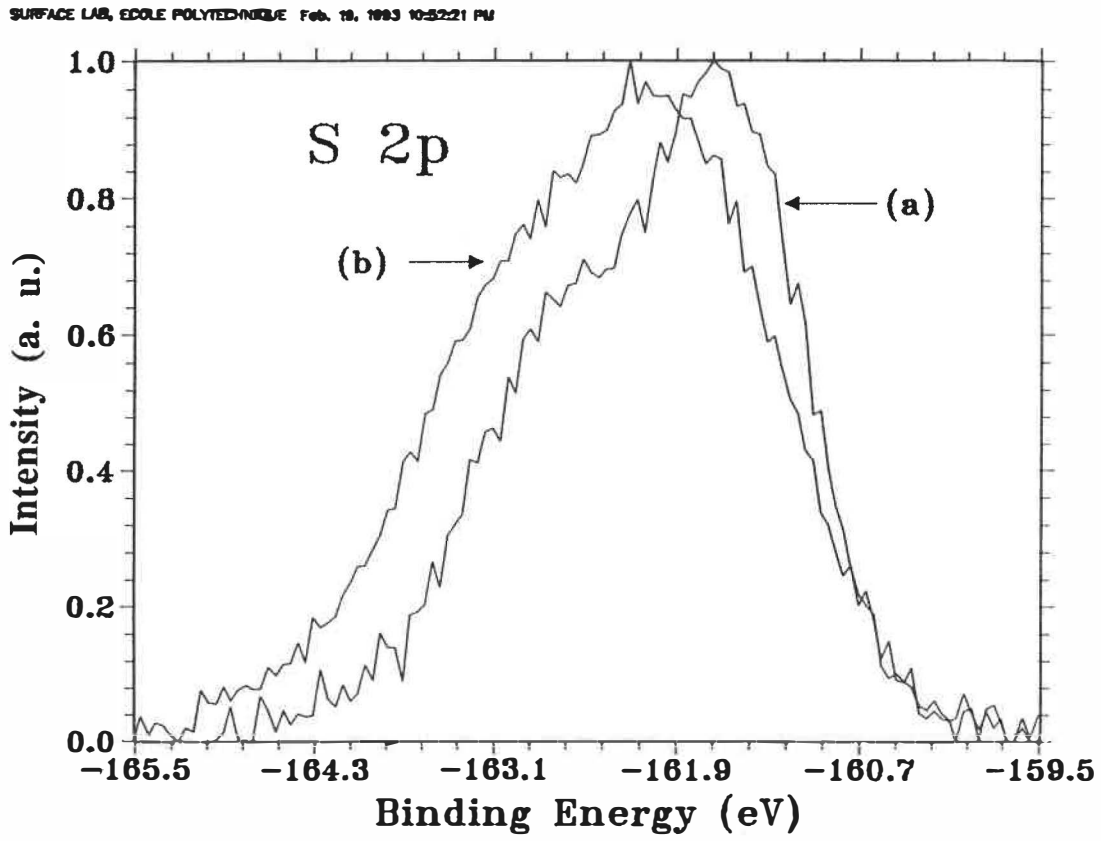

Figure A.1 S 2p spectra from: (a) S-passivated InP, (b) 90°C sulfur treated InP.

The preparation temperature also affects the band edge PL intensity. Fig.A.2 shows PL spectra from three differently treated InP samples. As indicated in the figure, one spectrum is from an InP sample sulfur treated at 90^{0}C and annealed. Another spectrum is from a sample passivated at 65^{0}C and annealed. The third is from an etched and annealed sample. The InP used in this measurement was a lightly doped n-type InP(100) wafer, of carrier density, N_d - N_a, is 5×10^{15} cm^{-3}. The PL peak at 1.417 eV is due to the recombination of excitons bound to neutral donors (D^0X). The one centered at 1.378 eV is probably due to two recombination processes. One is the recombination of (e-A^0) process (at 1.379 eV). Another is the recombination of (D^0–A^0) process (about 1.373 eV). The related intensities are listed in Table A.1. Like the results discussed in §4.3.2, the PL intensity of the S-passivated sample is about twice that of chemically etched sample. The PL intensity of a sample treated at 90^{0}C is lower than that of S-passivated sample, but is still higher than that of the chemically etched sample. It is not clear if the PL intensity decrease of the 90^{0}C treated sample was caused by the scattering of incident radiation and the emitted luminescence by the thicker In-S overlayer formed on InP by the sulfur treatment at that temperature. However, this cannot be the sole cause of the PL intensity decrease, since this was not the same for the two peaks. The peak due to (D^0–A^0) and (e-A^0) decreases much more than that due to (D^0X).

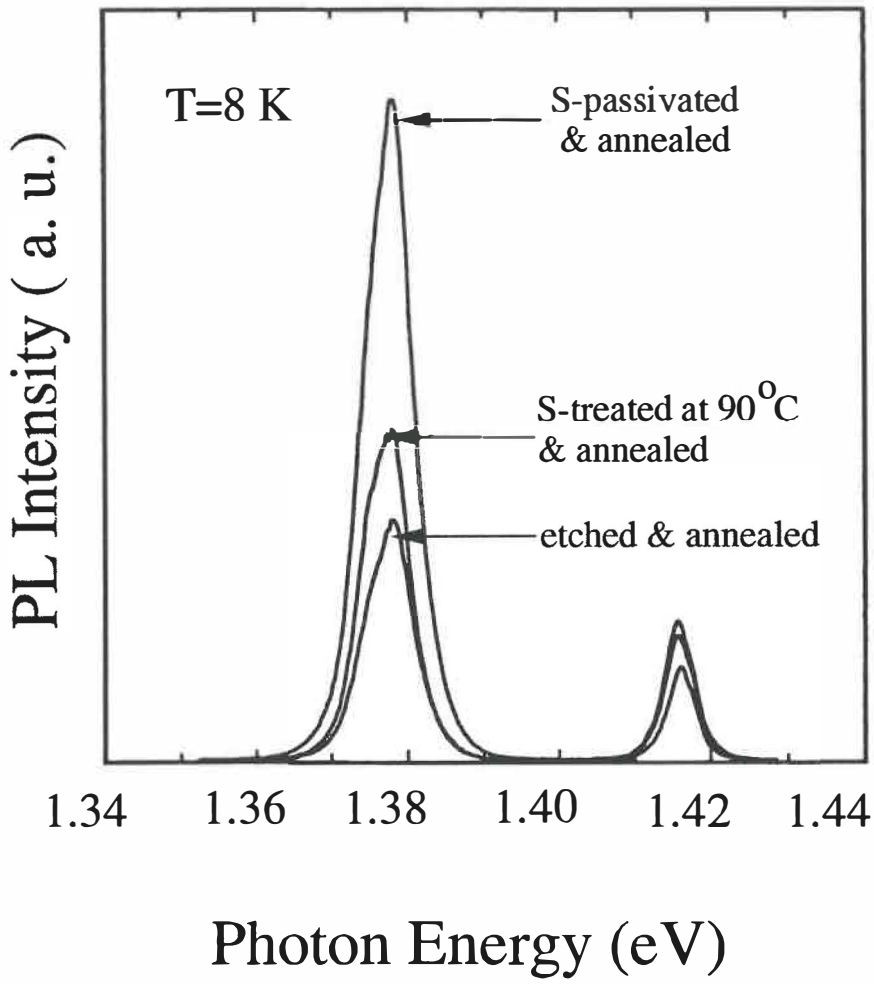

Figure A.2 Comparison of band edge PL spectra from differently treated n-InP at 8 K.

Table A.1 PL intensity at 8 K (lightly-doped n-type)

	D^0, X	D^0-A^0, e-A^0	D^0, X /e-A^0+D^0-A^0
Etched & annealed	0.64	0.36	0.38
Sulfur treated at 90^0 C &annealed	0.90	0.50	0.38
S-passivated & annealed	1.00	1.00	0.21

The temperature affects the I-V characteristics of Schottky diodes as well. Fig.A.3 shows the I-V curve from an Au/n-InP Schottky diode prepared on 90^0C sulfur treated samples. We obtain a barrier height of 0.50±0.02 eV, and an ideality factor of 1.8±0.1 for Au/n-InP; and a barrier height of 0.87±0.02 eV, an ideality factor of 1.4±0.1 for Au/p-InP. The reason for the barrier height change with the sulfur treatment temperature is not clear. However, the sum of the Schottky barrier heights on the n- and p-type samples is close to the value of the band gap, indicating Fermi level pinning at the interface between the Au and the 90^0C sulfur treated InP. The interface states which are responsible for this Fermi-level pinning are possibly related to the interaction between the metal and the thicker In-S surface compound on such samples. Since the ideality factor increases with the thickness of the interfacial layer [83], the existence of a thicker In-S layer can also be a reason for the

increased the ideality factors on these diodes.

The above results indicate that not only does the temperature used for S-passivation affect the surface chemical composition, the surface coverage of In-S species, and the surface structure of the samples, but also directly affect the surface and interface electronic properties of InP.

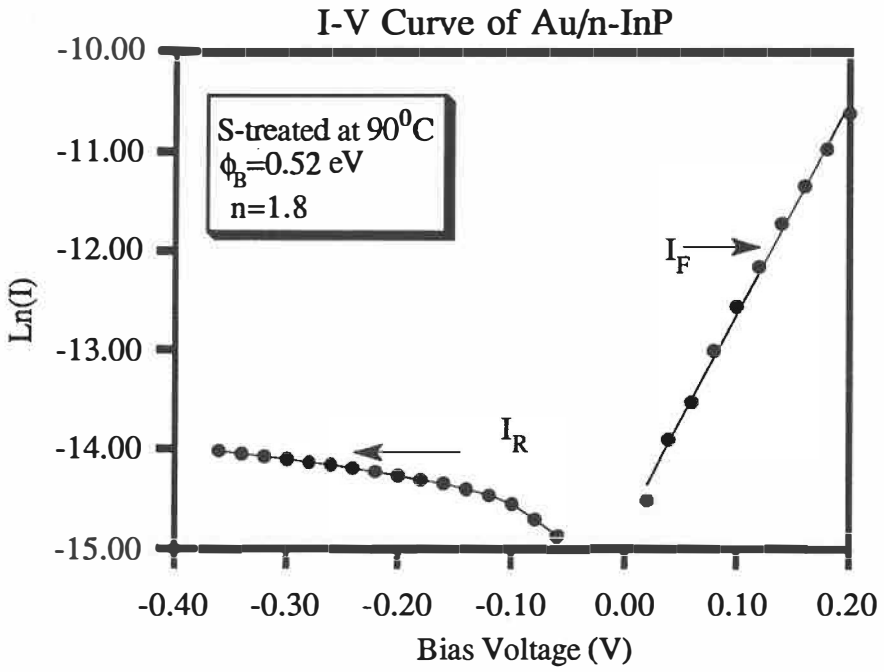

Figure A.3 The current-voltage (I-V) characteristics of the Au/n-InP Schottky diodes prepared on 90°C sulfur treated sample.

T

19